Stony Brook University

Structure and Dynamics of the Gulf Stream's Interannual Migration East of Cape Hatteras

A Dissertation Presented

by

Alejandra Sanchez Franks

to

The Graduate School

in Partial Fulfillment of the

Requirements

for the Degree of

Doctor of Philosophy

in

Marine and Atmospheric Science

Stony Brook University

May 2015

Stony Brook University

The Graduate School

Alejandra Sanchez Franks

We, the dissertation committee for the above candidate for the

Doctor of Philosophy degree, hereby recommend

acceptance of this dissertation.

Dr. Charles N. Flagg
Research Professor, School of Marine and Atmospheric Science

Dr. Robert Wilson
Associate Professor, School of Marine and Atmospheric Science

Dr. Sultan Hameed
Professor, School of Marine and Atmospheric Science

Dr. Thomas Rossby
Emeritus Professor of Oceanography, University of Rhode Island

Dr. Kathleen A. Donohue
Associate Professor of Oceanography, University of Rhode Island

This dissertation is accepted by the Graduate School

Charles Taber
Dean of the Graduate School

Abstract of the Dissertation

Structure and Dynamics of the Gulf Stream's Interannual Migration East of Cape Hatteras

by

Alejandra Sanchez Franks

Doctor of Philosophy

in

Marine and Atmospheric Science

Stony Brook University

2015

The Gulf Stream's (GS) main mode of interannual variability, its latitudinal migration, has been shown to be atmospherically forced by the North Atlantic Oscillation (NAO), taking a 2 year lag into account. Observational and model data were used here to examine the structure of the GS's migration and the dynamics linking it to atmospheric forcing.

The structure of the GS's interannual variability was investigated from different measures of GS position and transport at 38°N and 27°N (i.e. the Florida Current). Using a zonally averaged index, the local measurements of GS position at 38°N proved good representations of overall meridional shifting of the current. GS position and transport were shown linked to the NAO, though the relationship between the GS and the Florida Current transport was not found statistically significant. This indicated that the Florida Current does not have a detectable interannual signal downstream in the GS.

Further investigation of the link between GS position and the NAO revealed the GS position has a more robust correlation with the Icelandic Low (IL) component of the NAO rather

than with the NAO itself. Using Sea Surface temperature composites, it was shown that for anomalously low (west) IL pressure (longitude) corresponding to cooler surface temperatures in the Labrador Sea the GS position shifts north after a period of ~2 years. The relationship between GS and IL pressure (longitude) was further used to create a forecasting scheme for GS position one year ahead of time. The correlation between the resulting forecasted GS and the observed GS was 0.60, significant at 95% level.

Insight into the 2-year delay between the GS and atmospheric forcing was obtained from mean structure and interannual variability of the Slope Sea and Labrador Current. Observations suggested there is a statistically significant link between the Labrador Current, the Slope Sea, and GS position. On 0.5 to 1 year time scales, increases (decreases) in Slope Sea transport lags southward (northward) shifts in GS position by 1 year (r=0.48, significant at 95% level), and cooler (warmer) SSTs in the Slope Sea lead southward (northward) shifts in GS position by 0.5 years (r=0.65, significant at 95% level). On longer time scales, Labrador Current transport and GS position are found significantly correlated (r=-0.68, significant at 95% level) where increases in Labrador Current transport lead southern shifts in GS position taking a 2 year lag into account.

Finally, the connection between GS position, the Atlantic meridional overturning circulation (AMOC) and the regional biogeochemical cycle was investigated using coupled climate models and ocean temperature observations. GS position and the AMOC simulated from GFDL's Climate Model 2.1 found enhanced (weakened) AMOC significantly correlated with south (north) shifts in GS position on decadal time scale. Similarly, results from the GFDL Earth System Models indicated an enhanced (weakened) AMOC leads southward (northward) displacements in GS position and increases (decreases) in regional chlorophyll and nutrient concentrations.

Contents

List of Figures

List of Tables

Acknowledgements

I would like to thank all my committee members, Drs. Charles Flagg, Tom Rossby, Sultan Hameed, Robert Wilson, and Kathleen Donohue. First and foremost of these is my adviser, Charlie Flagg, to whom I would like to express my deepest and most heartfelt gratitude. Thank you for teaching me that science is so much more than data analysis and relevant research questions within the confines of the academically familiar. It is a willingness to be creative and unapologetically doing what needs to get done. It is driving out to New Jersey and negotiating with port authority officers, cajoling the ship's crew, wrestling outdated instrumentation, and teaching your grad student valuable lessons of what not do with soldering irons. It is finding any means necessary to advance the projects you believe in.

I am very grateful to my outside committee members, Tom Rossby and Kathleen Donohue, as well. Tom's contagious enthusiasm and passion for ocean sciences was always a welcome source of motivation, and Kathy's support and encouragement were integral for both the research project and career/life decisions. I am also thankful for the support of Sultan Hameed and Robert Wilson.

A very deep debt of gratitude is due to the friends, both classmates and staff, that I've met and have supported me during my time at SoMAS. To Katelin Childers, whose friendship I'd like to credit as the real reason I got through grad school. Thank you for all the late nights we spent laughing, commiserating, scheming and gossiping. From epic adventures to embarrassing moments, almost every great memory of my time at Stony Brook was shared with you. Thank you to Keith Roberts and Claudia Hinrichs for listening to me practice talks at every odd hour of the day and night. To Mark Bond for weekend warrior-ing and unexpected sources of support,

and special thanks to Kim Knoll and Carol Dovi, for seeing me through the trials and tribulations of being a bureaucratically inept foreigner.

To my family I can only say, thank you doesn't even begin to cover it. Your love and support has carried me from the moment I left home; every adventure and chapter of my life since has been built on your belief in me.

The Oleander Project was made possible thanks to the Bermuda Container Lines (now known as The Neptune Group) and the ship's engineers and crew. Data acquisition and processing for the Oleander-based data used here is a product of the work and attention to detail of Ms. Sandy Fontana. Financial support for this dissertation was provided by National Science Foundation grants OCE-0825418 to Stony Brook University and OCE-0825845 to the University of Rhode Island.

Chapter 1

Introduction

The Atlantic meridional overturning circulation (AMOC) is the complex density-driven system of currents responsible for the distribution of heat regulating climate in the north Atlantic (Fig. 1.1). The Gulf Stream is the surface limb of the AMOC's northward transport of warm, salty waters from low to high latitudes. The Stream's formation originates with the clockwise traveling waters of the Atlantic North Equatorial Current, which splits at the latitude of the northeastern coast of South America. One branch flows through the Caribbean Sea, past the Yucatan Straits, into the Gulf of Mexico and out again through the Florida Straits as the Florida Current. The second branch, the Antilles Current, flows east of the West Indies rejoining the first north of the Florida Straits. The Gulf Stream begins where the Florida Current exits the Florida Straits continuing its poleward flow past Cape Hatteras towards the Grand Banks, gradually evolving into the North Atlantic Current (NAC). At the latitude of the Flemish Cap, the Gulf Stream/NAC alternates between two basic circulation schemes, either 1) the NAC veers towards the Northwest Corner forming a loop and then turning east, or 2) the NAC splits and one branch proceeds north into the Northwest Corner/Labrador Sea while the other branch diverges east towards the Irminger and Nordic Seas [*Krauss et al.,* 1987]. As a result of these circulation patterns both Labrador and the Nordic Seas are regions of deep-water formation. In particular,

the combination of deep winter-convection and NAC inflow into the Labrador Sea via Greenland is responsible for the formation of Labrador Sea Water (LSW), a dense intermediate water mass that flows out of the Labrador Sea basin as three separate branches [*Talley and McCartney*, 1982]. The first limb flows out towards the European Basin, the second one goes southeast under the NAC, and the last one flows southwest around the Grand Banks as part of the Labrador Current, and also as part of the lightest surface layer of the NADW. This deep equatorward movement is an integral part of the AMOC's return flow out of the North Atlantic basin.

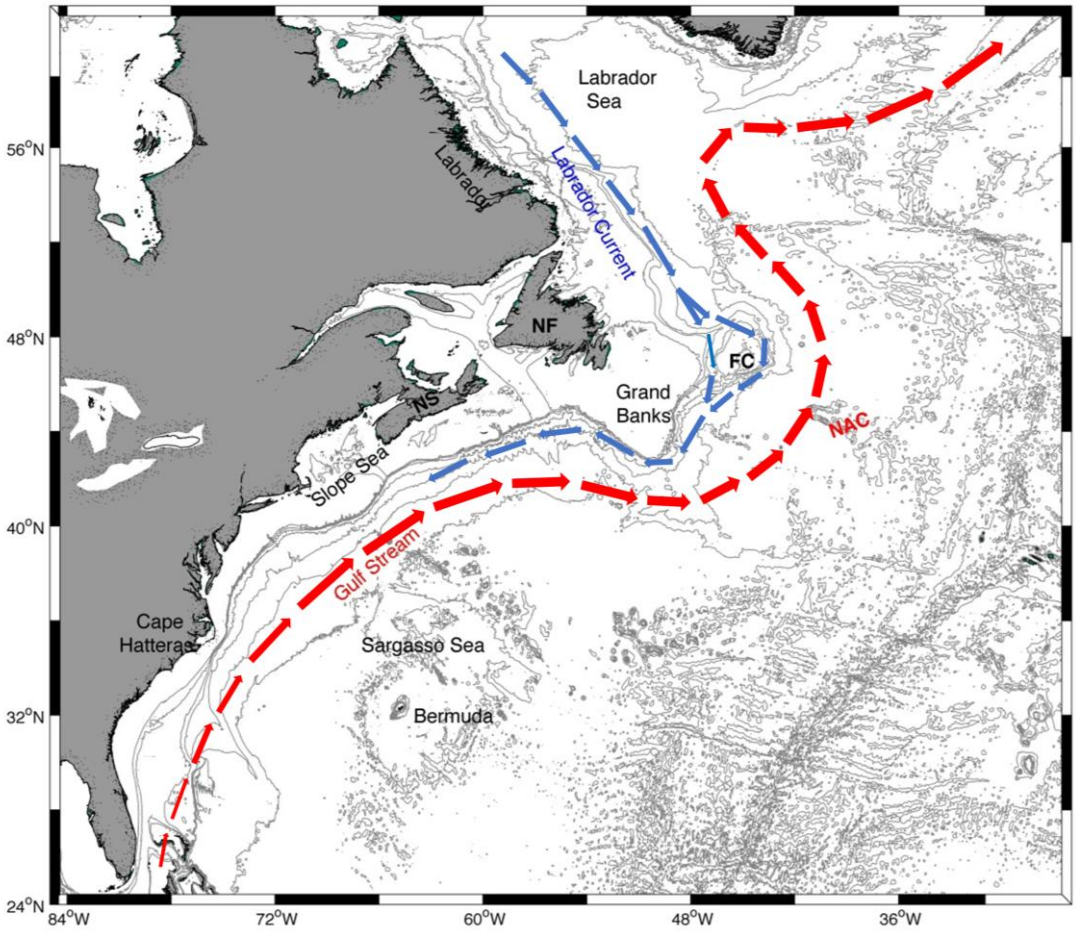

Figure 1.1: Map of study region with schematic diagram of Gulf Stream and Labrador Current circulation pathways. FC: Flemish Cap. NF: Newfoundland. NS: Nova Scotia. NAC: North Atlantic Current.

Because of its impact on the marine biological cycle [*Jennings and Allott*, 2006; *Planque and Taylor*, 1998] and storm tracks in the North Atlantic [*Joyce et al.*, 2000], the Gulf Stream component of the AMOC is of particular importance to the scientific community. Studies have shown that the Stream's interannual migration is linked to low frequency variability in the AMOC [*Joyce and Zhang*, 2010] and atmospheric forcing in the form of the North Atlantic Oscillation (NAO) [*Taylor and Stephens*, 1998]. *Taylor and Stephens* [1980] show positive (negative) phases in the NAO lead northward (southward) shifts in Gulf Stream position with a 2-year lag. Though the Gulf Stream's interannual variability is found strongly interconnected to the atmospheric field, studies have suggested that the intermediary link between the Stream and the NAO is oceanic and buoyancy driven by winter convection processes in the Labrador Sea. During negative NAO phases there is a reduced pressure gradient between the Azores High and the Icelandic Low leading to milder winters. Reduction of deep winter convection in the Labrador Sea implies a decrease in deep intermediate water formation (i.e. Labrador Sea Water). The resulting increase of equatorward Labrador Current transport around the Grand Banks, along the continental shelf and into the Slope Sea is believed to precede southward shifts in the Gulf Stream position. Conversely, during positive NAO phases the Icelandic Low pressure is lower than usual increasing cyclonic conditions, such as storms and harsher winters, in the northwestern North Atlantic. Deep winter convection increases and the newly formed Labrador Sea Water flows preferentially east under the NAC [*Bersch et al.*, 2007]. Enhanced deep eastward flow of the Labrador Sea leads to a decrease in the Labrador Current's southwest transport along the continental shelf. The subsequent reduced flow north of the Gulf Stream then allows for the Stream's northward shift.

Integral in the understanding of the Gulf Stream's interannual variability and its role in North Atlantic large-scale circulation is establishing a clear picture of the Gulf Stream general structure and its link to the surrounding water masses. This dissertation seeks to investigate the underlying driving force behind the Gulf Stream migration, both wind driven and buoyancy driven components. In the following dissertation outline, a brief description of the objectives of each chapter is presented.

1.1 Dissertation Outline

In the subsequent Chapter (2), Gulf Stream path is tracked using several different proxies. Combinations of in-situ and satellite measurements provide the sources for constructing and comparing estimates of Gulf Stream path. Local measures of Gulf Stream path are compared with a zonally averaged Gulf Stream position index to verify that the estimates are internally consistent. In the second component of this chapter, directly measured velocity is used for layer transport of the Gulf Stream east of Cape Hatteras. Gulf Stream transport and position are compared to Florida Current transport. The focus is on the relationship, or lack thereof, between the Gulf Stream east of Cape Hatteras and the Florida Current on interannual time scales.

Chapter 3 investigates the connection between the Icelandic Low component of the North Atlantic Oscillation (NAO) and the Gulf Stream's interannual migration. Long term records of ocean temperature are used to construct an index of the Gulf Stream's Northwall position, focusing on its interannual variability. Sea surface temperature composites of the North Atlantic during years of anomalously low Icelandic Low pressure are constructed to establish a physical basis for the connection between the Icelandic Low and the Gulf Stream Northwall through Labrador Current and Slope Sea circulation. Finally, based on the established connection between the Gulf Stream Northwall and the NAO, the Icelandic Low and the Southern

Oscillation Index are used as predictor variables to create a forecasting scheme, up to 1 year ahead, of the Gulf Stream Northwall position.

Circulation dynamics in the Labrador Current, Slope Sea, and Gulf Stream position on low frequency time scales are examined in Chapter 4. Directly measured velocity and temperature and salinity (T/S) from the Oleander Project are used to analyze structure and variability of the Slope Sea's velocity profile in the vertical, transport and T/S signal. Directly measured temperature is similarly used to create estimates for Gulf Stream path based on the 2°C temperature drop north of the Stream's core, while satellite data from satellite missions, ERS-2 and ENVISAT, provided a measure of Labrador Current transport flowing equatorward around the Grand Banks. The resulting Slope Sea, Gulf Stream position, and Labrador Current transport are analyzed to establish a connection between the water masses and the precise nature of their interaction.

Last, Chapter 5 compares results from observed and model output of the Atlantic meridional overturning circulation (AMOC) fingerprint, and its impact on Gulf Stream path and the regional biogeochemical cycle. First, observed subsurface temperature data are used to construct indices of Gulf Stream path and the AMOC fingerprint. The resulting observational estimates are compared with coupled climate model (CM2.1) derived Gulf Stream path and AMOC fingerprint. In the second part of the Chapter, GFDL Earth System Models (ESM) are used to analyze the biogeochemical cycle in the Gulf Stream region between Cape Hatteras and the Grand Banks. ESM constructed chlorophyll and nutrient concentrations are compared to Gulf Stream path and AMOC fingerprint with the objective of uncovering the underlying physical mechanism responsible for fluctuations in the region's interannual chlorophyll/nutrient signal.

Chapter 2

A comparison of transport and position between the Gulf Stream east of Cape Hatteras and the Florida Current

Abstract

The Florida Current (FC) transport and Gulf Stream (GS) transport and position have been measured almost continuously for many decades in the Florida Straits at ~ 27°N and for the last 20 years at ~38°N along the Oleander line, respectively. Variations in both currents have been linked to the North Atlantic Oscillation (NAO). Here we show five different proxies for the position of the GS near the Oleander line and find all five measures internally consistent. Further, using a zonally averaged index, the local measurements prove to be good representatives of overall meridional shifting of the current (between Cape Hatteras and the New England Seamounts). The second part of the study shows that the statistical relationship between the GS position proxies and the GS and FC transports, in turn, is inversely correlated with r values of ~-0.30, significant at 85% level. The GS and FC transport themselves, on the other hand, are not significantly correlated. Though both position and transport for the GS are shown to be linked to

the NAO, the lack of a robust relationship between GS and the FC transport indicates that the FC does not have detectable interannual signal downstream in the GS.

2.1 Introduction

The Gulf Stream (GS) is the western boundary current flowing north along the U.S. eastern seaboard. At its southernmost end it is known as the Florida Current (FC) emerging from the Florida Straits. Farther north the Stream veers eastward at Cape Hatteras beyond which it becomes a zonal-flowing meandering jet. East of ~50°W the GS splits in several directions with the northern branch known as the North Atlantic Current that continues the warm water transport towards Europe. These currents are components of (or links in) the Atlantic meridional overturning circulation (AMOC) responsible for transferring heat from low to high latitudes, a process of fundamental climatological and ecological importance to the North Atlantic and the surrounding landmasses.

East of Cape Hatteras, the GS experiences two modes of variability: meanders and lateral shifts [*Lee and Cornillon,* 1995]. The meanders are characterized by wave-like perturbations in the Stream's path, while the lateral shifts are the large-scale migration, or deviation from the mean, of the path itself [*Lee and Cornillon*, 1995]. The lateral shifts have been shown to account for most of the GS's low-frequency variability [*De Coetlogon et al.,* 2006; *Frankignoul et al.,* 2001] and have been linked to atmospheric forcing [*Frankignoul et al.,* 2001; *Joyce et al.,* 2000; *Kelly et al.,* 1996]. Several studies found the GS shift correlated to the NAO with a 2 year lag [*Hameed and Piontkovski*, 2004; *Taylor and Stephens*, 1998], and the GS northward (southward) displacement of the current associated with an increase (decrease) in transport, using a model , dynamic height [*Rossby and Rago*, 1985], and GEOSAT data [*Kelly*, 1991; *Kelly and Gille*, 1990]. As westward Slope Sea transport decreases, the GS is positioned farther north and the

Slope Sea's Sea Surface Temperature (SST) and salinity increase [*Rossby et al.*, 2005; *Schollaert et al.*, 2003]. Here we re-examine GS position and transport using over 20 years of direct observations (among other data sets) to determine if the results from previous studies are consistent over time and for in-situ measurements.

Among datasets available for investigating GS variability, one of the longest records comes from the Oleander project. The Oleander project is a long term observational program that has provided eXpendable BathyThermograph (XBT) sections since 1977 and more than 20 years, starting 1992, of upper ocean velocity and sea surface temperature data covering the continental shelf, the Slope Sea, GS and the Sargasso Sea on a line between New York and Bermuda (Fig. 2.1). The main objective of the Oleander project has been to monitor seasonal to long-term variability of the GS and western North Atlantic.

Similar to the GS east of Cape Hatteras, the Stream farther south (hereafter referred to as the FC) is also an integral part of the North Atlantic subtropical gyre. The Yucatan Channel provides the primary source of flow for the FC, which then pours out through the Florida Straits flowing northward, along the east coast of Florida. Historically, measurements of this current have been taken at 27°N [*Peng et al.*, 2009], where numerous studies have tracked the FC transport's variability and its connection to atmospheric forcing [*Baringer and Larsen*, 2001; *DiNezio et al.*, 2009; *Meinen et al.*, 2010]. In particular, *Baringer and Larsen* [2001] found a high negative correlation between the FC transport and the North Atlantic Oscillation (NAO) existed for a time period from 1982 – 1999. Subsequently, *DiNezio et al.* [2009] showed these results did not hold for longer periods of time, and suggested a connection between FC transport and the NAO via regional wind stress curl instead. They posited that Rossby waves were the underlying mechanism between the Current's variability and atmospheric forcing. The majority

of the aforementioned studies linking the FC transport to atmospheric forcing, wind stress curl and the NAO [*DiNezio et al.*, 2009; *Meinen et al.*, 2010] have been based on the Western Boundary Current Time Series (WBTS) project [*Baringer and Larsen*, 2001]. The primary objective of the WBTS is to archive the continuing changes of the western boundary current at the latitude of the Florida Straits.

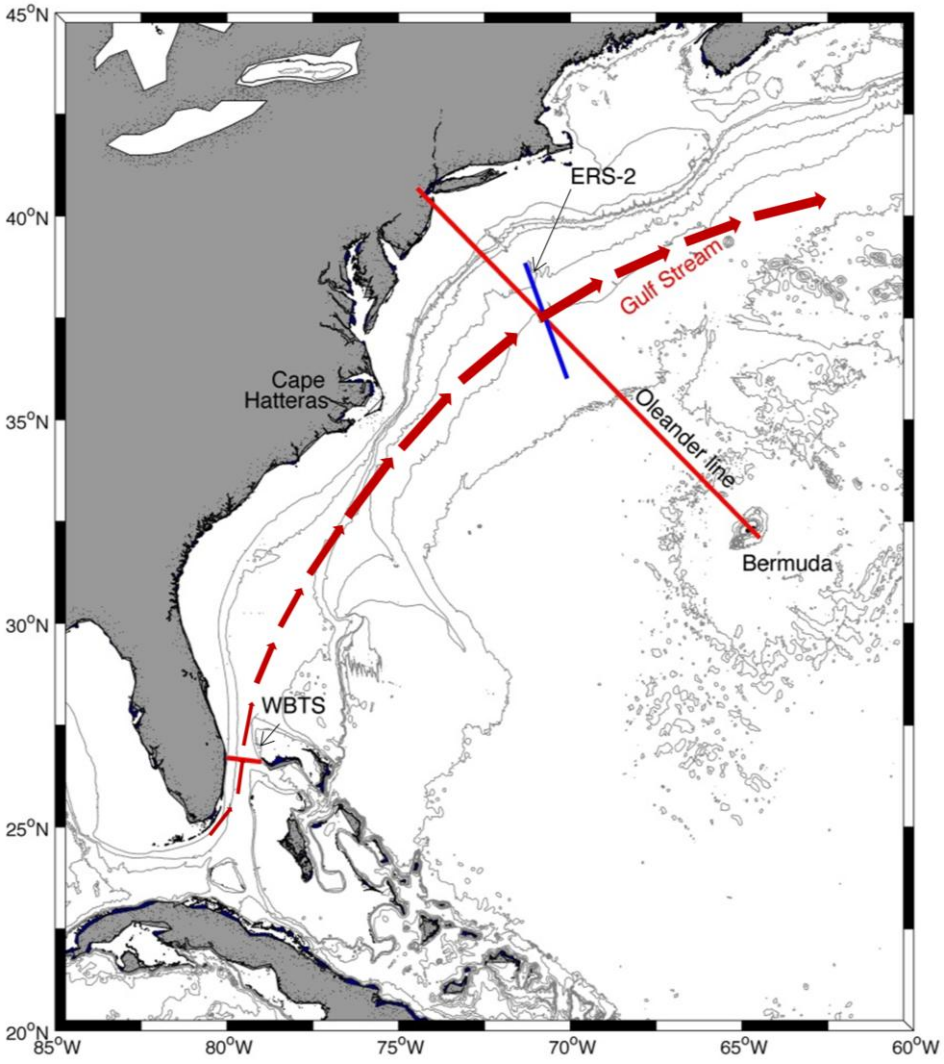

Figure 2.1: Map of the area of interest. The top red line indicates the Oleander trackline, traveling from New Jersey to Bermuda. The small lower red line is where the WBTS records FC data at ~ 27° N. The solid blue line indicates the section from satellite pass. Dotted lines indicate depth ranging from 0 to 5000 m and the red arrows are a rough estimate of the Gulf Stream's path.

Meinen et al. [2010] merged historical and modern observations of the FC into a 40-year record permitting longer term statistical analysis of the current's annual and interannual variability. Here we combine those long-term transport data from the FC with indices of GS position and transport to examine the extent to which the GS and FC are correlated and what this can tell us about the underlying processes involved. The next section (2) summarizes the data and methods used in this study. The principal findings are given in section 3, followed by a discussion and concluding remarks in sections 4 and 5. Given the continuity between the GS and the FC, and the connection between these currents and the larger-scale North Atlantic gyre and AMOC, we hope to better understand the inter-relationship between the prominent features of the western north Atlantic.

2.2 Data and Methods

Position and transport are the two measures of GS variability used here to characterize the GS's behavior. GS position is described using several proxies, remote and local, while GS ocean transport at 38°N and 27°N (FC) are estimated directly from Acoustic Doppler Current Profiler (ADCP; upper ocean only) and cable measurements, respectively. Measures for GS position are computed using data from the Oleander Project, satellite SST, and satellite Sea Level Anomaly (SLA)

The instruments installed and operated on the Oleander include an ADCP, an XBT, and a thermosalinograph (TSG). Since the Oleander program was first initiated, two different ADCPs have been in use, both of which also collect near surface temperature data. The first ADCP installed, a 150 kHz RD Instruments ADCP, ran from 1992 to 2004 yielding velocity profiles down to 250-400 m [*Flagg et al.*, 1998]. In 2005, the 150 kHz ADCP was replaced with the currently-running 75 kHz RD Instruments Ocean Surveyor, increasing the depth of the velocity

profiles to 500-600 meters depth. To obtain absolute current measurements, the Oleander is also equipped with a Global Positioning System (GPS) continuously recording precise estimates of the ship's heading and position. Final current velocity is acquired by subtracting the Oleander's GPS velocity from the ADCP derived current velocity. The resulting velocity's accuracy is of approximately 0.05 m s^{-1}. The Common Ocean Data Access System (CODAS) is the ADCP software package, developed at University of Hawaii [*Firing et al.*, 1995], used to process and store the final data which is served on the http://po.msrc.sunysb.edu/Oleander website. For this study, the surface temperature and velocity ADCP data used was from 1994 to 2012. The velocity was extracted from the 55 meter layer (data are binned in 8 m steps); and at least 60 profiles and gaps no larger than 20 km in the GS region were required for every transect. Technical difficulties in data collecting arose primarily from bubble entrainment. During poor weather and particularly on return trips northward when the ship is more lightly loaded, bubbles are more easily swept down under the vessel, impeding good data coverage [*Flagg et al.*, 1998]. In addition, the Oleander was taken out of service for a major overhaul in winter/spring 2011. Difficulties with the ADCP during the following startup led to a significant absence of data coverage for that year.

The Oleander also hosts an XBT program run by the Northeast Fisheries Science Center. Since 1977, the XBT program has been accumulating surface salinity from bucket samples, and temperature data from XBTs deployed monthly from the Oleander. The XBT sections generally covered most of the continental shelf, slope, and the GS. Starting in 2008, the Oleander Project has contributed XBTs to extend coverage through and south of the GS into the Sargasso Sea. The data are then processed at the NOAA Northeast Fisheries Science Center Narragansett Lab

and can be obtained from the Oleander website, http://po.msrc.sunysb.edu/Oleander/XBT/NOAA_XBT.html.

Another source of GS position information is from the Canadian Marine Environmental Data Service (MEDS) dataset, which from 1966 to the present provides the mean monthly position of the Northwall, i.e. the northern edge of GS marked by a sharp drop in temperature, from frontal maps constructed using satellite AVHRR SST imagery. The maps cover the area between 75°W - 50°W and 34°N - 44°N, though here we focus only on the SST anomaly found along 71°W. The SST data are mostly from NOAA and the Naval Oceanographic Office and can be found at http://www.meds-sdmm.dfo-mpo.gc.ca/isdm-gdsi/azmp-pmza/climat/gulf-golfe/slope-plateau-eng.htm.

The second satellite-based dataset is the along-track SLA from the Radar Altimeter Database System (RADS). RADS is a product of the Delft Institute of Earth Observation and Space Systems and is currently supported by both NOAA and Delft University of Technology (pers. comm. John Lillibridge). Measurements can be acquired from the website: http://rads.tudelft.nl/rads/rads.shtml. Here, for a section covering 36-39°N, data from the ERS-2 satellite track 0693 is used, operational from 1995 to 2011. Latitude, longitude and sea level (anomaly) measurements are obtained using the geoid height, from the Earth's Gravitation Model [*Pavlis et al.*, 2012] as a reference level. Figure 2.1 shows the region of interest and highlights the track used in this study.

Finally the WBTS project, funded by NOAA, is used for its long-term measurements on the FC. The WBTS has collected data centered on 26.5°N using submarine cable voltages and dropsondes or LADCPs since 1982. The transport time series presented here is obtained from cable measurements that have been recorded daily and dropsondes/LADCPs come from cruises

taken throughout the year since the start of the project. The WBTS project has almost complete coverage for the duration of the time period, except for the year 1999, which has almost no coverage due to technical difficulties the project experienced that year. All data are collected from the same line (Fig. 2.1) found on the website: http://www.aoml.noaa.gov/phod/floridacurrent/data_access.php.

For comparison purposes, all GS and FC time series are presented with the same time step. One of the difficulties in defining a common time base is that each subset of data has different types of coverage and gaps in their sampling. To deal with the different issues in temporal and spatial data coverage we construct annual averages, where 12 months is the averaging interval with 6-month steps, in order to make comparisons between the time series. Though the interannual signal is the focus of this study, the GS and FC's annual cycle was also considered (further details in Appendix A). In particular, we found that removing the seasonal variations from the original data before applying a moving average had a negligible effect on the overall results.

2.3 Results

2.3.1 Overview

Two parameters have been used over the years to describe GS variability east of Cape Hatteras, namely the lateral shifting of the GS and the upper ocean transport (or sea level difference across the current). Position of the GS and its relation to the NAO has been quantified in several papers [*Hameed and Piontkovski*, 2004; *Peña-Molino and Joyce*, 2008; *Taylor and Stephens*, 1998] although significant questions about the mechanisms by which the NAO affects GS position remain. Since FC transport has also been linked to the NAO [*Baringer and Larsen*, 2001], it is of interest to investigate whether the GS's variability shows any similarities with the Florida Straits.

In the following we present results for two objectives, 1) to evaluate the various possible GS position measures to determine which yields the most robust measure, and 2) compare those measures to the GS and FC transports to establish a connection between lateral position and along GS transports.

2.3.2 Gulf Stream position proxies

To define the GS's position or path variability, a number of proxy measures have been used over the years. Here six of those measures are reviewed: 1) the 15°C isotherm at 200 m (the classic measure), 2) the Stream's position via the Northwall (indicated by the 2°C drop in surface temperature northward from the location of maximum velocity), 3) the position of the velocity maximum at 55 m (from the Oleander transects), 4) the SST anomaly along 71°W from satellite imagery, 5) the location of the maximum along-track gradient in SLA, and 6) the zonally averaged SST gradients, from *Taylor and Stephens* [1998]. The principal variables used will be velocity and temperature from the Oleander Project, frontal data from the MEDS data set, and the altimeter-derived along-track SLA from the ERS 2 satellite (RADS), all of which have been annually averaged in 6-month steps. All the time series are processed this way to overcome spotty data issues and to focus on the longer interannual time scales. The objective of creating this database of GS parameters is to assess the connection between the different time series and their effectiveness at following the GS's interannual migration, using and contrasting in-situ and satellite measurements. The 6th proxy, i.e. the Taylor index, is not shown or discussed again until the following (Discussion) section.

First the structure of the GS's velocity and its variability over space and time is investigated. Thanks to the Oleander's 20 (and running) year program, position of maximum velocity is tracked using direct measurements (Fig. 2.2). Here we take the position of velocity

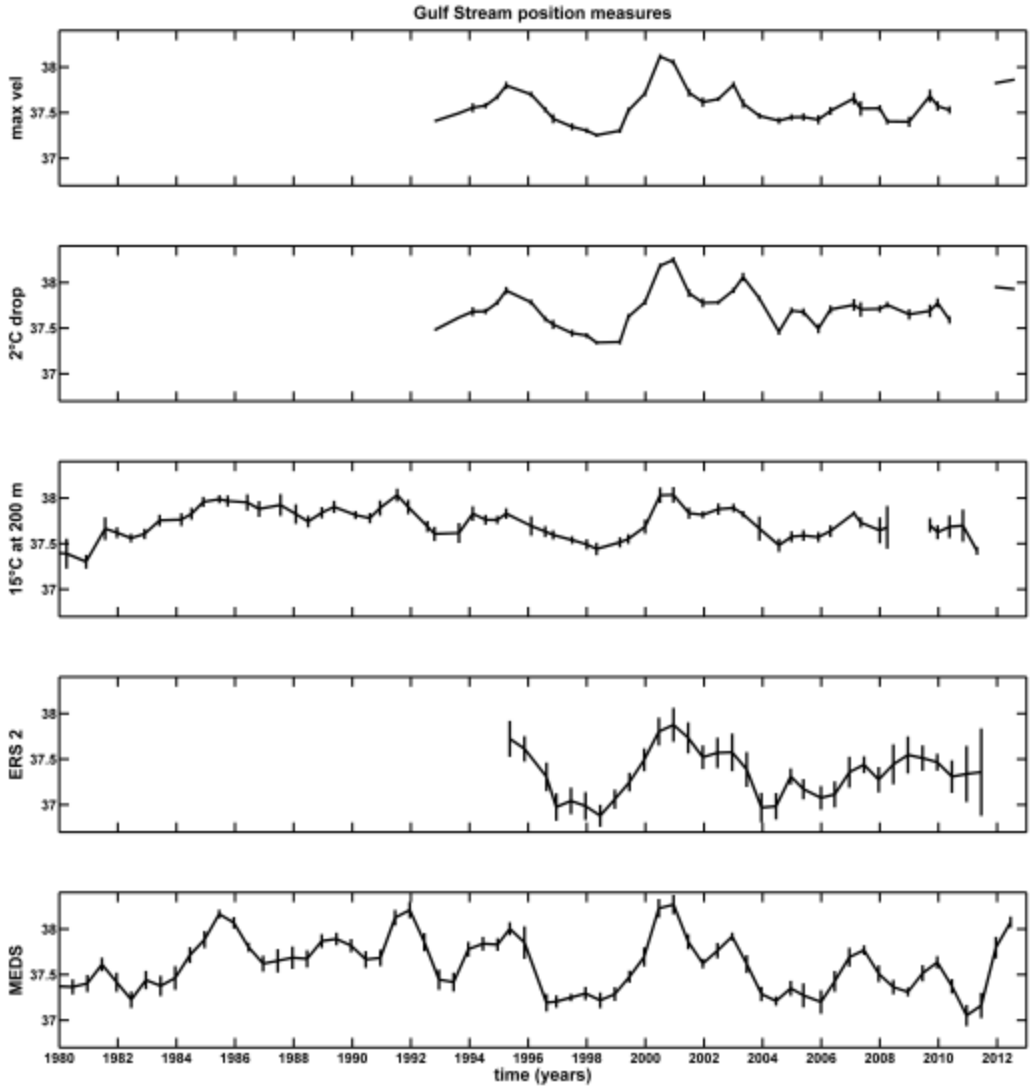

Figure 2.2: Five indices of GS position from the Oleander's ADCP and XBT, i.e. position of max velocity, location of 2°C drop and the 15°C isotherm at 200 meters, and from satellite data, i.e. ERS 2 and MEDS.

maximum at 55 m to be our 'true' estimate of GS position, from which we can determine how well the other indices approximate the Stream's path. Even though the maximum velocity has embedded small scale eddy variability, this gets reduced by the running mean and as such serves as our best measure of GS position at the Oleander line. The 55m depth for the position of maximum velocity is chosen for two reasons: 1) it is the layer closest to the surface with a high

degree of coverage, important for comparisons with the ADCP's surface temperature measurements (see 2° C drop measure), and 2) for consistency with the GS layer transport, also measured at 55 m. The position of the GS's lateral velocity maximum is unchanging with depth within the first couple of hundred meters (results not shown), thus the 55 m choice of depth is as good a representative as any of the Stream's position of maximum upper level velocity (the minimum depth sampled by the ADCP is 22 m).

Before satellite or ADCP data became available, a widely used characterization of the GS Northwall position was the 15°C isotherm at 200 m [*Cornillon and Watts*, 1987; *Fuglister and Voorhis*, 1965] using XBTs or the earlier mechanical bathythermographs. Another metric that was developed for comparison with satellite thermal imagery was the location where SST had dropped 2°C from its maximum in the current [*Rossby and Gottlieb*, 1998]. These metrics can be estimated from the Oleander's XBT and ADCP data sets, respectively, and compared with the location of maximum velocity.

The position of maximum velocity in the GS, Figure 2.2, indicates that the most significant southward shifts occurred in 1998, 2004 and 2011 and the northward shifts during mid-1995, 2000 and 2012. Similarly, the 15°C isotherm at 200 m and the 2°C temperature drop (where available) indicate a northward shift in the mid-80s, 1991 and, more markedly, the year 2000. As expected both temperature proxies for GS position are located north of the Stream's maximum velocity because the position of maximum velocity is in the GS's core whereas the temperature drop occurs where the Stream's warm water meets the Slope Sea's cold water north of it. Overall the time series indicate periods of quiescence mostly between 1982 to about 1996, and then again from the 2003 until about 2011. The highly active periods when the GS shifts south occur, data permitting, for 1981 and then 1998 to 2002. These time periods correspond

with the two strongest El Nino recorded in the last century [*Fedorov and Philander*, 2000]. The mean standard errors of the ADCP-derived Gulf Stream position are significantly smaller than the GS's displacement, especially for the maximum velocity and the 2°C drop measures. Notable exceptions occur in the 15°C isotherm at 200 m index for 2008-2009 and 2011. The XBT time series is less complete in 2009 and the ADCP data are spotty during 2011. Despite some interruptions in the record there is no discernable trend in any of the Oleander position indicators over the 30-year record.

The other measures of GS position near the Oleander line come from satellite data. MEDS records the Northwall position from satellite SST anomalies. The MEDS GS position index is then obtained by tracking its latitude from the SST anomalies at longitude 71°W. Similar to MEDS, data from the ERS 2 satellite is used to estimate the latitudinal position of the maximum SLA gradient, representative of the GS's maximum geostrophically balanced velocity.

In the MEDS index, the most abrupt southward shifts occur during the mid to late 90s, and then again in 2004 and 2011 (Fig. 2.2). The northward shifts occur in the early 90s, 2001, 2007, and 2012. Likewise the ERS 2 shows the position of the GS to be more northerly during 1995, 2001, and 2009; and more southerly during 1998, 2004, 2006, 2008, and 2010. The positional accuracy of the MEDS index is on par with the ADCP-derived GS position measures as its standard error bars appear considerably smaller than the GS's displacement about its mean. The ERS-2 index, on the other hand has slightly larger standard errors but again these are smaller than the indicated GS movements. The large magnitude of the 2011 error bar is consistent with the lack of data points from that year due to the early termination of the satellite mission. Similar to the Oleander data, the satellite data also show the late 90s to be the most active period, which coincides with the 1998 El Nino episode.

Overall both in-situ and satellite observations agree very well for large-scale variations and (to a certain extent) for small scale variations as well. In particular, all position measures are found to be highly correlated, significant at 99% levels (Table 2.1, shown in discussion section). The most active time periods, reflected in all the proxies during the early 80s and late 90s, coincide with the two strongest El Nino documented in the last 100 years [*Fedorov and Philander*, 2000]. We have also found, using thermosalinograph data (not shown here), that salinity proxies are in phase with results presented in this study. This is expected since large temperature excursions are associated with water mass changes.

2.3.3 Gulf Stream and Florida Current Transport Estimates

The GS transport is obtained from the Oleander's ADCP following *Rossby et al.* [2010] methods wherein layer transport is calculated at the 55 m depth across the width of the GS along the Oleander line. The transport is then generated by integrating the velocity normal to the Oleander's track between the two points whose downstream velocity goes to zero on either side of the GS's center. The downstream direction is determined by the direction of the maximum observed velocity. The layer transport is the 12-month running mean average, estimated at 6 month intervals (Fig. 2.3).

The GS layer transport at the Oleander section ranges between 0.122 and 0.146 Sv m^{-1} (or from 85 to 102 Sv using a scale factor of 700, *Rossby et al.*, 2014]. The overall mean for this 20-year record is 0.134 Sv m^{-1} (with a ±9% peak-to-peak range) similar to past studies [e.g. *Rossby et al.*, 2010]. The Figure does not suggest any overall trend, but quite high transport values occur in 1993, 2001, and 2003 and lower transports in 1994-95 and 2007.

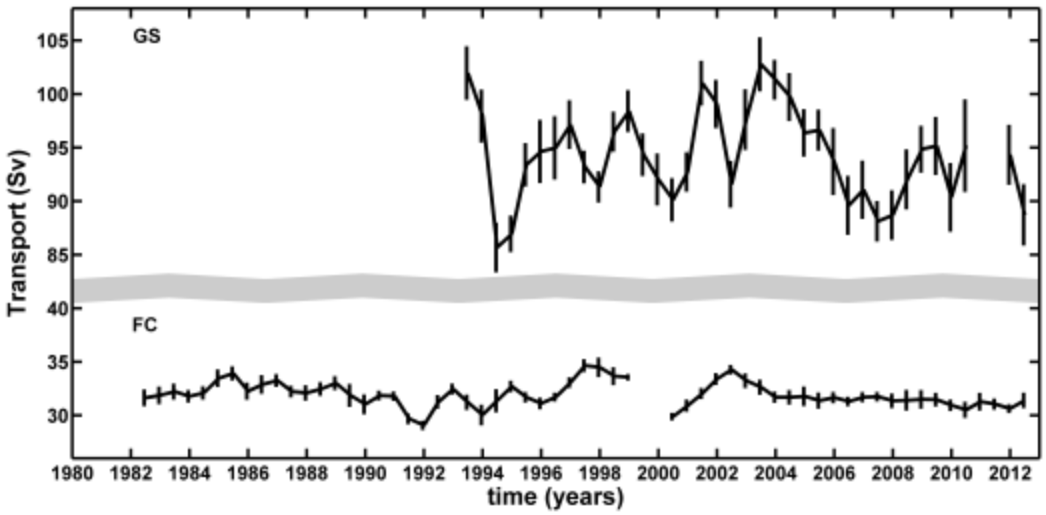

Figure 2.3: GS and FC transport (Sv) annually averaged and stepped every 6 months. A break in the y axis is introduced to eliminate blank space between 40 and 80 Sv.

The FC transport shows much greater variability for the first half of the time series (1982-2000), ranging between transport values of 29 and 34.6 Sv, whereas the second half of the time series appears to be more or less restricted to between 30 and 34.2 Sv. The overall mean transport, 31.93 Sv, agrees with estimates previously reported by *Baringer and Larsen* [2001] and *Meinen et al.* [2010].

To summarize, GS layer transport shows a 9% peak-to-peak range and a 4.6% standard deviation over the twenty-year period. The Stream's transport is highest during 1994 and 2004 and lowest during 1995, 2000, and 2008. The FC transport shows much greater fractional transport variability (overall range is about ±8%) for longer time periods during the first half of the time series (1982-2002) compared to the second half (2002-2012). A visual inspection of the two transport estimates, Figure 2.3, shows no evident pattern common to both currents.

2.4 Discussion

Cross-correlations are used here to establish whether there are links between the various GS position indices and the two transport measurements. The position measures and transports calculated previously are also compared with the zonally averaged *Taylor and Stephens* [1998] index (hereafter referred to as the Taylor index). The Taylor index is computed by taking the first principal component of the position of the maximum SST gradient at 6 different longitudes between 79°W to 65°W. This is followed by an analysis of the relationship between both currents and the NAO index.

Table 2.1 shows cross correlations between the six GS position measures, the GS transport and the FC transport. Zero lag correlations show the best results. This is expected as any lag between these two currents would likely not be longer than a few months, due to their physical proximity. All correlation coefficients between the position indices were found to be significant at the 99% level, while the correlation coefficients between position and transports were significant between the 85 and 95% levels.

	15°C at 200 m	**Max Vel**	**2°C drop**	**MEDS**	**ERS 2**	**Taylor Index**	**GS trans**	**FC trans**
15°C at 200 m	**1**	**0.67**	**0.69**	**0.75**	**0.81**	**0.64**	-	-
Max Vel		**1**	**0.94**	**0.90**	**0.85**	**0.70**	-0.25	**-0.44**
2°C drop			**1**	**0.83**	**0.82**	**0.59**	-	**-0.48**
MEDS				**1**	**0.81**	**0.67**	-0.34	-0.21
ERS 2					**1**	**0.79**	-	-
Taylor index						**1**	-0.30	-0.25
GS trans							**1**	-
FC trans								**1**

Table 2.1: Cross-correlations between all GS position and transport time series and the FC transport. Values that are statistically significant at 99% level are in bold. The rest are significant at 85% level, at least.

When comparing correlation coefficients between the position proxies, the highest r-values correspond to correlations between the maximum velocity vector, 2°C drop, MEDS, ERS 2 and Taylor Index. The high agreement of the satellite (ERS 2 and MEDS) and temperature front indices with our 'true' estimate of GS position, max velocity, shows that the various local measures of GS position are internally consistent. Given the stiff structure of the GS [*Rossby*, 1999; *Rossby et al.*, 2005; *Rossby and Zhang*, 2001] this is not unexpected. The advantage of the Taylor index is that it is a zonal average and it has been shown to be closely linked to the NAO [*Taylor and Stephens*, 1998]. Despite this high correlation the max velocity index shows smaller amplitude than the Taylor Index. This may be because the Oleander line crosses the GS where the meandering envelope is near a minimum [*Lee and Cornillon*, 1996]. Nonetheless, the high correlation shows that even the local measurements of GS position along the Oleander line can represent the low-frequency shifting of the stream as a whole quite well.

In Figure 2.4 the maximum velocity and Taylor indices are considered, along with both transport datasets and the NAO index, where the NAO is the leading variable. As noted earlier the position indices are significantly correlated, but the GS and FC transports by themselves are poorly correlated. Further, the noticeable southward shift of the GS position mid-to-late 90s is not at all reflected in the GS transport, but the time series suggests that when the GS shifts north transport decreases temporarily and vice versa: in 1994, 1999 northward GS shifts and decreases in transport are visible while in 2001, 2003 the corresponding southward shifts and increases in transport occur. Curiously, the (negative) correlation of GS position with FC transport looks stronger (e.g. 1996-2001), however, both transports exhibit more rapid variability than does position.

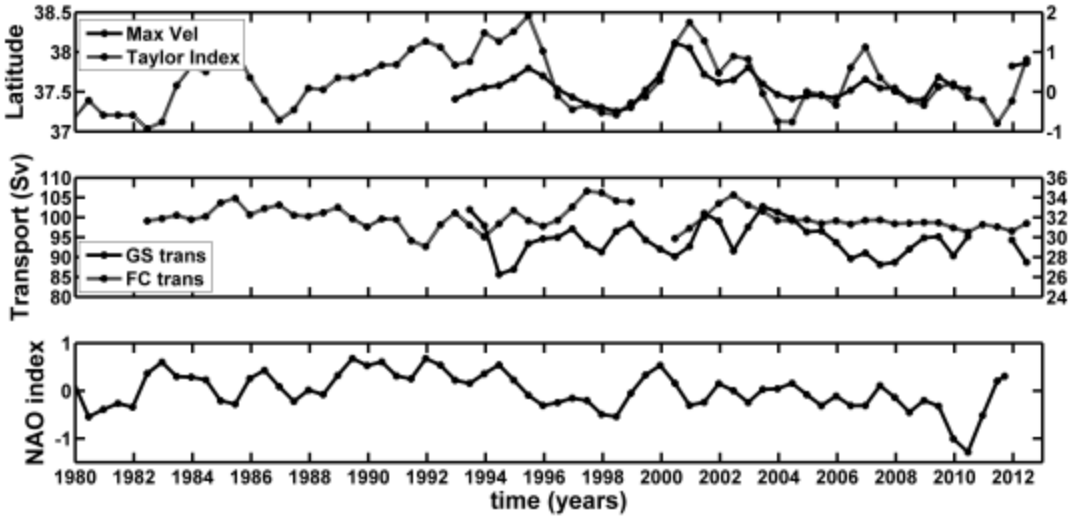

Figure 2.4: Top panel shows position of maximum velocity (solid line) corresponding to the left y-axis (latitude) and the Taylor Index (dashed line) associated with the right y-axis (no units). Both GS (solid line) and FC (dashed line) transport can be seen in the middle panel; left (right) axis corresponds to the GS (FC) transport and units are in Sverdrup. The NAO index is indicated in the bottom panel. All time-series are annually averaged and 6 month stepped.

The NAO index shows agreement with the position proxies and an inverse correlation with GS transport, significant at 95% level (Table 2.2). Analysis indicates that the NAO can account for 13% of the max velocity position with a 1.5 year lag and 20% of the Taylor Index with a 1-year lag. For transports, a correlation of -0.37 was found between the NAO and GS at a 1-year lag. This indicates that during high NAO the GS position is shifting north, taking corresponding lags into account. We note that it is reasonable for the Taylor index to be more highly correlated with the NAO than the max velocity since the zonally averaged index covers a much wider region in comparison to the Oleander's ADCP line, which reflects more local variability. No statistically significant relationship between the FC transport and the NAO could be established.

Variable	n	Lag (years)						
		0	**0.5**	**1**	**1.5**	**2**	**2.5**	**3**
Max Vel	**37**	-0.39	-	-	0.37	0.34	-	-
MEDS	**92**	0.20	**0.34**	**0.43**	**0.40**	**0.32**	**0.31**	**0.28**
Taylor	**92**	-	0.26	**0.45**	**0.44**	**0.39**	**0.35**	**0.29**
GS Trans	**37**	-	-0.36	-0.37	-	-	-	-
FC Trans	**60**	-	-	-	-	-	0.19	0.21

Table 2.2: The sample size, n, and cross-correlations between position measures and transports with the NAO as the leading variable. Values that are statistically significant at 99% level are in bold. The rest are significant at 85% level, at least.

Both GS position and transport have been shown to have significant regional impact as the GS's latitudinal migration has been connected to North Atlantic atmospheric storm tracks [*Joyce et al.*, 2000], plankton abundance [*Borkman and Smayda*, 2009; *Jennings and Allott*, 2006; *Planque and Taylor*, 1998], and the mid-Atlantic Bight shelfbreak currents [*Bane Jr. et al.*, 1988]. However caution is advised when interpreting estimated correlations – a high correlation does not prove causality. This is illustrated very effectively by the fact that the FC transport exhibits its highest correlation with the position based upon the 2°C drop, higher than with the velocity or Taylor indices; there is no physical basis for this that we can see.

There is some indication that when the Stream shifts to the north transport decreases temporarily, but position and transport do not appear to co-vary in a consistent fashion. *Rossby et al.* [2010] showed that variations in westward flow in the Slope Sea north of the Stream are much smaller than those in the Stream. The Sargasso Sea exhibits large variations in westward transport, comparable to those in the Stream, but they have not yet been shown to co-vary [*Rossby et al.*, 2010]. Thus GS transport comprises not only the 'throughput' of the large-scale GS, but also transport associated with re-circulations, some involving the full southern

recirculation gyre [*Worthington*, 1976], some associated with the meandering structure of the GS [*McGrath et al.*, 2010].

The mechanism responsible for the lateral shifting of the GS, on the other hand, likely has its origins to the north through variations in the Slope Sea probably due to a variable outflow from the Labrador Sea [*Peña-Molino and Joyce*, 2008]. When the NAO is in a strong positive phase (very cold winters) large volumes of water are exported to the east as dense intermediate water [*Bersch et al.*, 2007], but when the NAO is in a negative phase, this intermediate water production is sharply curtailed or ceases, and instead export tends to take place to the west along the continental shelf and slope [*Bersch et al.*, 2007]. It is this increased westward flow that leads to a southward displacement of the GS. Hence the poor correlation between the GS position measures and the FC.

2.5 Concluding Remarks

Though it would seem that the FC transport has no detectable signal downstream in the GS, several studies, consistent with results presented here, have linked both currents to the NAO. Here we have tested for and have not been able to establish a direct correlation in transport variability between the FC and the GS. The reason we suggest is that the correlation with the NAO comes along different physical pathways.

The GS position has been linked to the NAO with correlations of ~0.6 following a 1 to 2 year lag in various studies [*Hameed and Piontkovski*, 2004; *Joyce et al.*, 2000; *Taylor et al.*, 1998; *Taylor and Stephens*, 1998]. At 27°N *Baringer and Larsen* [2001] found that for a time period ranging from 1992-1998 the FC was inversely correlated with the NAO with an r-value of -0.5. *DiNezio et al.* [2009] found results consistent with a mechanism where the NAO affects the current via Rossby waves forced from the wind stress curl for a time period in the range of 1982

to 2007. Some differences in results could be attributed to the fact that we used year-round data for the NAO, instead of the NAO's active (winter) months.

For the GS position *Rossby* [1999] and *Rossby et al.* [2005] suggested that the process linking GS and NAO is likely through an increased westward transport of shelf and slope water, which then pushes the GS offshore (to a more southerly position), while a decrease or retreat in transport allowed the GS to shift northward. During years of low NAO winters are milder in the Labrador Sea and dense water production ceases. This evidently forces an increased Labrador Sea Water transport south and west into the slope region; however, when the NAO is high, winters are colder and transport from the Labrador shelf decreases [*Rossby and Benway*, 2000; *Rossby et al.*, 2005; *Smith et al.*, 2001]. Thus based on our results and past studies we posit that the GS east of Cape Hatteras does not have a robust connection with waters upstream from it and its connection to the NAO is via buoyancy forcing from the north. We also note that, contrary to previous literature mentioned here [*De Coetlogon et al.*, 2006; *Kelly*, 1991; *Kelly and Gille*, 1990], the Gulf Stream position and transport do not necessarily co-vary nor appear to be forced by the same mechanisms. This requires further investigation.

Appendix A

The question addressed here is the seasonal cycle in transport and whether its removal alters the transport correlation estimates. To do this we use a least squares sinusoidal fit to transport measurements to determine the annual cycle of transport in the GS east of Cape Hatteras and the FC at 27°N. We found that removal of the annual cycle from the data had a negligible effect on the correlation estimates. This is not surprising for two reasons, first, the seasonal amplitude is not large (discussed in next paragraph), and second, the 1-year boxcar average averages over a complete annual cycle.

For a time period 1993-2013, from the Oleander data, and a period of 1982-2012, following WBTS data, the amplitude of the annual cycle is 0.006 Sv m^{-1} (4.51 Sv) or 4.7% of the mean flow for the GS, and 1.12 Sv or 3.5% of the mean flow for the FC (Fig. 2.5). Instantaneous measurements of the GS transport have a scatter around the sine curve of 15.5% (as a percentage of mean) with the annual cycle peaking in the fall months. In contrast, the FC has a lower scatter of 10.2%, with a peak around the end of the summer months.

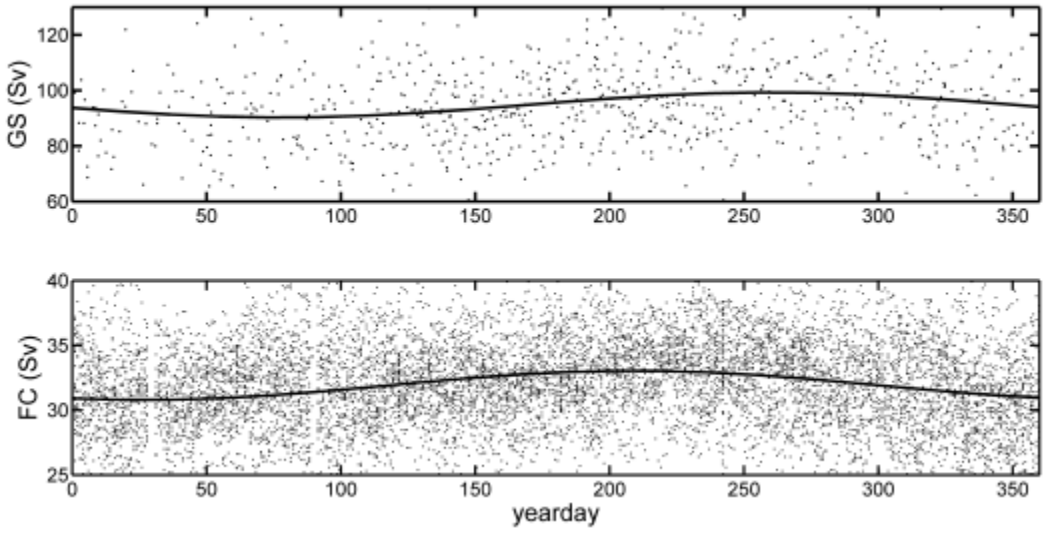

Figure 2.5: Annual cycle of the GS and FC volume transport. The amplitude of the least squares fit to the data is 0.006 Sv m^{-1} (4.51 Sv) for the GS and 1.12 Sv for the FC. The scatter is 15.5% and 10.2% of the mean for each current, respectively.

Chapter 3

The Icelandic Low as a predictor of Gulf Stream Northwall position

Abstract

The Gulf Stream's Northwall east of Cape Hatteras marks the abrupt change in velocity and water properties between the Slope Sea to the north and the Gulf Stream itself. An index of the Northwall position constructed by *Taylor and Stephens* [1998], called GSNW, is analyzed in terms of interannual changes in the Icelandic Low (IL) pressure anomaly and longitudinal displacement during 1966-2012.

Sea Surface Temperature (SST) composites support the view that when the IL pressure is anomalously low, its cooler and more intense winds lower temperatures in the Labrador Sea and southwards to the Gulf of Maine. Two years later, warm temperature anomalies are seen south of the Grand Banks as the warm slope water spreads over the continental shelf. At this time warm SST anomalies are seen over the whole domain of the Northern Recirculation Gyre and a northward shift in the GSNW occurs. Similar changes in SSTs occur during winters in which the IL is anomalously west resulting in a northward displacement of the GSNW three years later. Although time lags of 2 and 3 years between the Icelandic Low and the Northwall are used in the

calculations, it is shown that lags with respect to each of the atmospheric variables, the Icelandic Low pressure, Icelandic Low longitude, and the NAO are statistically significant over a range of years. The calculated lags between atmospheric perturbations in the Labrador region and the Gulf Stream Northwall are consistent with those estimated from observational data.

Utilizing the appropriate time lags between the GSNW index and the IL pressure and position, as well as the Southern Oscillation index, a regression-prediction scheme is developed for forecasting the GSNW with a lead time of one year. This scheme, which uses only prior information, was used to forecast the GSNW from 1994 to 2012. The correlation between the observed and forecasted values for this period was 0.60, significant at 99% level.

3.1 Introduction

Labrador Sea Water (LSW), formed in convective processes in the Labrador Sea, makes up the upper component of the deep western boundary current in the North Atlantic. The deep western boundary current crosses under the Gulf Stream, near 36°N, an important region of interaction between the two different water masses. Hydrographic and tracer surveys of the crossover region show that most of the LSW transported by the deep western boundary current turns away from the shore at the crossover and becomes incorporated with the northern part of the Gulf Stream [*Bower and Hunt*, 2000; *Pickart and Smethie Jr.*, 1993]. At the northern edge of the Gulf Stream, where its warm waters meet the cold Labrador Sea-derived flow, a sharp temperature gradient known as the Northwall (GSNW) is created. Interannual fluctuations of the latitude at which the Northwall occurs are associated with changes in Sea Surface Temperature (SST) distribution northwards and therefore regional climate and plankton distributions.

The analysis presented in this paper is based on the GSNW index of *Taylor and Stephens* [1980, 1998]. This index has been used in studies of plankton abundance in the northeast

Atlantic, the North Sea [*Planque and Taylor*, 1998; *Taylor*, 1995], Narragansett Bay [*Borkman and Smayda*, 2009], and the lakes in Ireland [*Jennings and Allott*, 2006]. From current measurements in the Slope Sea, *Bane Jr. et al.* [1988] found the southwestward shelfbreak current is stronger when the Gulf Stream shifts northward and is closer onshore and it is weaker as the Gulf Stream shifts south offshore. They suggested this relationship is driven by the Gulf Stream's impact on the Northern Recirculation Gyre from both its shift in position and the shedding of warm core rings.

Taylor and Stephens [1998] also showed that the GSNW is significantly correlated to the North Atlantic Oscillation (NAO). They presented a regression model of the GSNW using a 1-year lagged GSNW and a 2-year lagged NAO index. In this scheme, southward (northward) shifts of the Gulf Stream are associated with a low (high) NAO phase. *Taylor et al.* [1998] showed that more of the Gulf Stream's variability could be explained when the Southern Oscillation Index (SOI), lagged 2 years, was added as an independent variable in the regression equation. They found that, for 1966-97, 60% of the GSNW's variance was explained using the GSNW (lagged one year) and the NAO (lagged two years); another 9% was explained by the SOI, also lagged two years. Later, *Hameed and Piontkovski* [2004] discovered that the variance of the GSNW explained in the regression model of Taylor and Stephens [1998] increased significantly when the NAO was de-coupled into its component centers of action, the Icelandic Low (IL) and the Azores High (AH) characterized by their pressure, latitude, and longitude. Their regression model was dominated by the IL pressure (lagged 2 years) and IL longitude (lagged 3 years). The direct contribution, or partial correlation coefficient, of the AH to the variation of the GSNW was insignificant. Because the northerly winds around the IL cause cooling in the Labrador Sea their results suggested that variations in the southward flow of LSW

is the main influence on the Northwall position. This result supported the suggestion by *Rossby and Benway* [2000] and *Rossby* [1999] that interannual variations in the flow of water from the Labrador Shelf to the Slope Sea is the main process that influences the north-south fluctuations of the Gulf Stream.

This paper has a three-fold purpose. First, we report that the relationship between the GSNW and the IL pressure and longitude position described by *Hameed and Piontkovski* [2004] has been maintained up to present. Secondly, we examine SST anomalies in the north Atlantic for winters when the IL pressure is anomalously low, and for winters in which the Low has shifted anomalously west. These anomalies are indicative of dynamical changes in the ocean consequent to changes in wind stress that accompany the fluctuations in the strength and position of the IL. The SST changes are found to be consistent with recent hydrographic observations in the Labrador Sea and the Gulf of Maine. A third purpose of this paper is to show that GSNW can be forecasted a year in advance. Noting the GSNW is correlated with IL pressure and longitude position, and the SOI, each with a 2-3 year lag, we develop a statistical model for predicting GSNW position with a lead-time of one year. This is used to make one-year forward forecasts of GSNW position for each year from1994 to 2013.

3.2 Update of relationship between the Icelandic Low and the Northwall

The GSNW dataset used here is the index computed by *Taylor and Stephens* [1980] from the first principal component of the position of the Northwall's latitude from six different longitudes: 79ºW, 75ºW, 72ºW, 70ºW, 67ºW, and 65ºW. The temperature measurements used to identify the Gulf Stream position have been collected since 1966 by the U.S. Naval Oceanographic Office, NOAA, Oceanographic Monthly Summary, and the U.S. Navy, respectively. Both monthly and

annual means are available at *http://www.pml*-gulfstream.org.uk/default.htm. In order to maintain continuity with previous studies of the GSNW this paper uses only annual means of the index.

The second dataset used was the IL pressure and longitude indices, constructed from gridded NCEP-NCAR reanalysis monthly sea level pressure (SLP) data [*Kalnay et al.*, 1996] as described by *Hameed and Piontkovski* [2004]. Objective indices for the IL are calculated by using the air mass distribution over its domain. By examining the monthly SLP maps over the north Atlantic since 1900, the latitude-longitude domain of the IL was chosen as 40°N-75°N, 90°W-20°E. The monthly averaged pressure of the IL is then estimated as the area weighted mean pressure over all the grid points in the domain where the pressure is less than a threshold value of 1014 mb. The longitude position index is defined as the pressure weighted longitudinal location of the centroid of the air mass over the grid points where the pressure is less than the threshold value. Further details on the calculation of the indices are given by *Hameed and Piontkovski* [2004].

Hameed and Piontkovski [2004] investigated the relationship between the GSNW and the NAO for the years 1966-2000. By decoupling the NAO into the IL and the AH, they found that the largest correlations with the GSNW were with the IL pressure lagged two years and the IL longitude lagged three years. The first row of Table 3.1 gives the statistics of these correlations for the 1966-2000 years. We have updated these results for 1966-2012 (last rows of Table 3.1) and find the lagged correlations between GSNW and IL pressure and longitude have stayed robust through the longer period. Since GSNW and IL pressure and longitude have significant autocorrelations, the effective sample size n' for the correlations was estimated using the method of *Quenouille* [1953] as:

$$n' = n/\left(1 + 2r_1 r_1' + 2r_2 r_2' + 2r_3 r_3' + \ldots\right)$$

where n is the number of data in each series, r_1 and r_1' are the autocorrelations at lag 1 in the two data series, r_2 and r_2' the autocorrelations at lag 2, etc.

Variable	n	n'	r
IL Pressure 1966-2000	**35**	**21**	**-0.59**
IL Longitude 1966-2000	**35**	**25**	**-0.50**
IL Pressure 1966-2012	**47**	**27**	**-0.52**
IL Longitude 1966-2012	**47**	**34**	**-0.40**

Table 3.1: The sample size n, the effective sample size n' and the correlation coefficient r between the GSNW and IL pressure and longitude position compared between the 1966-2000 and 1966-2011 periods. All correlation coefficients are statistically significant at the 99% level.

3.3 Time lags between changes in the Icelandic Low and the Northwall

There are multiple intraseasonal and interannual time scales for variations in the IL pressure and position. Similarly, there are multiple time scales that influence the western boundary current. As a result the time lags between the changes in the IL and changes in GSNW vary over a range of years. *Hameed and Piontkovski* [2004] showed correlations with lags of 0-5 years in their Table 1, where it was seen that the correlations between IL pressure and GSNW were statistically significant for lags of 0, 1 and 2 years, and for IL longitude the correlations for lags 3 and 4 years were statistically significant. However, the percentage of GSNW variance explained was maximized for a 2-year lag for IL pressure and 3-year lag for IL longitude. The lags at which the correlations are statistically significant for the extended data 1966-2012 are shown in Table 3.2, where we again see that the correlations of GSNW are significant for lags of 0, 1, 2 years and those for IL longitude are significant for lags of 3 and 4 years. The Table shows the interesting result that the correlation between the NAO and GSNW is statistically significant for lags of 0, 1, 2 and 3 years. The highest correlation is at lag of one year, although a lag of 2 years

with respect to the NAO was used in the regression model of *Taylor and Stephens* [1998]. Table 3.2 also indicates that the correlation between the SOI and the GSNW is statistically significant with only the lag of 2 years. The physical mechanism that would explain this relationship between ENSO and GSNW remains unidentified.

Variable	0	1	2	3	4	5
NAO	**0.40**	**0.62**	**0.53**	**0.34**	0.21	0.18
IL Pessure	**-0.37**	**-0.48**	**-0.57**	**-0.37**	-0.19	-0.24
IL Longitude	-0.05	0.10	0.02	**-0.37**	**-0.43**	-0.26
SOI	-0.13	0.07	**-0.32**	-0.17	-0.15	-0.12

Table 3.2: Correlation between the GSNW and the atmospheric variables with lags from 0 to 5 years. Results in bold indicate the correlation coefficient is significant at 95 % level or higher.

Bower and Hunt [2000] deployed floats at the levels of upper LSW and overflow water in the deep western boundary current between the Grand Banks and Cape Hatteras to measure the spreading rates of these two water masses. They estimated mean advection velocities along the upper Labrador Current as 2–4 cm s^{-1}. These estimates translate to a travel time of 2 to 4 years for a water parcel to travel the 1700 km between the Grand Banks and Cape Hatteras, consistent with the multiyear lag times between the IL and the GSNW shown in Table 3.2.

More recently, *Han et al.* [2010] measured Labrador Current variations in the Labrador Sea north of the Hamilton Bank (56°N) over 1993–2004. They found the multiyear changes in the Labrador Current transport to be primarily barotropic and positively correlated with the NAO at zero lag. This shows a fast response of the Labrador Sea circulation to the atmospheric variability and is consistent with earlier observations made by *Pickart et al.* [2002] showing that when very cold air blows over the Labrador Sea, deep convection occurs on a time scale of days to weeks.

Another evaluation of time lags was reported by *Mountain* [2012] who estimated the percent of Labrador Slope Water entering the Gulf of Maine (GoM) at depth (150–200 m) through the Northeast Channel from temperature/salinity measurements for the period 1964–2008. Analysis of this long time series data showed that the percent of LSW in the GoM is negatively correlated with the NAO, where the NAO leads the LSW by two years.

3.4 Sea Surface Temperature Response to Icelandic Low Variations

In this section relationships between IL pressure and longitudinal position, and the distribution of SST in the north Atlantic are examined. NOAA Optimum Interpolated (OI) sea surface temperatures v2 available from 1981-2012 with a 1^o x 1^o resolution are used for the SST composites. The SST data may be found on NOAA's physical sciences division website: http://www.esrl.noaa.gov/psd/data/gridded/data.noaa.oisst.v2.html.

Figure 3.1a shows a composite of SST anomalies during 1981-2012 in winters for which the area averaged IL pressure was more than one standard deviation lower than its mean value (Fig. 3.2). We see cold anomalies of -0.2°C to -0.5°C extending from the Labrador Sea to the east and northeast across the north Atlantic, and southward to the south of the Grand Banks, as would be expected from the impact of intensified cyclonic winds that accompany very low IL pressures. Figure 3.1b shows SST anomalies 2 years later, i.e. winters with a 2-year lag with respect to those shown in Figure 3.1a. where the cold SST anomalies in the GoM, observed two years prior, have been replaced by warm SSTs spanning the Northern Recirculation Gyre. This is consistent with the results of *Mountain* [2012] who showed that the percent of LSW in the GoM near the Northeast Channel is negatively correlated with the NAO, where the NAO leads

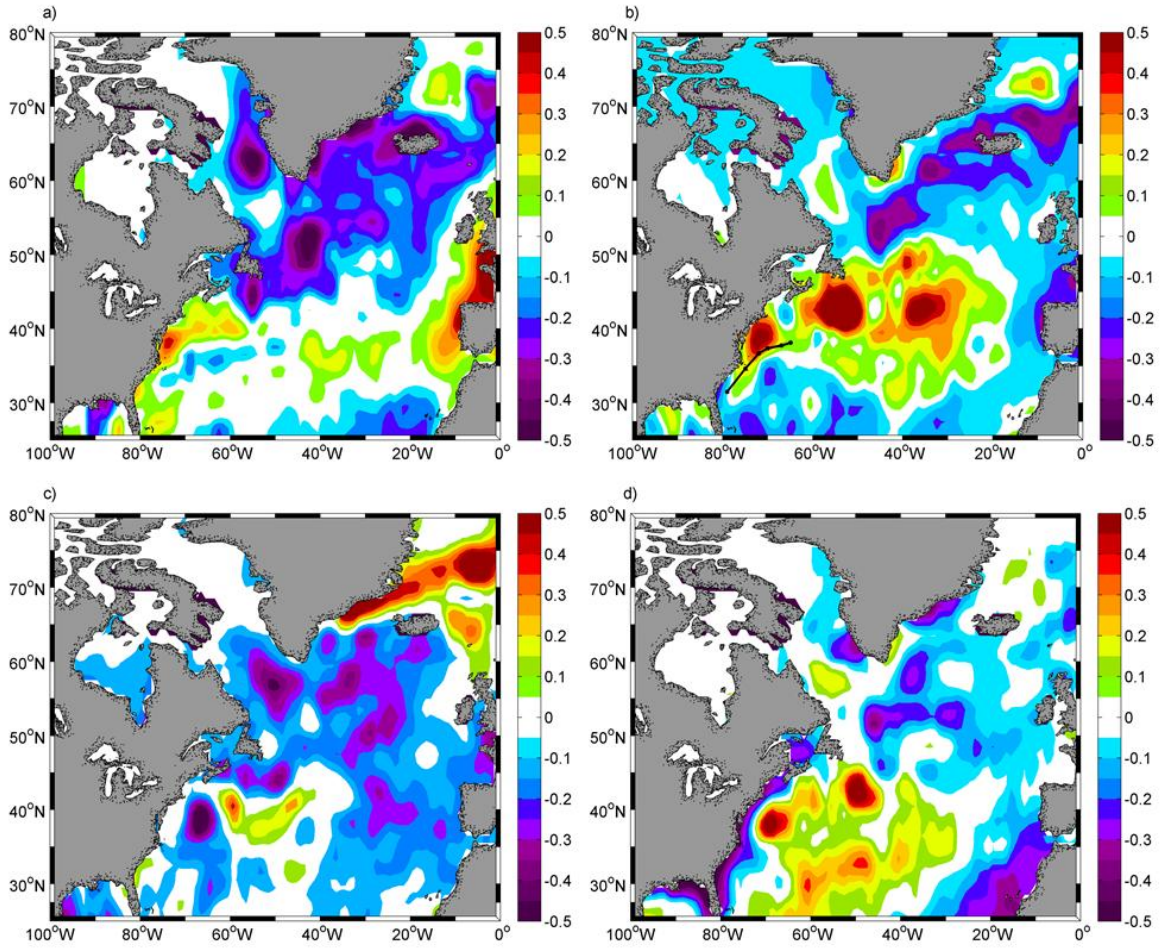

Figure 3.1: Winter (DJF) composite SST anomalies for the time range 1981 to 2012. The ILP during its lowest years is depicted in the top left (with no lag) and top right (with a 2 year lag) images. The ILL during its westernmost years appears in the lower left (no lag) and lower right (with a 3 year lag) images. The Gulf Stream path is superposed (black line) on the SST in panel b. The units are degrees Celsius.

the LSW by two years. Since a positive NAO index corresponds to deeper than average IL and northern shifts in Gulf Stream position, the warm anomalies in the GoM region in Figure 3.1b verify the results reported by *Mountain* [2012]. *Pena-Molino and Joyce* [2008] estimated position of the Gulf Stream from sea surface height anomalies during 1993-2007. They lag-correlated the Gulf Stream position with SST over the north Atlantic and found warm anomalies extending northeastward from Cape Hatteras along the 1000 m and 3500 m isobaths. Warm

anomalies of 0.1°C to 0.5°C are found in the same region in Figure 3.1b. Warm anomalies in the Slope Sea were attributed by *Rossby and Benway* [2000] to a reduction of cold water flux from the Labrador shelf, consistent with the warm temperature anomalies south of the Grand Banks in Figure 3.1b.

Figure 3.1c depicts composite SST anomalies in the winters when the IL was displaced westward by more than one standard deviation of its mean longitudinal position. Cold SST anomalies of up to -0.5°C are seen at the mouth of the Labrador Sea, extending eastward and southward to the Grand Banks and the Scotian shelf. Figure 3.1d shows the composite SST anomalies 3 years after those shown in Figure 3.1c, i.e. lagged 3 years with respect to extreme westward positioning of the IL, as is suggested by the correlation calculations. SSTs in Figure 3.1d are seen to be warmer south of the Grand Banks in comparison with Figure 3.1c indicating a reduction in the spilling of cold waters from the north into the Slope Sea, as hypothesized by *Rossby and Benway* [2000]. Warm anomalies over the North Recirculation Gyre somewhat similar to Figure 3.1b are also seen in Figure 3.1d. The observational evidence reported by *Han et al.* [2010] and *Mountain* [2012] is based on correlations of Labrador Current variations with the NAO index that does not take account of shifts in the position of the IL. Observations so far have not been analyzed to detect influence of changes in the position of the IL, and therefore it is not possible to interpret Figures 3.1c and 3.1d in terms of their dynamical implications. The lower panel of Figure 3.2 shows that the mean position of the IL varied over a longitudinal range of about 25^{o} during 1965-2012; it is reasonable to assume that such shifts in IL position would impact geographical distribution of atmospheric forcing over the Labrador Sea, and thereby contribute to Labrador Current variability.

Figure 3.2 shows the IL pressure index in the upper panel and the IL longitude index in the lower panel. The two dashed lines in each panel represent one standard deviation away from the mean value. The winters for which the index is beyond one standard deviation are used to make the composites in Figure 3.1a and 3.1c. For ILP in Figure 3.1a (no lag) these are 1989, 1990, 1993, 1995, 2000, and 2007. For IL longitude Figure 3.1c (no lag) these are 1985, 1987, 1991, 1992, 1996, 2003, and 2006.

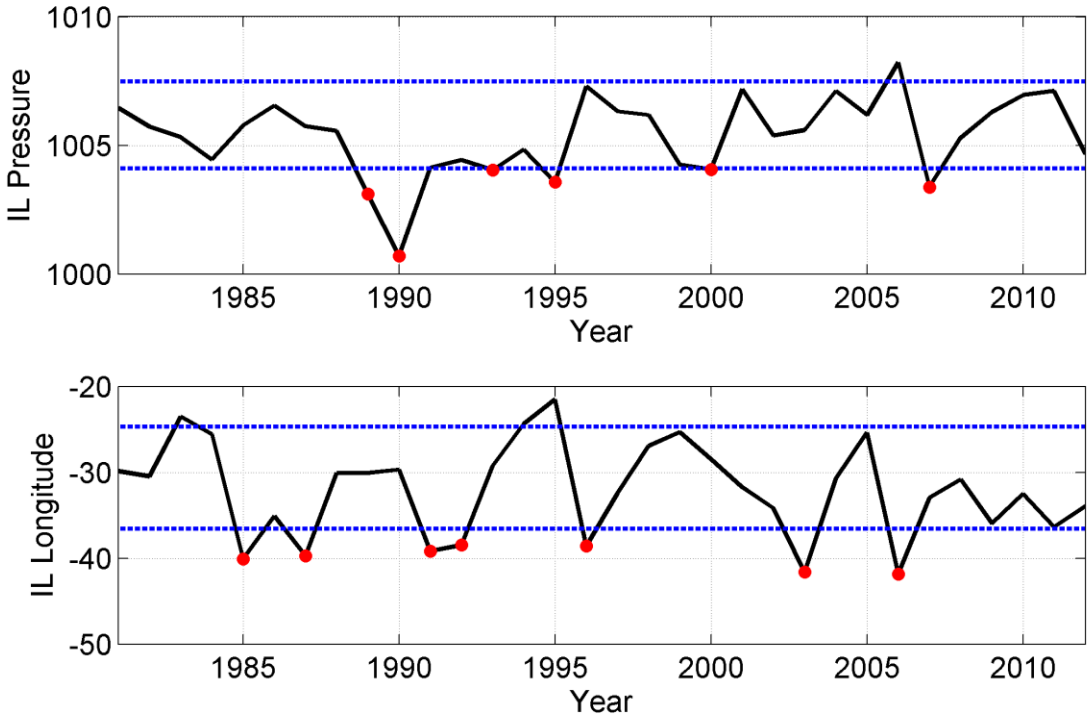

Figure 3.2: Upper panel: The horizontal lines represent one standard deviation above and below the mean IL pressure for 1966-2012. Lower panel: The horizontal lines represent one standard deviation above and below the mean IL longitude for the same years.

3.5 Forecasting the Northwall Position

Taylor and Stephens [1998] and *Taylor et al.* [1998] showed that the GSNW is autocorrelated with a lag of one year, and correlated with the NAO with lag of 2 years and the SOI with a lag of 2 years. Thus it seems plausible that it should be possible to forecast the GSNW using these

variables. A reliable scheme for predicting the GSNW should have practical value in view of the GSNW's known impact on zooplankton distribution in the north Atlantic. *Taylor and Gangopadhyay* [2001] used the one-dimensional model developed by *Behringer et al.* [1979] to *hindcast* the interannual variations in the latitude of the GSNW. The model was forced by the monthly NAO index with a lag of one year.

Based on the results presented in Table 1 and by *Taylor and Stephens* [1998] and *Taylor et al.* [1998] we developed a regression-prediction model for the GSNW as:

$$GSNW_i = a \cdot GSNW_{i-1} + b \cdot ILp_{i-2} + c \cdot ILl_{i-3} + d \cdot SOI_{i-2} + e$$

where *i* represents a particular year and the subscripts of the independent variables represent the lag for each. *a, b, c, d* are regression coefficients and *e* is the residual. The variables on the right hand side of the equation $GSNW_{i-1}$, ILp_{i-2}, ILl_{i-3}, and SOI_{i-2} are statistically independent of each other, i.e. correlations between all pairs of them are smaller than needed for 95% significance. In the first step we developed a regression using the data from 1966 to 1993; the regression coefficients obtained were used to predict the GSNW index for 1994. Then, moving one year forward by developing a regression equation for 1966 -1994 we obtained a prediction for 1995, and so on until we had forecasts for each of the years during 1994-2013. In each of these calculations only *prior* information was used to make the prediction. In Figure 3.3 the solid line shows the observed values of the GSNW index and the dashed line shows the predicted values. The amplitude of variations in the observations is under-estimated by the predicted values. However, the maxima in the northward shifts of the Gulf Stream in 1995, 2000, 2006, and 2009 are captured in the predicted values. Similarly, the extreme southward shifts in 1998, and 2008 are reproduced in the predicted values. The correlation coefficient between the observed and forecasted values during 1944-2013 is 0.60 (significant at the 99% level) and the

Mean Absolute Error (MAE) is 0.53. We tested the stability of this prediction scheme by examining the values of R and MAE for four different durations. These are shown in Table 3.3, where it is seen that the correlation coefficient and the MAE were stable as the length of the forecast period increased.

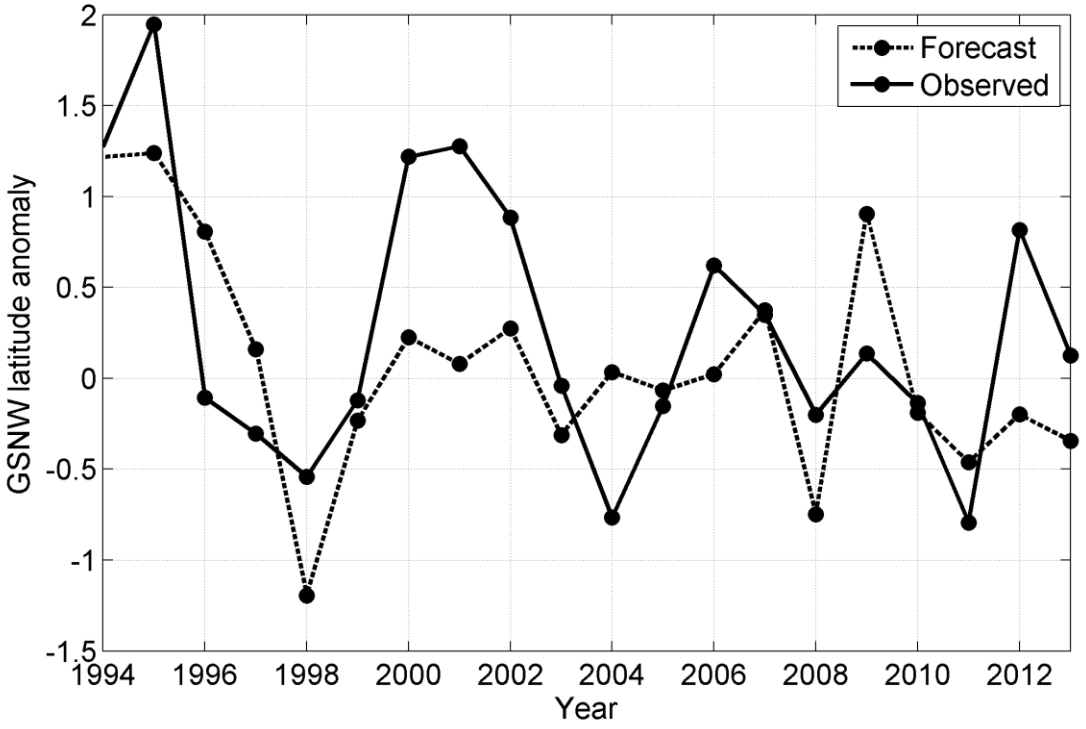

Figure 3.3: The observed Gulf Stream Northwall Index (solid line) compared with its one year ahead forecasted values (dashed line).

As a further check on consistency, cross-correlations between GSNW and IL pressure during 1966-1994, and then for each succeeding year until 2012, were also calculated. The maximum correlation was found to be always with a lag of two years. A similar consistency was found in the correlation of GSNW with IL longitude being maximum at the lag of 3 years. However, the lag for maximum correlation between GSNW and the NAO index fluctuated between 1 and 2 years.

	1994-2002	1994-2005	1994-2008	1994-2012
R	**0.65**	**0.65**	**0.65**	**0.60**
MAE	**0.63**	**0.57**	**0.53**	**0.53**

Table 3.3: Correlation coefficient R and the mean square error MAE during four segments of the forecast period. All correlations are significant at the 5% level.

3.6 Conclusions

While previous studies have noted that the meridional fluctuations of the Gulf Stream Northwall are associated with the NAO, this paper specifically relates these changes in the Gulf Stream to changes in the IL pressure and its longitudinal position.

The SST composite presented in Figure 3.1a suggests that when the IL pressure is anomalously low its cooler and more intense winds lower Labrador SST, which would lead to more intense deep winter convection. The corresponding increase in the production of deep water results in LSW flowing preferentially eastward [*Bersch et al.*, 2007], thus allowing for the observed northward shift in the Gulf Stream. A similar change in SSTs is seen in Figure 3.1c for winters in which the IL is located anomalously west. These changes are followed by circulation changes that produce shifts in the Gulf Stream position after a few years. Lags of 2 years for the Icelandic Low pressure and 3 years for its longitude position were used in the calculations in this paper. However, lags between changes in the IL and the Northwall can vary over a range of years as shown in Table 3.3, and is to be expected from the variable nature of processes in the atmosphere and the ocean.

There are other known processes that can influence the GSNW position, as summarized by *Zhang and Vallis* [2007], not accounted for in this paper. Noteworthy among these is the impact by westward propagating Rossby waves in the ocean generated by fluctuation of westerly

winds related to the changes in the NAO [*Parsons*, 1969; *Taylor and Stephens*, 1998]; and the impact of the bottom topography on the western boundary current and the recirculation gyre.

Finally, utilizing the result that the GSNW index is correlated with the IL pressure and position as well as the SOI with time lags of 2-3 years, a statistical prediction scheme was developed for forecasting the GSNW one year ahead of time.

Chapter 4

Role of the Slope Sea and the Labrador Current on the Gulf Stream's interannual migration

Abstract

The Slope Sea is composed of shelf and Labrador Sea waters coming in from the north and west, and Gulf Stream waters coming in from the south. Interannual Slope Sea transport variability has been linked to changes in Labrador Sea Water just as fluctuations in Gulf Stream position follow variations in Slope Sea Temperature/Salinity (T/S) [*Peña-Molino and Joyce*, 2008] and phase reversals in the North Atlantic Oscillation (NAO) [*Taylor and Stephens*, 1998] when lagged 6 months and 2 years, respectively. It has been hypothesized that the signal from the NAO reaches the Gulf Stream via the Labrador Current and the Slope Sea [*Rossby*, 1999].

Directly measured current velocity is used here to show the mean structure and variability of the Slope Sea. Flow in this region is dominantly (south) westward, with an intensified subsurface jet ~100 km offshore of the shelf break. Slope Sea transport and T/S anomalies are compared with Gulf Stream position, focusing on the low frequency signal. Statistically significant correlations are found, establishing in particular that 1) Slope Sea T/S signal is shown to precede shifts in Gulf Stream position, and 2) variations in Slope Sea transport lead Slope Sea

T/S, yet follows changes in the Gulf Stream's position. Last, comparisons of satellite-derived Labrador Current transport are shown to be correlated (r=-0.68, significant at 95% levels) with a 2 year lagged Gulf Stream position.

4.1 Introduction

The Slope Sea is the water mass between the continental shelf and the Gulf Stream that extends from Cape Hatteras to the tail of the Grand Banks. It is characterized by a mixture of the less saline, cool waters from Coastal Labrador Sea Water [*Csanady and Hamilton*, 1988] and the saltier, warmer, (subsurface) nutrient rich waters from the Gulf Stream [*Schollaert et al.*, 2003]. The continental shelf and slope waters in this area are dominated by the southwest flowing shelf-break jet, a deeper southwestward flow offshore of the shelf break [*Flagg et al.*, 2006; *Linder and Gawarkiewicz*, 1998] and the northeast flowing return slope current/jet under the Gulf Stream's north wall. Changes in this slopewater jet are correlated with Labrador Current variability [*Pickart et al.*, 1999].

Both the Slope Sea and the Labrador Current have been linked to Gulf Stream dynamics. The Gulf Stream's interannual migration follows variations in Labrador shelf water; increases (decreases) in Labrador shelf transport result in the Gulf Stream's shift to more southerly (northerly) positions [*Rossby and Benway*, 2000]. In turn, as the Gulf Stream flows east, it interacts at different points with the Slope Sea and the Labrador Current. At the tail of the Grand Banks, the Gulf Stream breaks up into 3 branches, a southern return flow, a flow east that eventually joins the Azores Current, and the North Atlantic Current (NAC) that flows northeast offshore of the Grand Banks. The relationship between the Slope Sea and the western boundary current has been correspondingly documented [*Peña-Molino and Joyce*, 2008; *Rossby et al.*, 2005; *Rossby and Gottlieb*, 1998]. *Rossby and Gottlieb* [1998] found variations in Slope Sea's

Sea Surface Temperature (SST) anomalies showed a strong correlation with the displacement in Gulf Stream position. Periods of warm SST anomalies in the Slope Sea coincided with the Gulf Stream being recorded closer to the shelf; conversely, cooler SSTs find the Gulf Stream positioned farther offshore [*Rossby and Benway*, 2000].

The atmosphere is the driving force behind the Labrador Current, the Slope Sea, and the Gulf Stream. Shifts in Gulf Stream position [*Hameed and Piontkovski*, 2004; *Taylor et al.*, 1998; *Taylor and Stephens*, 1998] and interannual variations in the Slope Sea [*Flagg et al.*, 2006; *Pershing et al.*, 2001] follow changes in the North Atlantic Oscillation (NAO) index, taking temporal lags into account. Similarly, Labrador Sea transport has a statistically significant non-lagged correlation with the NAO [*Han et al.*, 2014; *Han and Tang*, 2000]. In general, it is hypothesized that during years of low NAO, when winters are milder, Labrador Sea transport around the tail-of-the-bank flows preferentially westward into the slope region; during high NAO, however, winters are colder and the Labrador Sea experiences deeper winter convection. During these years the increased dense-intermediate water produced gets exported preferentially eastward [*Rossby and Benway*, 2000; *Rossby et al.*, 2005; *Smith et al.*, 2001]. Westward transport of shelf and slope water from the Labrador Sea, during periods of low NAO, then lead to southward shifts in Gulf Stream position, while the decrease in westward transport during high NAO allows the Gulf Stream to shift northward. This postulate, wherein the Labrador Sea Water and the Slope Sea are links in the Gulf Stream's latitudinal position and remote atmospheric forcing in the North Atlantic, was introduced by *Rossby* [1999] and is (hereafter) referred to as the buoyancy-driven hypothesis.

Despite the previously referenced work, the relationships between the Labrador Current, the Slope Sea, and the Gulf Stream's latitudinal displacement are still poorly established. The

main objective of this study is to further investigate the connection between the three water masses on interannual time scales. Observational datasets are used to determine the low frequency structure of each current and the nature of the lead-lag relationship among them. The next section provides a brief overview of the datasets and methods used here. This is followed by the results section, which is split in three components. The first part focuses on structure and variability of westward flow north of the Gulf Stream where Slope Sea transport, Slope Sea SST, and the vertical cross section profile of velocity are presented. Second, Gulf Stream position is compared to Slope Sea transport and its Temperature/Salinity (T/S) properties. The third part investigates the relationship between the Labrador Current and the Gulf Stream position, where satellite altimetry and statistical analysis are used to determine the link between currents and the nature of the propagating signal's dynamics. The last sections present a discussion and concluding remarks.

4.2 Data and Methods

The Slope Sea and Gulf Stream regions are investigated using data from the Oleander project. The Oleander is a merchant vessel running once a week between Port Elizabeth, New Jersey and Hamilton, Bermuda. The weekly trips provide long term, high resolution transects of the continental shelf and slope, the Slope Sea, the Gulf Stream, and the Sargasso Sea (Fig. 4.1). This project has been operational for longer than 20 years, providing upper ocean temperature, salinity and velocity from an Acoustic Doppler Current Profiler (ADCP) and eXpendable BathyThermographs (XBT's). Between 1992 and 2004, a 150 kHz ADCP operated aboard the Oleander yielding velocity profiles down to 250-400 meters. In 2005, the ADCP was upgraded to the 75 kHz RD Instruments Ocean Surveyor, increasing the profiling depth to 500-600 meters.

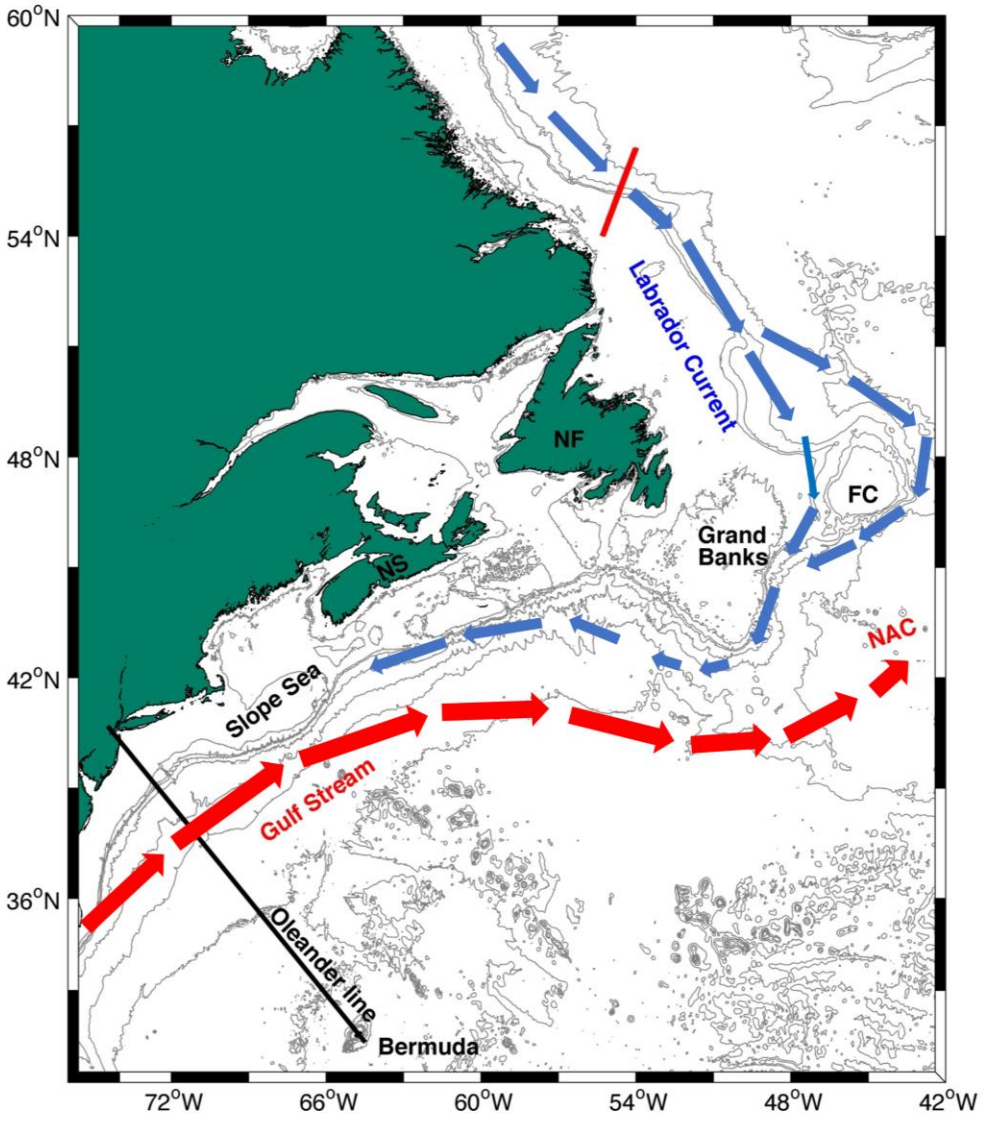

Figure 4.1: Region of interest. Gray lines indicate bathymetry at 200 and 500 m. The long black line indicates the Oleander trackline traveling from New Jersey to Bermuda, and the short red line is the location of the ERS-2/ENVISAT 250 pass. NS: Nova Scotia. NF: Newfoundland. FC: Flemish Cap. NAC: North Atlantic Current.

Based on the ship's average 16-knot speed and a 5- minute averaging interval, spatial resolution in the horizontal is about 2.4 km. In the vertical, for waters shallower than 100 meters, 2 to 8 meter bins are used. In deeper waters, usually 16-meter bins are used. The processing and storing of raw data from the instruments is executed by the Common Ocean Data Acquisition (CODAS)

Access System software package. Limitations in quality data acquisition due to bubble entrainment occur particularly during northbound return trips when the vessel is lighter and more air gets swept down, yielding spottier data during those times. Further technical details can be found in *Flagg et al.* [1998] and *Flagg et al.* [2006]. The Oleander ADCP also provides SST as well as the velocity measurements along its route. The velocity estimates are used to compute transports and Gulf Stream position. All data are accessible on the website: http://po.msrc.sunysb.edu/Oleander/.

The Oleander's XBT program collects surface salinity and temperature from bucket samples and after 2000, from a thermosalinograph (TSG), as well as temperature at depth from the monthly-deployed XBT casts. The program, operated by the Northeast Fisheries Center since 1977, covers the continental shelf, slope, and the Gulf Stream. In 2008, the Oleander Project added XBTs so that coverage was extended south, past the Gulf Stream, into the Sargasso Sea. NOAA's Northeast Fisheries Science Center Narragansett Lab processes the data, obtainable on http://po.msrc.sunysb.edu/Oleander/XBT/NOAA_XBT.html. Near surface temperatures are also provided by the ADCP at the depth of the transducer, ~6m.

Finally, satellite altimetry Sea Surface Height (SSH) data distributed by Archiving, Validation, and Interpretation of Satellite Oceanographic data (AVISO) and the Radar Altimeter Database System (RADS) is used to investigate the connection between Gulf Stream position and the northward waters from the Slope Sea to the Labrador Sea. Maps of SSH anomalies, available at 10-day intervals, are constructed from altimeter missions (Jason-1&2, ENVISAT, TOPEX/Poseidon, GFO, ERS, and GEOSAT)) and processed by the Ssalto/Duacs system, gridded at 1/3° resolution (http://www.aviso.oceanobs.com/duacs/). The Mean Dynamical Topography (CNES-CLS13 MDT) and the associated surface geostrophic velocity field are

obtained from the Ssalto/Duacs altimetry datasets, the CNES-CLS11 Mean Sea Surface, hydrographic and drifter datasets, and the Gravity and Ocean circulation Experiment (GOCE) and Gravity Recovery and Climate Experiment (GRACE) geoid models. The mean field was computed for a 1993-2013 time period and has a spatial resolution of 1/4 ° (auxiliary products are available on the AVISO website: http://www.aviso.altimetry.fr/en/data/products/auxiliary-products/mdt.html). Along-track satellite data from RADS (http://rads.tudelft.nl/rads/rads.shtml) used the ERS-2 and ENVISAT satellite missions to obtain measures of Labrador Current. From 1995 to 2010, between 54° N and 56.5° N, satellite track 250 provided estimates of Labrador Current transport (Fig. 4.1).

All in-situ based time series are presented at six-month intervals with a one-year running mean filter. The purpose of the running mean is to facilitate comparisons between variables and circumvent issues arising from different sampling among datasets.

4.3 Results

4.3.1 Overview

The Slope Sea is characterized by cold, fresh waters [*Csanady and Hamilton*, 1988] composed primarily of Coastal Labrador Sea Water and North Atlantic Central Water [*McLellan*, 1957]. Though the slope water mass was first identified in *Iselin* [1936], its properties and composition were initially defined by *McLellan* [1957].

In the first sub-section, structure and variability of the Slope Sea's westward flow north of the Gulf Stream, i.e. mean velocity, transport, SST, and T/S anomalies, are presented. The next sub-section investigates the link between Gulf Stream position and Slope Sea parameters. Last, measurements of Labrador Current transport north of mainland Labrador and SSH

anomalies in the western North Atlantic are compared to the Gulf Stream's interannual variability.

4.3.2 The Slope Sea structure

4.3.2.1 Mean velocity and temperature profiles

The vertical velocity structure of the Slope Sea is investigated using ADCP measurements from the Oleander. ADCP data are binned 8 m vertically, from 17 to 400 m depth. In the horizontal direction they are averaged over 0.02 degrees latitude, ~3km, between 38.2°N and 40°N, covering the northern edge of the Gulf Stream, the Slope Sea and the outer shelf beyond the 50 m isobath. The temperature records from the Oleander's XBT program are temporally meaned with a vertical and horizontal resolution of 4 m and 0.04 degrees latitude, respectively. Velocity and temperature span the period from 1993 through 2013.

High frequency variability and energetic occurrences, such as warm core rings, are also taken into account. These distort the background dynamics of the region and need to be omitted to the extent possible. To eliminate the effect of the Gulf Stream's warm rings and meanders in the Slope Sea transects in which easterly velocities of over 0.5 m s^{-1} were found, were omitted.

Figure 4.2 depicts the mean velocity structure in the Slope Sea region separated into components alongshore (positive to the northeast) and offshore (positive onshore) to the mean topography. In the neighborhood of the shelf break, the alongshore velocity component shows a subsurface shelfbreak jet with velocities ranging from -0.15 to -0.40 m s^{-1} (negative to the southwest), in the 50 to 250 m depth band. Off the shelfbreak/slope there is a weak northeast flow between 150 – 400 m, followed by a wide band, ~50 km, down to at least 400m flowing southwest. Alongshore standard error suggests the southwest flow is quite robust, but there is some increased variability in the northeastward component. The offshore component of velocity

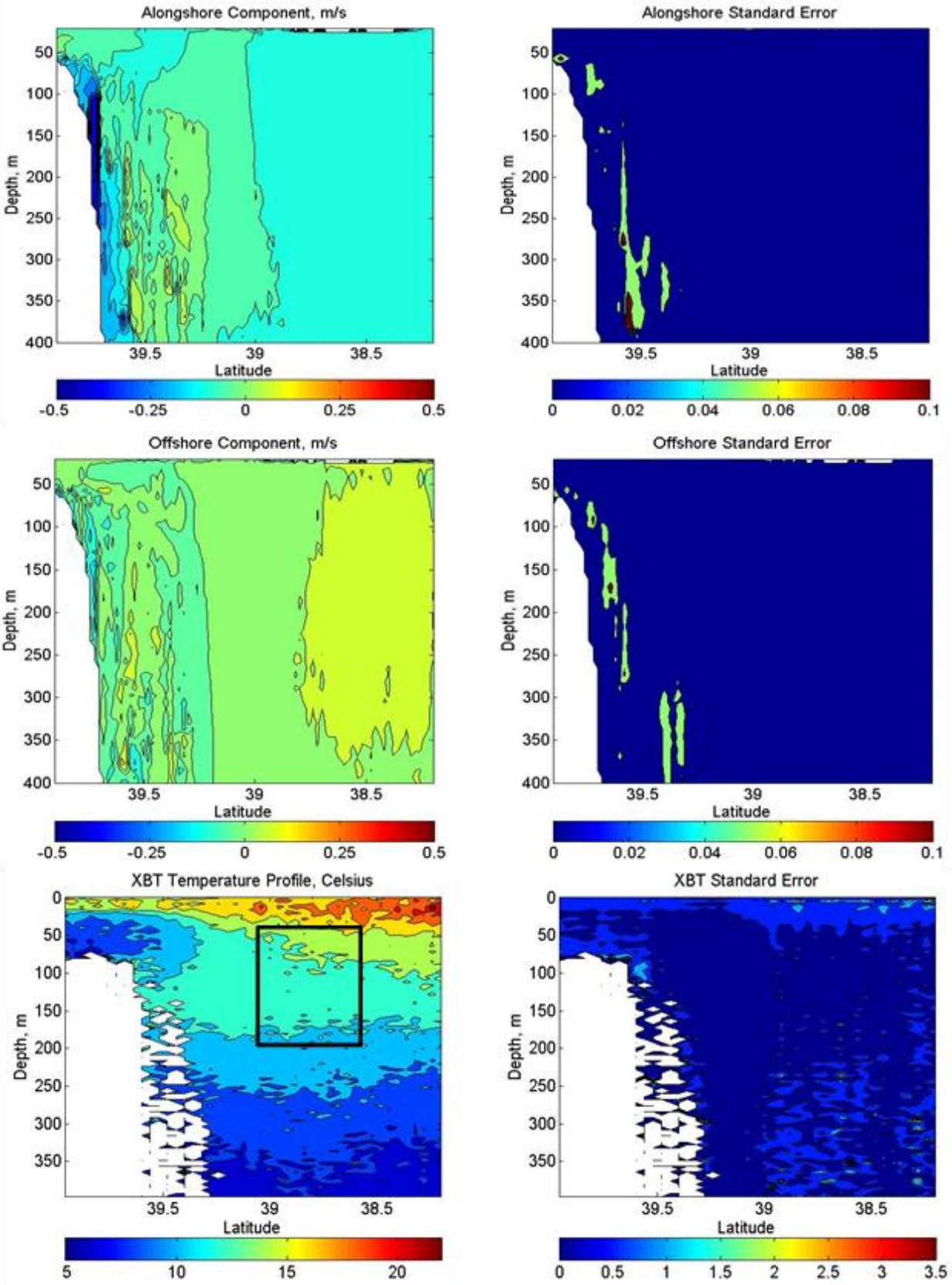
Alongshore Component, m/s
Depth, m
Latitude
Alongshore Standard Error
Offshore Component, m/s
Offshore Standard Error
XBT Temperature Profile, Celsius
XBT Standard Error

Figure 4.2: (a) Alongshore and (b) Offshore to topography components, and the respective standard errors, of the vertical velocity profile in the general Slope Sea and shelf region, averaged over 1993 - 2013. Positive velocities indicate flow is northeast and northwest for the alongshore and offshore components, respectively. Warm core rings have been removed. (c) Mean temperature profile and standard error from XBT casts over the Slope Sea and the shelf. Black box indicates area over which XBT Slope Sea temperature anomaly was calculated.

depicts narrow, subsurface offshore (i.e. southeast) flow of waters in the shelf break/slope region followed by onshore flow. In general, waters flow in the onshore direction most everywhere, except for the weak offshore flow observed near the shelf break. The XBT temperature profile is dominated by a cold band, temperatures of 10°C or less, which cover the shelf and extend offshore.

This system suggests a southwest flowing subsurface jet in the Slope Sea, with associated temperatures ranging from 8° to 12°C (Fig. 4.2). The standard error for the velocity components is less than 0.01 m s^{-1} everywhere south of 39.4°N, meaning the alongshore and offshore velocity components are statistically significant. The areas around ~39.5°N of higher standard error are indicative of both higher variability in the water column (for that region) and a decrease in data points. Small pockets of weak northeast-flowing water may reflect sections in the water column that experience frequent reversals in the direction of the current.

4.3.2.2 Layer Transport

The limits of the Gulf Stream are determined by the location of the point where downstream (northeastward) velocity, on either side of the velocity maximum, goes to zero. The Slope Sea's southern limit can then be defined the same way as the Gulf Stream's northern limit. Based on past Slope Sea studies [*Flagg et al.*, 2006; *Peña-Molino and Joyce*, 2008] and velocity profiles (Fig. 4.2), the Slope Sea's northern limit is fixed at 39.4°N, around 190 km offshore from Ambrose Light in the vicinity of the 1000 m isobath. Between these limits the Slope Sea layer

transport, Sv m^{-1}, is calculated from the Oleander ADCP data at the 55 m depth. Transport is obtained by integrating the velocity normal to the Oleander line and averaging yearly in 6 month steps (Fig. 4.3).

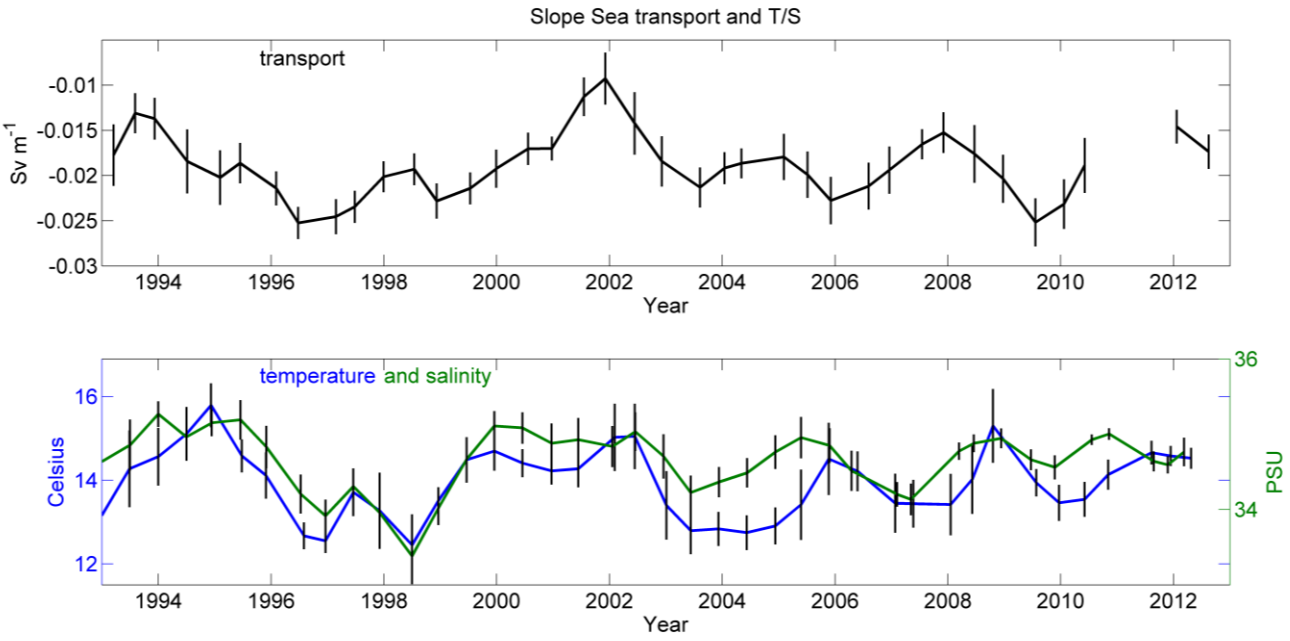

Figure 4.3: Slope Sea layer transport (Sv m^{-1}), temperature (°C), and salinity (PSU) annually averaged and stepped every 6 months. The minus sign in Slope Sea transport indicates the water is moving east to west normal to the Oleander line.

The overall mean layer transport of the Slope Sea, over 20 years, is 0.018 Sv m^{-1} to the southwest. During this time period transport for the Slope Sea ranges between 0.009 Sv m^{-1} and 0.025 Sv m^{-1} and shows no evident long-term trend. From 1993 to 1997 southwestward layer transport increases (note the inverted axes in Figure 4.3), followed by a prominent decrease in 2002. Other periods of low transport occur during 2005 and 2008, interrupted by increases in transport in 2003, 2006, and 2009. The transport highs occurring in the late 90s and the all-time low in 2002 have been similarly observed in this region by *Schollaert et al.* [2003]. In particular,

the high during 1997 is coincident with the one of the largest El Ninos recorded in the last 100 years [*Fedorov and Philander*, 2000].

The data gap in 2011 is from a period when the ship was put in dry dock for an extended period and technical difficulties with the Oleander's ADCP following the ship's repairs lead to an extended interruption of coverage for that year.

4.3.3 The Slope Sea and the Gulf Stream's position

SST sections of the continental shelf and the Slope Sea are useful to understand the relationship between water mass changes in the Slope Sea and the coincident changes in Gulf Stream position. A Hovmöller plot of SST anomaly from the Oleander's ADCP shows interannual variations in near surface (5-6 m depth) temperature. Temperature data is averaged monthly with a spatial resolution of 0.02 degrees latitude. The seasonal cycle is then removed from the SST at each latitude point separately by a least squares fit. The resulting SST anomalies depict interannual variations in the Sargasso Sea, the Gulf Stream, the Slope Sea and the shelf, with the Gulf Stream position plotted overtop (Fig. 4.4). Gulf Stream position is defined here as the location of the 2°C drop in SST north of the Gulf Stream's core as defined by the location of its maximum velocity. The location of the maximum temperature gradient north of the Gulf Stream's maximum velocity, the Gulf Stream's "Northwall", used to track Gulf Stream position was obtained using the Oleander's ADCP temperature records.

The Slope Sea experiences marked interannual variability in surface temperature, especially in contrast with the Sargasso Sea (the region approximately south of 36.5°N). Fluctuations in Gulf Stream position are clearly correlated with the Slope Sea SST's long-term variability. The Gulf Stream shifts south during the cold periods of the mid-90s and north for the 2000-2001 warm SST anomalies. The only marked disparity between the Gulf Stream position

and the SST occurs during the cold south-reaching anomalies of 2003 and 2005 when the Gulf Stream position appears relatively unaffected, and does not shift south following these events.

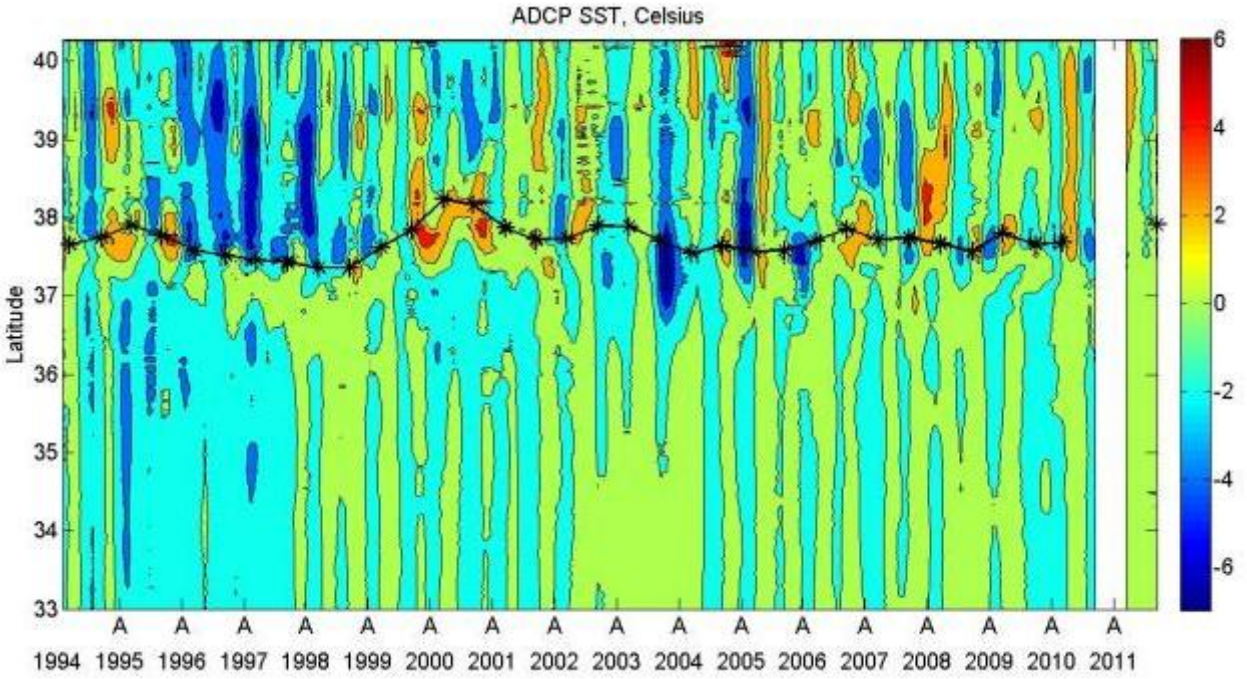

Figure 4.4: De-seasoned SST (°C) anomaly Hovmöller plot along the Oleander line. Gulf Stream position (black line), i.e. the 2°C drop in SST north of the Gulf Stream's maximum velocity, is plotted overtop the SST anomaly. The month of April is noted on the x-axis as 'A'.

To properly quantify the relationship between Gulf Stream position and Slope Sea T/S signature, XBTs and surface water samples are used to estimate spatially averaged Slope Sea temperature and salinity (Fig. 4.3). The XBT Slope Sea temperature is computed by averaging temperature from the 30 to 200 m depth, between 38.6°N and 39.4°N (see boxed area in Fig. 4.2c). Surface salinity is also averaged between 38.6°N and 39.4°N. The resulting temperature and salinity time series show similar interannual variations as the SST Hovmöller and Gulf Stream position. The general pattern depicted by Slope Sea SST, Slope Sea T/S, and Gulf Stream position is akin to the Slope Sea transport time series over the same time period (Fig. 4.5). Cold/fresh phases dominate in the late nineties and 2003-2005, extending as far south as 36.7°N,

around the same time the Slope Sea experiences an increase in southwest Slope Sea transport, and the Gulf Stream shifts south. The warm/salty anomalies predominant in 1995, 2000-2002, 2006-2008, and 2011, are followed by decreases in southwest Slope Sea transport, yet preceded by northern shifts in Gulf Stream position. In general the Slope Sea's cooler (warmer) temperature anomalies follow the Slope Sea's increase (decrease) in southwest flow (r=0.46, significant at 95% level), yet precede the Gulf Stream southward (northward) migration (r=0.64, significant at 95% level) with 0.5 year lags; increase (decrease) in Slope Sea transport follows a southward (northward) shift in Gulf Stream position (r=0.48, significant at 95% level) with a 1 year lag (Fig. 4.5).

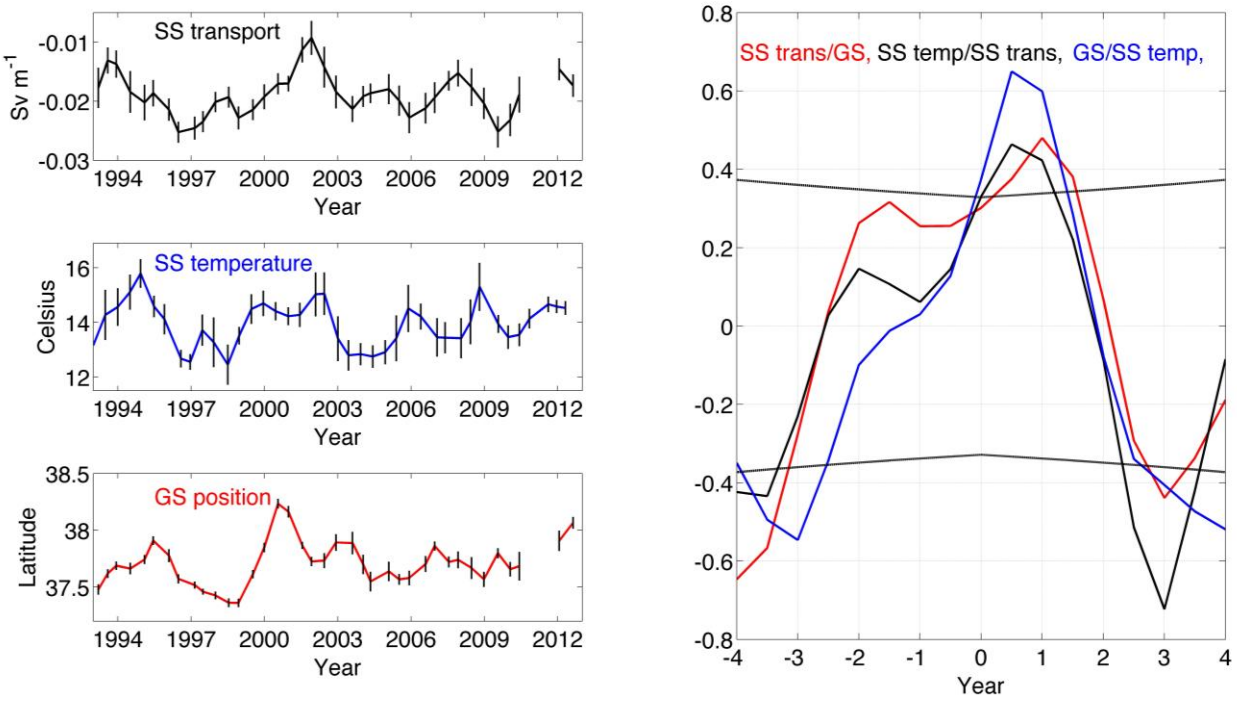

Figure 4.5: Time series of the Slope Sea transport (Sv m^{-1}, black line), Slope Sea temperature (°C, blue line), and Gulf Stream position (latitude of 2° drop, red line). All variables are annually averaged, 6 month steps. The vertical lines represent the standard errors. Correlation coefficients between Slope Sea transport (SS trans) and Gulf Stream position (GS, red line), Slope Sea temperature (SS temp) and SS trans (black line), and GS and SS temp (blue line). The second

variable listed leads the first variable in the positive direction. Dotted black lines indicate statistical significance at 95% level.

Slope Sea temperature and salinity have a correlation coefficient of 0.70, significant at 95% level. The relationships between Slope Sea salinity, and Slope Sea transport and Gulf Stream path show similar high correlations to those found with Slope Sea temperature. Thus in the following sections, where relevant, only Slope Sea temperature is considered.

4.3.4 Circulation in the northwestern North Atlantic

4.3.4.1 Mean Sea Surface Structure

The link between the Labrador Current and Gulf Stream position is investigated first by looking at the patterns of general circulation in the northwestern North Atlantic using satellite altimetry maps of SSH. This is useful as it gives detailed insight into [exact] location of where currents experience their strongest and least contaminated signals.

Mean dynamic topographic (MDT) and geostrophic surface velocities are calculated for a 21-year time period, 1993-2013, from Ssalto/Duacs altimetry products, in-situ data, MSS_CNES-CLS11 Mean Sea Surface, and the EGM-DIR-R4 geoid model, which combines data from both GOCE and GRACE geoid models. Both MDT and associated surface velocity field depict a pattern consistent with known general circulation in the western North Atlantic (Fig. 4.6). The Gulf Stream is seen flowing northeastward from the general vicinity of Cape Hatteras to south of the tail of the Grand Banks, its mean location observed in both the MDT's maximum gradient between the anti-cyclonic subtropical gyre and the Northern Recirculation Gyre (NRG), and the prominent surface geostrophic velocities. Figure 4.6a shows the lowest SSH on the northern side of the Gulf Stream to be -0.29 m, and the highest SSH on the southern end is ~0.93 m; thus difference in sea level across the Gulf Stream (along the Oleander line) is of

approximately 1.22 m. South of the maximum MDT gradient, representative of the Gulf Stream, dynamic height is maximized and generally follows dynamics of the anti-cyclonic gyre. Moving north, at the tail of the Grand Banks, the Gulf Stream evolves into the meandering North Atlantic Current (NAC), protruding/curving in and out of the Northwest Corner. In the Labrador basin region, the patterns of low dynamic height are characteristic of the cyclonic subpolar gyre.

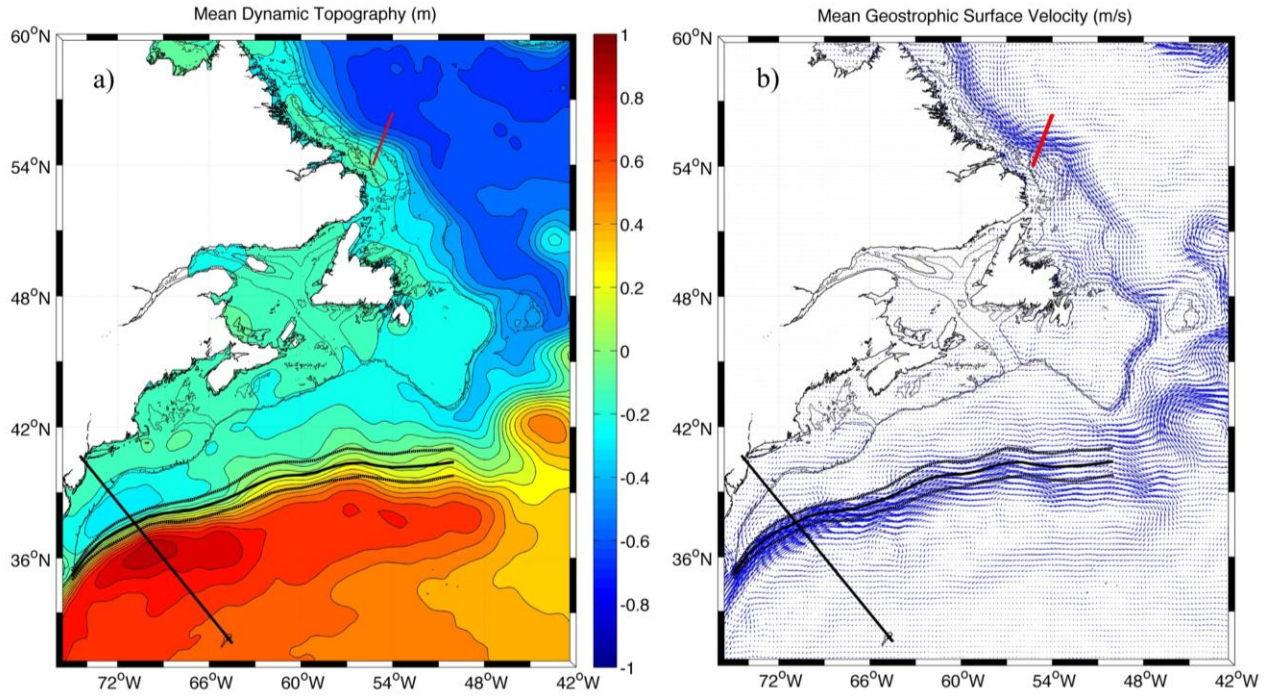

Figure 4.6: (a) Mean Dynamic Topography (m) and corresponding (b) geostrophic surface velocity field (m/s). Dashed black lines indicate bathymetry at 200 and 500 m. The long, black line represents the Oleander track, and the short red line is the location of the ERS-2/ENVISAT 250 pass. The elongated, undulating black line tracks the mean Gulf Stream Northwall position from MEDS data, and the adjacent black, dashed lines are the associated standard deviation for the Stream's mean position. The MEDS mean Gulf Stream position is estimated from SST anomalies at every degree longitude between 75° W and 50° W.

Geostrophic surface velocity vectors (Fig. 4.6b) confirm the general large-scale features observed in the MDT: the conspicuous Gulf Stream flowing northeastward, evolving into the NAC, and the Labrador Current flowing southeast and equatorward around the Grand Banks. It

is interesting to note that the signal for the Labrador Current weakens considerably by the time it reaches the tail of the Grand Banks and is imperceptible thereafter.

The surface velocity field is particularly useful in that it gives us a better idea of where the Labrador Current might be sampled to obtain a signal both strong and removed from the influence of the Gulf Stream/NAC system. For the first of those criteria, we note the strongest signal for the equatorward Labrador Current runs along the 500 m isobaths from the north just off Labrador, south through the Flemish Cap and around the Grand Banks. The next consideration is the Labrador Current's proximity to the Gulf Stream/NAC. Between the southern Grand Banks and the northern latitude of the Newfoundland, we found that the Labrador Current is in too close to the Gulf Stream/NAC to obtain a signal unaffected by the meandering stream. Thus, the strongest, cleanest signal for changes in the Labrador Current can be found in a segment between 54°N - 56.5°N, and 55.3°W - 54°W, just north of mainland Labrador. The along-track satellite pass that falls in this region is ERS/ENVISAT pass 250 (red line, Fig. 4.6). A Labrador Current index is thus computed from pass 250 SSH data and compared to Gulf Stream position in the following section.

4.3.4.2 The Labrador Current and Gulf Stream position

In order to compare variability of the Gulf Stream's position to processes much farther north, in the Labrador Sea, it is advantageous to consider a zonally averaged index for Gulf Stream position. Analysis of the relationship between Oleander-derived Gulf Stream position and satellite altimetry data in the Labrador Sea region (not shown here) suggests the Oleander line may be positioned too far south (and the localized index may have too much noise) to provide robust results. The *Taylor and Stephens* [1998] proxy for Gulf Stream position (hereafter referred to as the Taylor index), however, is a zonally-derived index, computed from Principal

Component Analysis of the latitude of the Gulf Stream Northwall at the following longitudes: 79°W, 75°W, 72°W, 70°W, 67°W, and 65°W. The link between the Gulf Stream position from the Taylor index and the Labrador Current from the along-track satellite pass is also supported by an analysis of AVISO SSH in the northwestern North Atlantic.

Based on the mean field and surface velocity of the previous section, pass 250 is chosen as representative of the Labrador Current for comparison with the Taylor index. The Labrador Current index (hereafter referred to as LC index) is constructed from the along track 250 pass between 54° N and 56.5° N, using both ERS-2 and ENVISAT satellite missions. The general structure of the SSH along this segment is high to low SSH going in the offshore direction (indicated by the higher latitudes), consistent with Labrador Current equatorward/southwest flow at this location. The LC index is computed from the height difference between 54° N and 56.5° N from each 250 pass and then annually averaged for the 1995 to 2010 time period (Fig. 4.7).

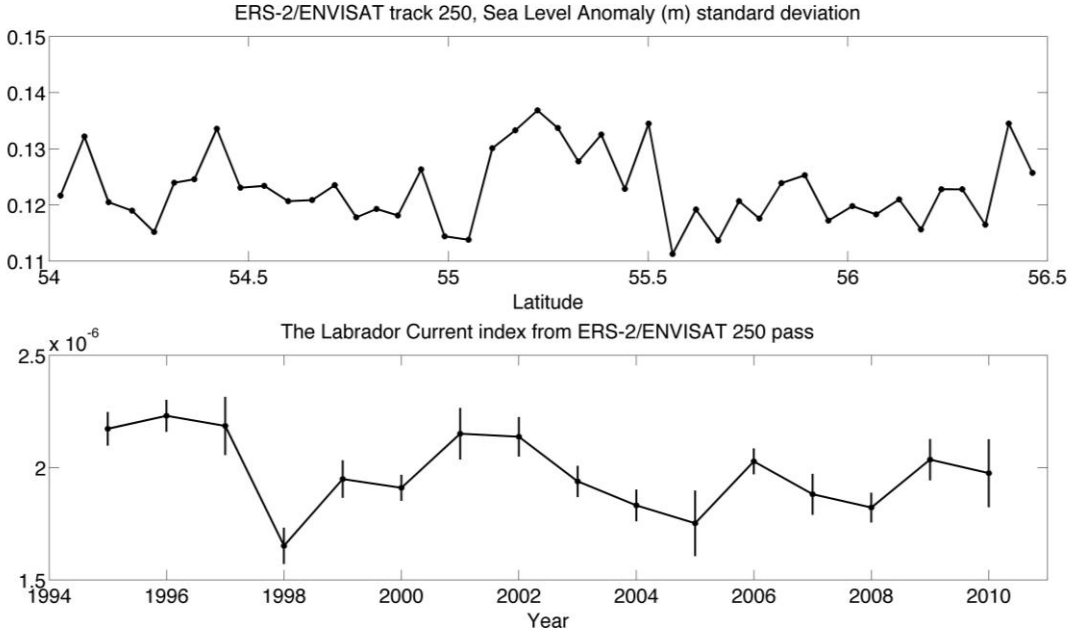

Figure 4.7: (a) Standard deviation of the Sea Level Anomaly (m) from 1995 to 2010 by ERS-2/ENVISAT satellite missions along pass 250, between 54° N and 56.5° N. (b) Labrador Current

index estimated from the slope of line of each cycle of the 250 pass between 54° N and 56.5° N, annually averaged. The vertical lines indicate standard error.

Comparison of the annual Taylor index with the satellite-derived LC index shows Gulf Stream position to be highly correlated with the Labrador Current (r=-0.68, significant at 95% level) with the LC index leading the Taylor index by 2 years (Fig. 4.8). In particular, the LC index experiences lows during 1996, 2001, 2006, and 2009 followed two years later by the Taylor index; meaning increases in Labrador Current transport are followed two years later by southward shifts in Gulf Stream position. Similarly, the decreases in Labrador Current transport observed in 1998, 2005, and 2008 are followed two years later by northward shifts in the Gulf Stream's position (as represented by the Taylor index). The anomalously low event of 1996, high transport to the south, has been previously described as the Labrador Current 'pulse' in previous studies [*Han*, 2006].

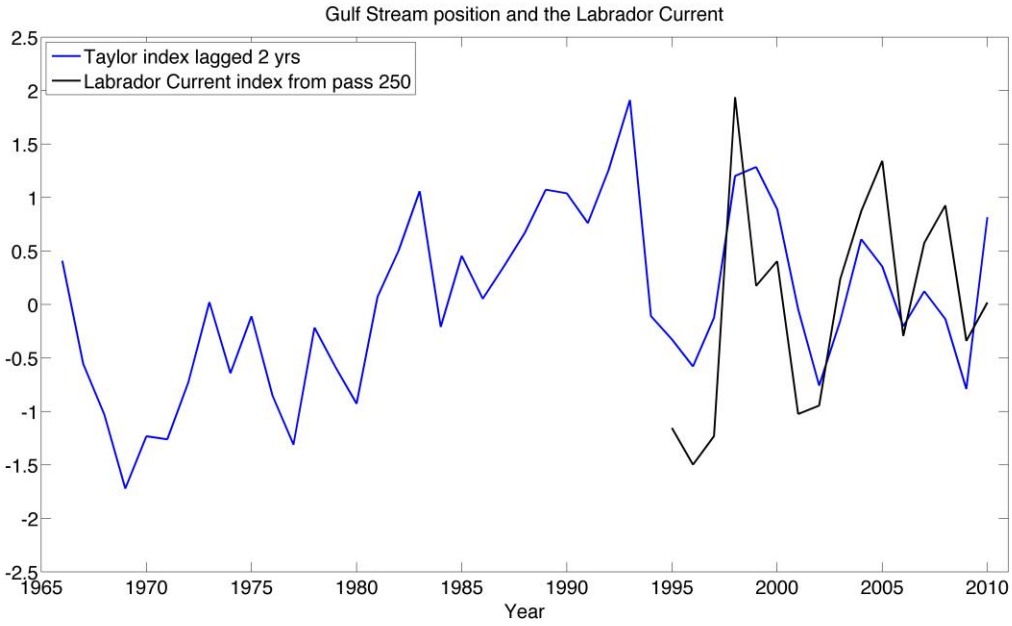

Figure 4.8: Taylor index (blue line) and the inverse, normalized LC index (green line) computed from the ERS-2/ENVISAT 250 pass. Both time series are yearly averaged.

To further investigate the link observed between the Taylor and the LC indices, AVISO SSH is used. The AVISO SSH is obtained from several altimeter missions and has a spatial resolution of 1/3°. For a 21 year time period, from 1993 to 2013, daily AVISO SSH was yearly averaged at every grid point in western North Atlantic, between 31°N - 60°N, and 76°W - 42°W. This region was chosen as it comprises a large part of the Labrador Sea basin, circulation around and east of the Grand Banks, the shelf, slope, and Gulf Stream region north and east of Cape Hatteras.

Figure 4.9a shows a map of the correlation between the Taylor index and each gridded SSH point for a time period going from 1993 to 2013, at zero lag. The highest positive correlation (r=0.85, significant at 99% levels) between the Taylor index and the gridded AVISO SSH is along the general mean path of the GS (black line in Fig. 4.9). This is expected, as at 0 lag, variability of sea level anomaly along the mean path of the Gulf Stream is the variability of the Gulf Stream position itself, which is represented by the Taylor index. Regions of high negative correlation (r=-0.50 to -0.65, significant at 99% levels) are observed across the Labrador Sea (northeast of the Labrador province), in the west Greenland Current, and along the shelf and the slope between continent and the Gulf Stream, and Cape Hatteras and Nova Scotia. This suggests that decreases in SSH in these regions are strongly associated with northern shifts in the Gulf Stream and vice versa. The simultaneous correlations in the shelf/slope region indicate the spatial extent of the processes that lead to the displacement of the Gulf Stream. The associated p-values suggest these correlations are statistically significant at 99% levels (Fig. 4.9b).

The overall strength of the correlations decreases when the Taylor index lags the SSH anomalies by a year (Fig. 4.9c). The dominant features in the 1-year lag correlation are the high

Correlation between the AVISO SSH and the Taylor Index

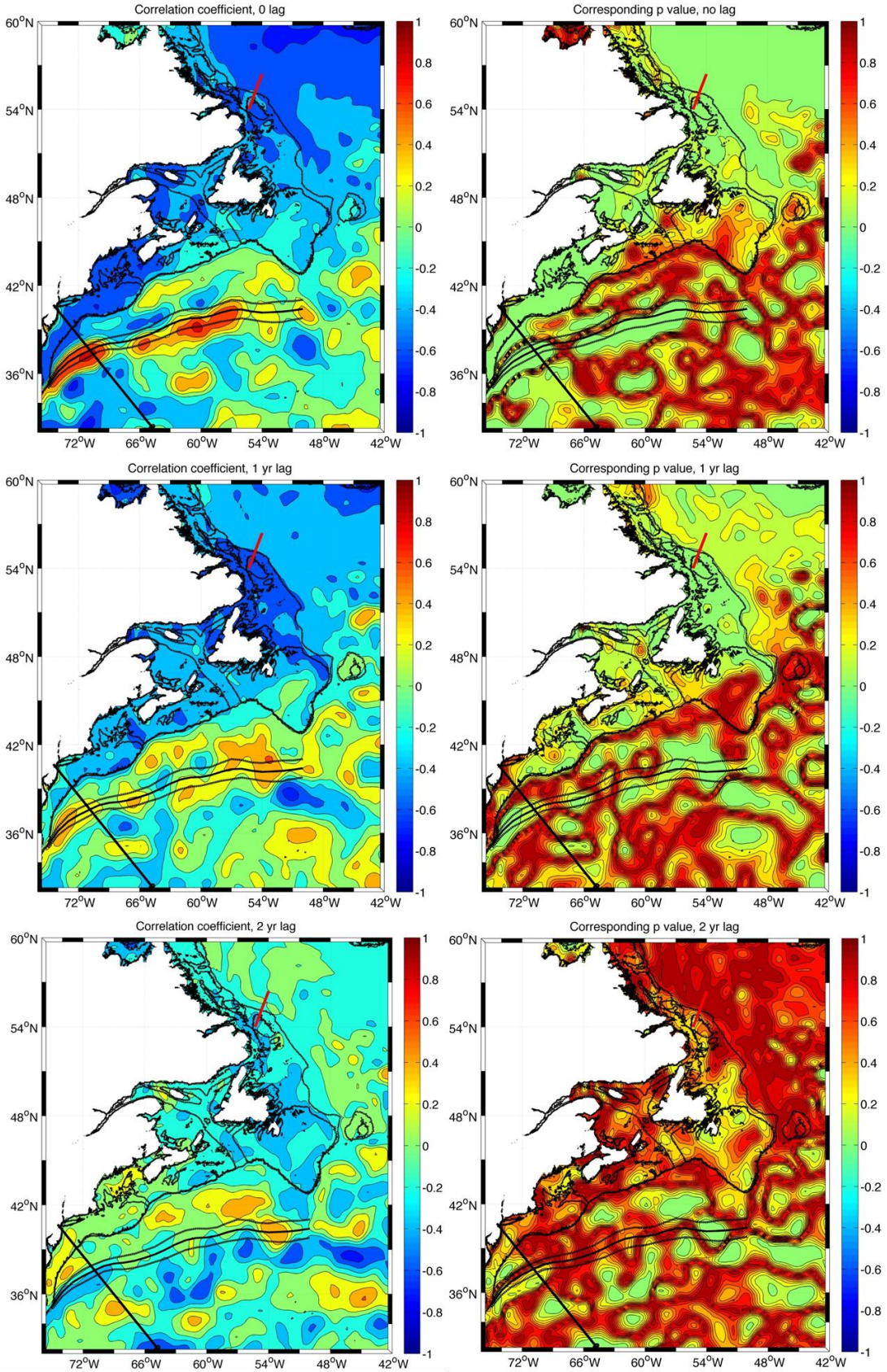

Figure 4.9: Correlation coefficient and p-value maps for the correlation between AVISO SSH over the northwestern North Atlantic and the Taylor index for a 0 year lag (a, b), a 1 year lag (c, d), and a 2 year lag (e, f). AVISO SSH is always the leading variable. Dashed black lines indicate bathymetry at 200 and 500 m. The long, black line represents the Oleander track, and the short red line is the location of the ERS-2/ENVISAT 250 pass. The elongated, undulating black line tracks the mean Gulf Stream Northwall position from MEDS data, and the adjacent black, dashed lines are the associated standard deviation for the Stream's mean position. The MEDS mean Gulf Stream position is estimated from SST anomalies at every degree longitude between 75° W and 50° W.

negative correlation north of Newfoundland and Labrador (r=~-0.50, significant at 95% levels), indicating that decreased SSH in this region precedes a northern shift in Gulf Stream position 1 year later, and vice versa. Statistically significant positive correlations (r=0.45 to 0.54, significant at 95% levels) are found north of the Gulf Stream's mean path, suggesting positive SSH anomalies in this area are followed by a northward shift in Gulf Stream position, and vice versa, 1 year later. The difference in negative correlations along shelf, and the positive correlations in the Slope Sea and north of the Stream's path point to the Gulf Stream position's link to the Slope Sea's spin up/down, i.e. the gyre spins up, and the Gulf Stream shifts north a year later, and vice versa. P-values indicate correlations discussed are statistically significant at 95% levels (Fig. 4.9d).

Finally, the mapped correlation between (leading) AVISO SSH and the 2-year lagged Taylor index shows an overall decrease in the gridded correlation coefficients (Fig. 4.9e). Negative correlations (r=-0.30, significant at 85% levels) are apparent in the region of the Grand Banks, and along (and just south) of the mean path of the Gulf Stream. The latter negative correlation likely indicates that the Gulf Stream shifts south 2 years after it has shifted north, and vice versa. Positive correlations (r=0.42 to 0.53, significant for at least 90% levels) along the shelf and slope suggest high SSH anomalies are followed two years later by Gulf Stream shifts north, and vice versa. The most noteworthy feature is the low correlation coefficient values along

the ERS-2/ENVISAT 250 pass. As both AVISO SSH and the RADS ERS-2/ENVISAT time series are constructed from almost the same satellite data, high negative correlations (r=-0.68, significant at 95% level) as observed in Fig. 4.8 should be apparent in the vicinity of the 250 pass, where the Taylor index lags 2 years behind the SSH data (Fig. 4.9e). However, the correlations in the locality of the 250 pass are at best of r=-0.25 (not statistically significant). These results suggest the Gulf Stream position has a statistically significant relationship with the fluctuation in SSH *difference* between the 250 pass endpoints (i.e. Labrador Current cross-current endpoints), and not just (or not necessarily) SSH fluctuations at a single grid point.

4.4 Discussion

The combination of direct velocity measurement with altimetry enables us to address the connection between the Labrador Current, the Slope Sea, and Gulf Stream position. The measurements used include accurate estimates of upper ocean transport and altimetry to examine their space-time characteristics. In particular we show not only that the lateral shifting of the Gulf Stream is associated with time-varying flows, but also give a breakdown of how these signals propagate along the continent from the Labrador Sea to Cape Hatteras.

In the first part of this study, the Slope Sea's velocity structure, transport and T/S signature are investigated with the purpose of explaining the Slope Sea's basic framework and to illustrate how the Slope Sea and the Gulf Stream's position are interconnected. The mean structure of the Slope Sea's velocity profile depicts southwest flow as the dominant signal in this region (Fig. 4.2), in agreement with *Flagg et al.'s* [2006] results. The mean southwest flow intensifies onshore, nearer to the shelfbreak, in the form of a subsurface jet. Temperatures associated with the southwest current range from 11°C to 14°C.

Interannual fluctuations in the Slope Sea transport show very marked increases from 1993 to 1996, followed by a rapid decrease (Fig. 4.3). The prevailing event in the transport time series was the low of -0.009 Sv m^{-1} in 2002. The remaining time period saw increases in transport to the southwest, with fluctuations between -0.025 and -0.014 Sv m^{-1}. Slope Sea T/S was generally in phase and presented interannual fluctuations similar to those of the Slope Sea transport and Gulf Stream position (Fig. 4.5). In particular, two large-scale fluctuations are present in all 4 of the time series, taking slight lags among the variables into account. The first event was the peak in the late 90s (1997 for the Slope Sea transport and 1999 for the Gulf Stream position – for this event Slope Sea transport leads Gulf Stream position). During this time the Slope Sea transport experienced significant increases in southwest flow at the same time the averaged Slope Sea T/S became cooler (~12.5°C) and fresher (~33.9 psu). Shortly after, the Gulf Stream migrated south to a latitude of 37.3°N. The highs/lows of 1997 are coincident with an abnormally strong El Nino event [*Fedorov and Philander*, 2000] and the anomalously negative NAO of 1996 [*Greene and Pershing*, 2003]. The second event followed the first almost immediately, occurring in 2001-2002. The Slope Sea transport showed a noticeable decrease in southwest transport, coincident with warmer waters for the same region. This was preceded by a dramatic shift north in the Gulf Stream's position; for this event, the warm Slope Sea anomalies, record low transport, and northern Gulf Stream position concur/follow a strong positive NAO phase [*Pershing et al.*, 2001].

Next, the MDT and surface geostrophic velocity fields in the northwestern North Atlantic were examined to give a wider geographical context to the Gulf Stream's low frequency variability and to search for a connection with the Labrador Current. The MDT and velocity field for the region chosen highlighted Gulf Stream and subpolar gyre dynamics (Fig. 4.6). Further,

the surface geostrophic velocity field gave insight into optimal regions for sampling Labrador Current transport. Based on Figure 4.6b, an along track pass between 54° N and 56.5° N was chosen to obtain Labrador Current estimates. The resulting LC index proved highly correlated (r=-0.68, significant at 95% level) with a zonally averaged index of Gulf Stream position, taking a 2-year lag into account where the LC index was the leading variable (Fig. 4.8). In general, increases in Labrador Current transport are followed 2 years later by southward shifts in Gulf Stream position, and vice versa. The time period for the lag is consistent with studies showing NAO phase reversals lead Gulf Stream with a 2 year lag [*Taylor et al.*, 1998; *Taylor and Stephens*, 1998], and the Labrador Current at 0 lag [*Han et al.*, 2010], meaning the 2 year time lapse lies between the Labrador Sea and the Gulf Stream east of Cape Hatteras, as observed here.

Further insight into the dynamics/linking processes originating in the Labrador Sea, traveling equatorward along the shelf and in the Slope Sea, and affecting Gulf Stream position were explored using mapped correlations between AVISO SSH and the Taylor index, for 0 to 2 year lags. For 0 lag correlation between the Taylor index and SSH between 1993-2013, high positive correlations (r=0.85, significant at 99% levels) were found along the mean track of Gulf Stream position (Fig. 4.9a). These correlations are the SSH tracking the Gulf Stream's low frequency variability. High negative correlations (r=-0.50 to -0.65, significant at 99% levels) were predominant across the Labrador Sea, and along the shelf and the Slope Sea. Negative correlations in the Slope Sea suggest that as SSH increases in this region, the Gulf Stream shifts south, and vice versa. If increases in SSH in the Slope Sea region are incoming from the Labrador Current variability, then the Slope Sea is shown to be a key link between the Labrador Current and Gulf Stream position variability. The fact that changes in the Slope Sea and the Gulf

Stream occur simultaneously (at 0 lag) is not unreasonable due to the yearly averages and considering the proximity of the water masses.

The correlation between the Taylor index and the SSH, with a SSH leading by 1 year showed negative correlation (r=~-0.50, significant at 95% levels) north of Newfoundland and Labrador (Fig. 4.9c). This correlation could be indicative of increased convection in the Labrador Sea, which would result in the water column compressing The newly formed convected waters are known to flow preferentially southeast [*Bersch et al.*, 2007], leading to a decrease in waters flowing southwest, allowing for the Gulf Stream to shift north a year later.

Last, the correlation between the SSH and the Taylor index lagging behind by 2 years showed a general decrease in correlations all over the chosen region (Fig. 4.9e). Particularly surprising was the lack of a statistically significant correlation in the region marked by the ERS-2/ENVISAT 250 pass. We posit the reason the along-track 250 pass has a high correlation with the Taylor index, where the gridded AVISO SSH does not is that the Gulf Stream position must be correlated with the SSH difference across the Labrador Current, and not just the simple fluctuation of SSH at a single point. If this is the case, the correlation maps are a useful tool for linking processes in adjacent circulation fields, but might not a definitive measure for or against variability in the Labrador Current being linked to Gulf Stream position.

4.5 Concluding remarks

Variability in the Slope Sea and position of the Gulf Stream are important for regional climate as the Gulf Stream is an important source of heat transport from low to high latitudes. Thus far the relationship between the Labrador Current, the Slope Sea, and Gulf Stream position has been investigated and a significant link has been established between them.

Based on the statistically significant results shown here, we offer the following scheme on the impact of the Slope Sea and the Labrador Current on the Gulf Stream's interannual migration east of Cape Hatteras (Fig. 4.10). For Slope Sea/Gulf Stream circulation, Slope Sea transport is shown to follow changes in Gulf Stream position, where Gulf Stream southward displacement leads Slope Sea transport increases, and Slope Sea temperature (cool) anomalies follow changes in (increased southwest) Slope Sea transport. Though findings offered here suggest that direction of the lead-lag relationship is statistically significant, it is important to stress that they are only valid for this particular time period and may not be representative of the Gulf Stream/Slope Sea system as a whole (i.e. on longer time scales). Further, correlation between Gulf Stream position and Labrador Current transport showed Gulf Stream position follows Labrador Current transport off mainland Labrador region, where Labrador Current transport increase (decreases) lead to southward (northern) shifts in Gulf Stream position. This relationship is in keeping with the buoyancy-driven hypothesis, where increases in equatorward transport off the Labrador coast lead to southward shifts in Gulf Stream position.

Some discrepancies among datasets suggest longer observational data and further analyses are needed to resolve the mechanisms affecting the Gulf Stream's interannual migration and establish the connection between interannual variations at these three regions.

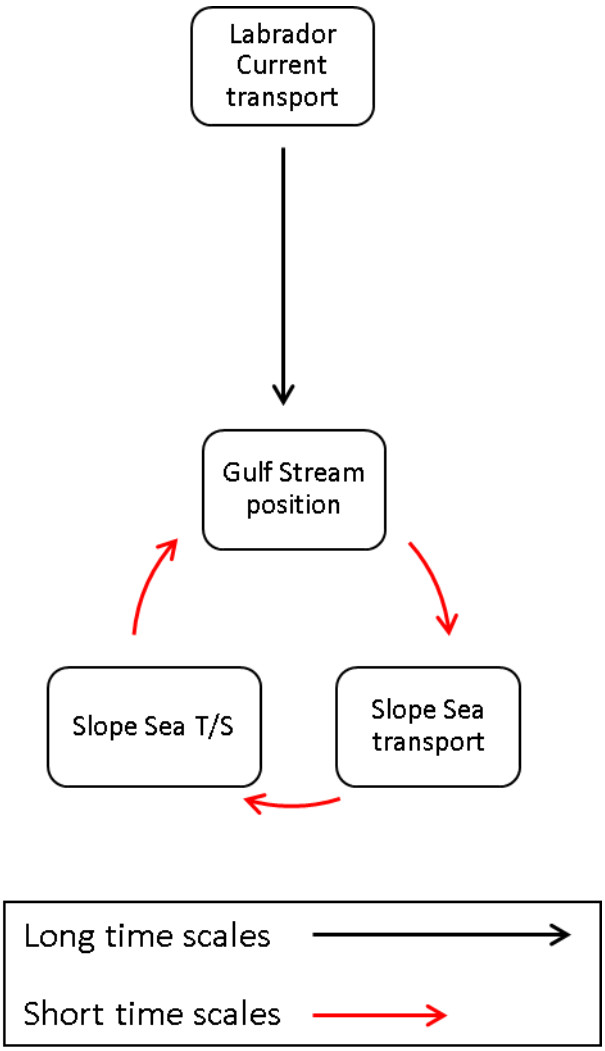

Figure 4.10: Suggested circulation scheme for the effect of the Slope Sea and the Labrador Current on the Gulf Stream's interannual migration east of Cape Hatteras.

Chapter 5

Impact of the AMOC fingerprint on the decadal variability of the Gulf Stream path and regional chlorophyll and nutrient concentrations

Abstract

In this study, we show that the underlying physical driver for the decadal variability in the Gulf Stream (GS) path and the regional biogeochemical cycling is linked to the low frequency variability in the Atlantic meridional overturning circulation (AMOC). The results suggest that the coherence between AMOC variations and the anti-correlated shifts of the GS path are much higher at decadal time scale than that at inter-annual time scale in both observations and modeling results, and the chlorophyll and nutrient concentrations in the GS region are strongly correlated with AMOC and anti-correlated with the GS path at decadal time scale in two Earth system models. Our results illustrate how changes in large-scale ocean circulation, such as AMOC, are teleconnected with regional decadal physical and biogeochemical variations near the North American east coast. Such linkages are useful for predicting future physical and biogeochemical variations in this region.

5.1 Introduction

The Gulf Stream (GS) is an important component of the Atlantic meridional overturning circulation (AMOC) transporting warm salty water from the subtropical region to mid-latitudes. The GS is found to have climate influence on the entire troposphere [*Minobe et al.*, 2008]. Changes in the GS path can also induce changes in winter synoptic atmospheric variability [*Joyce et al.*, 2009] and are highly correlated with changes in spatial distribution of silver hake over the last 40 years [*Nye et al.*, 2011]. The inter-annual migration of the GS path has been linked to the winter North Atlantic Oscillation (NAO) [*De Coetlogon et al.*, 2006; *Frankignoul et al.*, 2001; *Joyce et al.*, 2000; *Taylor and Stephens*, 1998], where a positive (negative) winter NAO leads to a northward (southward) displacement in the GS path. Meanwhile, *Thompson and Schmitz* [1989] suggest that near Cape Hatteras the deep western boundary current (DWBC) at depth advects the GS southward, and *Spall* [1996] found that the GS position near Cape Hatteras is affected by the entrainment of the upper DWBC. The meridional shift of the GS path in the open ocean, as well as the strength of the cyclonic northern recirculation gyre (NRG) north of the GS are found to be linked to the strength of the deep branch of AMOC through the interaction with bottom topography and associated bottom vortex stretching, in both high resolution and coarse resolution GFDL models [*Zhang et al.*, 2011; *Zhang and Vallis*, 2007]. Similar results are also found in the NCAR ocean general circulation model [*Yeager and Jochum*, 2009]. These modeling results are supported by observations that the GS path is significantly anti-correlated with the AMOC fingerprint [*Joyce and Zhang*, 2010].

In this study, we revisit the linkage between the migration of the GS path and the AMOC variability at decadal time scale, using both observed data and a 1000-year segment of the control simulation from a widely used climate model (GFDL CM2.1). The results suggest that

the coherence between AMOC variations and the anti-correlated shifts of the GS path are much higher at decadal time scale than that at inter-annual time scale. If the AMOC variability is a prime driver for the meridional migrations of the GS path at decadal time scale, it may also affect the decadal variability of the biogeochemical cycle in the GS region. Hence we further investigate the impact of AMOC variability on the marine biogeochemical cycle in the GS region using the control simulations from two Earth system models (GFDL ESM2M and ESM2G).

Regionally, chlorophyll concentrations are found highest in the area between the GS and the Grand Banks whenever the GS path is in a southerly position [*Brown et al.*, 1985]. It is generally believed that the increase in chlorophyll concentration in the northern NRG during the GS's southward displacement is linked to the increase of nutrient-rich Labrador Sea water in the Slope Sea [*Yoder et al.*, 2002]. Other studies have suggested that the nutrient supply along (and north of) the western boundary current is actually caused by the along-isopycnal nutrient advection in the GS [*Jenkins and Doney*, 2003; *Pelegri and Csanady*, 1991; *Schollaert et al.*, 2003]. *Csanady* [1990] found that the nutrient supply advected by the GS isopycnals originates from the nutrient rich subsurface-waters in the western Sargasso Sea (the 'nutrient stream' under the GS's core velocity). This is consistent with *Kremeur et al*. [2009] investigation on the dynamics of biogeochemical cycle variability related to Subtropical Mode Water, where nutrient distribution and primary production were largely dependent on the advection through gyre circulation. Satellite observations reveal anti-correlated relationship between sea surface temperature (SST) and chlorophyll concentrations in world oceans, and warmer SSTs are proposed as indicators for increased stratification in the upper ocean which can prevent nutrients from upwelling into the euphotic zone and lead to the reduction of phytoplankton biomass [*Behrenfeld et al.*, 2006; *Martinez et al.*, 2009]. In regions with abundant light, increased

(decreased) vertical mixing can bring more (fewer) nutrients to the phytoplankton population and enhance (reduce) the phytoplankton bloom [*Doney,* 2006; *Follows and Dutkiewicz,* 2002]. In addition to changes in SSTs, vertical mixing and phytoplankton biomass can also be strongly impacted by changes in wind and buoyancy forcing [*Lozier et al.*, 2011].

In this study using two Earth system models (ESMs) with different oceanic physical components (z-coordinate in ESM2M and isopycnal-coordinate in ESM2G), we found that the chlorophyll and nutrient (phosphate) concentrations in the GS region are strongly correlated with the AMOC fingerprint and anti-correlated with the GS path at decadal time scale. Our results from the two ESMs suggest that physical processes rather than biogeochemical processes (remineralization) are the primary driving mechanism for the simulated decadal biogeochemical variability in the GS region. In particular, we found that nutrient reservoirs in the GS region move along with the steepened isopycnals in the GS front induced by the enhanced AMOC, resulting in increased nutrient along the GS path as well as north of it. Meanwhile the chlorophyll concentrations are increased north of the GS path mainly due to enhanced upwelling there induced by the enhanced AMOC. Such AMOC induced decadal variability in chlorophyll and nutrient concentration is important for changes in carbon cycle and fisheries at decadal time scale in the GS region.

5.2 Data and Methods

The linkage between AMOC variability and the migration of the GS path at decadal time scale is investigated using both observed and modeled results. The observations are derived from the objectively analyzed datasets of ocean temperature anomalies from 1955 to 2013 [*Levitus et al.*, 2005], and the model results are derived from a 1000-year segment of the control simulation from GFDL CM2.1 [*Delworth and al*, 2006].

A classic measure for the GS path is the 15°C isotherm at 200 m characterization [*Cornillon and Watts*, 1987; *Fuglister and Voorhis*, 1965]. Here, for both simulated and observed results, estimates for the position of the GS path are obtained from the averaged locations of the annual mean 15°C isotherm between 75°W – 55°W, similar to the approaches used in previous studies[*Joyce et al.*, 2009; *Joyce and Zhang*, 2010]. The linear trend of the observed position of the GS path over the entire period (1955-2013) is removed to compare it with the results from the GFDL CM2.1 control simulation. For AMOC estimates, because there were no continuous observations of AMOC before the RAPID program started in 2004 [*Cunningham et al.*, 2007], AMOC fingerprints are used to construct past AMOC variations as suggested in previous studies [*Mahajan et al.*, 2011; *Zhang*, 2008]. One extra-tropical AMOC fingerprint is the leading mode of the annual mean ocean subsurface temperature at 400 meter (or upper ocean heat content) in extra-tropical North Atlantic, which shows a dipole spatial pattern of opposite signs in the subpolar North Atlantic and in the GS region. A positive AMOC fingerprint corresponds to warming in the subpolar gyre and cooling in the GS region (Fig. 1b, d in Zhang 2008]. The principal component of this leading mode (PC1) is highly correlated with the volume transport-derived AMOC index [*Zhang*, 2008]. In this study, this AMOC fingerprint is used for both observed and simulated results. When deriving the AMOC fingerprint, the linear trend of the observed ocean subsurface temperature over the entire period (1955-2013) is removed before taking the empirical orthogonal function (EOF) analysis, to compare with the results from GFDL CM2.1 control simulation. For reference, volume transport-derived AMOC index and the AMOC fingerprint, both with 5-year running smooth, have a correlation of 0.80 in the 1000-year segment of GFDL CM2.1 control simulation, statistically significant at 99% level.

To further investigate the impact of AMOC variability on marine biogeochemical cycle in the GS region, the 500-year control simulations from two Earth system models (GFDL ESM2M and ESM2G) [*Dunne et al.*, 2012; *Dunne et al.*, 2013] is used. The main differences between the two Earth system models are the vertical coordinates in the ocean components; ESM2M employs z-coordinate, while ESM2G employs isopycnal-coordinate. The index for the biogeochemical variables in the GS region are derived using EOF analysis over the subdomain, 80°W-50°W and 35°N to 45°N. The chlorophyll index in the euphotic zone is defined as the leading principal component (PC1) of the annual mean chlorophyll concentration at 35 m depth over the subdomain. Correspondingly, the nutrient index at the base of the euphotic zone is defined as the leading principal components of the annual mean phosphate (PO_4) concentrations at 150 m depth over the subdomain. The GS path and AMOC fingerprint are also derived from the two ESMs using the same approaches discussed above for comparison with the biogeochemical variables.

To focus on the variability at decadal time scale, all indexes (both physical and biogeochemical variables) in this study are smoothed with a 5-year running mean unless otherwise specified. The statistical significance levels of the correlations discussed in the paper are calculated with the 2-tailed Student t-test with the effective degree of freedom derived from the decorrelation time scale.

5.3 Results

5.3.1 Decadal variability of observed and modeled GS path and AMOC fingerprint

The observed GS path and AMOC fingerprint shows anti-correlated variations at the decadal time scale (Fig. 5.1a, r = -0.82 at zero lag, smoothed with a 5-year running mean, significant at

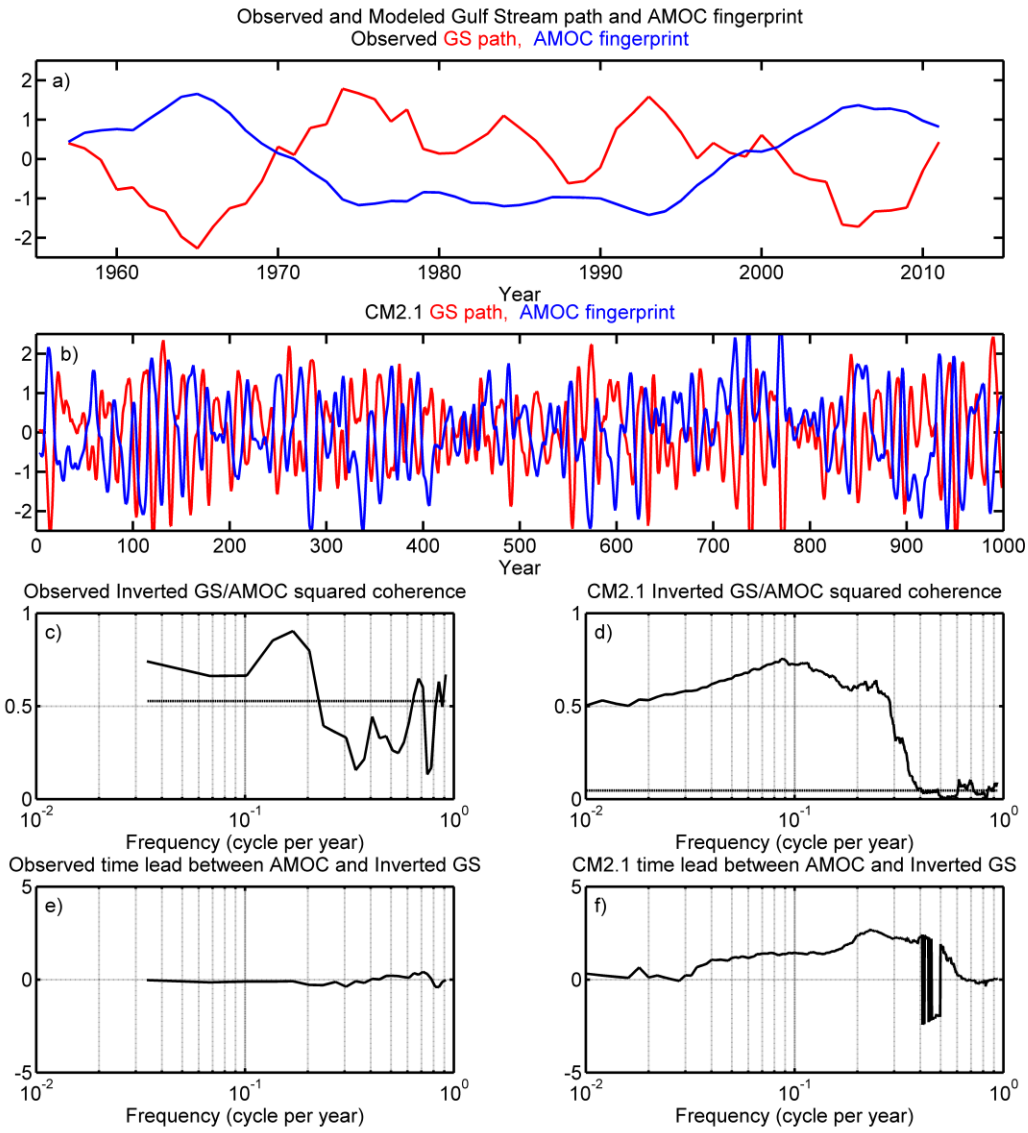

Figure 5.1: Observed and simulated time series and squared coherences of the GS path and AMOC fingerprint. (a) Observed and (b) CM2.1 simulated GS path (red line) and AMOC fingerprint (blue line). Both variables are filtered with a 5 year running mean and normalized by their standard deviations. (c) Observed and (d) CM2.1 simulated squared coherence between the unfiltered inverted GS path and AMOC fingerprint, (e, f). Corresponding time lag between these unfiltered variables for the observed and CM2.1 simulated results.

99% level). The observed AMOC fingerprint exhibits two strengthening periods, one from 1955 to 1965 and the other from ~1993 to 2005. The strengthening of AMOC is coincident with the

southerly shifting in the GS path. Similarly, for the two periods of AMOC weakening from 1965 to 1974 and from 2005 to present, the GS path is seen shifting northwards. The weakening of AMOC since 2005 indicated by its fingerprint (Fig. 5.1a) is consistent with the recent direct observational studies [*Robson et al.*, 2014; *Smeed et al.*, 2014] and the statistical prediction using the AMOC fingerprint [*Mahajan et al.*, 2011]. Meanwhile the northward shift of the GS path since 2005 is opposite to what is expected from the declining winter NAO index over this period, thus is not induced by changes in the NAO since 2005. Because the 5-year running mean smooth provides less degrees of freedom for the limited observed time series, the squared coherence between the unsmoothed observed inverted GS path and AMOC fingerprint is also examined. There is significant high (95% level) squared coherence between the observed inverted GS path and AMOC fingerprint at near-decadal time scale, meanwhile the coherence is much lower at inter-annual time scale shorter than 5 years (Fig. 5.1c). These findings are consistent with that found in the *Joyce and Zhang* [2010] study using unfiltered data, and here the anti-correlation between the observed GS path and AMOC fingerprint is much higher at decadal time scale.

Analogous to the observed results, the GS path and the AMOC fingerprint in the GFDL CM2.1 control simulation show similar anti-correlated variability at decadal time scale (Fig. 5.1b). Their anti-correlation coefficient is r = -0.79 smoothed with a 5-year running mean, significant at 95% level, when the enhanced (weakened) AMOC is leading southward (northward) GS path by ~2 years. The squared coherence between simulated inverted GS path and AMOC fingerprint at decadal time scale is significantly high, 0.72, at 95% levels, and again much lower at inter-annual time scale (Fig. 5.1d). A closer inspection of the cross spectra also indicates the unfiltered AMOC fingerprint leads the inverted GS path by ~2 years. This 2-year time lead is due to the model bias in GFDL CM2.1 and not the observational data (Fig. 5.1e).

The GS region temperature anomaly in the simulated AMOC fingerprint is located too further east (near 50^{o}W) than that observed (near 75^{o}W) [*Zhang*, 2008], and it takes a few years for this simulated temperature anomaly to propagate westward from east of 50^{o}W to 75^{o}W. On the other hand, both modeled and observed GS path mainly reflect the averaged temperature anomalies between 75°W – 55°W, thus the inverted GS path lags the AMOC fingerprint by ~2 years in the model, while the inverted GS path is in phase with the AMOC fingerprint in the observation. As discussed in previous studies [*Zhang*, 2008; *Zhang et al.*, 2011; *Zhang and Vallis*, 2007], a stronger (weaker) AMOC is associated with a stronger (weaker) North Atlantic deep flow, which interacts with the steep bottom topography near the North American east coast, and induces positive (negative) vorticity through bottom vortex stretching effects, resulting in a strengthening (weakening) of the cyclonic NRG and a southward (northward) shift of the GS path.

5.3.2 Decadal variability of chlorophyll and nutrient concentrations in the GS region

In this section the impact of AMOC variability on the chlorophyll and nutrient concentrations in the GS region is analyzed using the 500-year control simulations from two Earth system models (GFDL ESM2M and ESM2G). For consistency, the GS path and the AMOC fingerprint are derived from the two Earth system models (ESMs) in the same way as they are from the observations and the GFDL CM2.1 controlled simulation.

In ESM2M, the chlorophyll index in the GS region (PC1 of annual mean chlorophyll concentration over the subdomain in the euphotic zone at 35 m) is anti-correlated with the GS path at zero lag (r = -0.93 smoothed with a 5-year running mean, significant at 95% level), and the nutrient (PO_4) index in the GS region (PC1 of annual mean PO4 concentration over the subdomain at the base of the euphotic zone at 150 m) is also anti-correlated with the GS path at

zero lag (r = -0.97, smoothed with a 5-year running mean, significant at 95% level) (Fig. 5.2a, e). The AMOC fingerprint is positively correlated with both the chlorophyll index and the nutrient index with 2-year lead (r = 0.81, 0.81 respectively, smoothed with a 5-year running mean, both significant at 95% levels) (Fig. 5.2c, e).

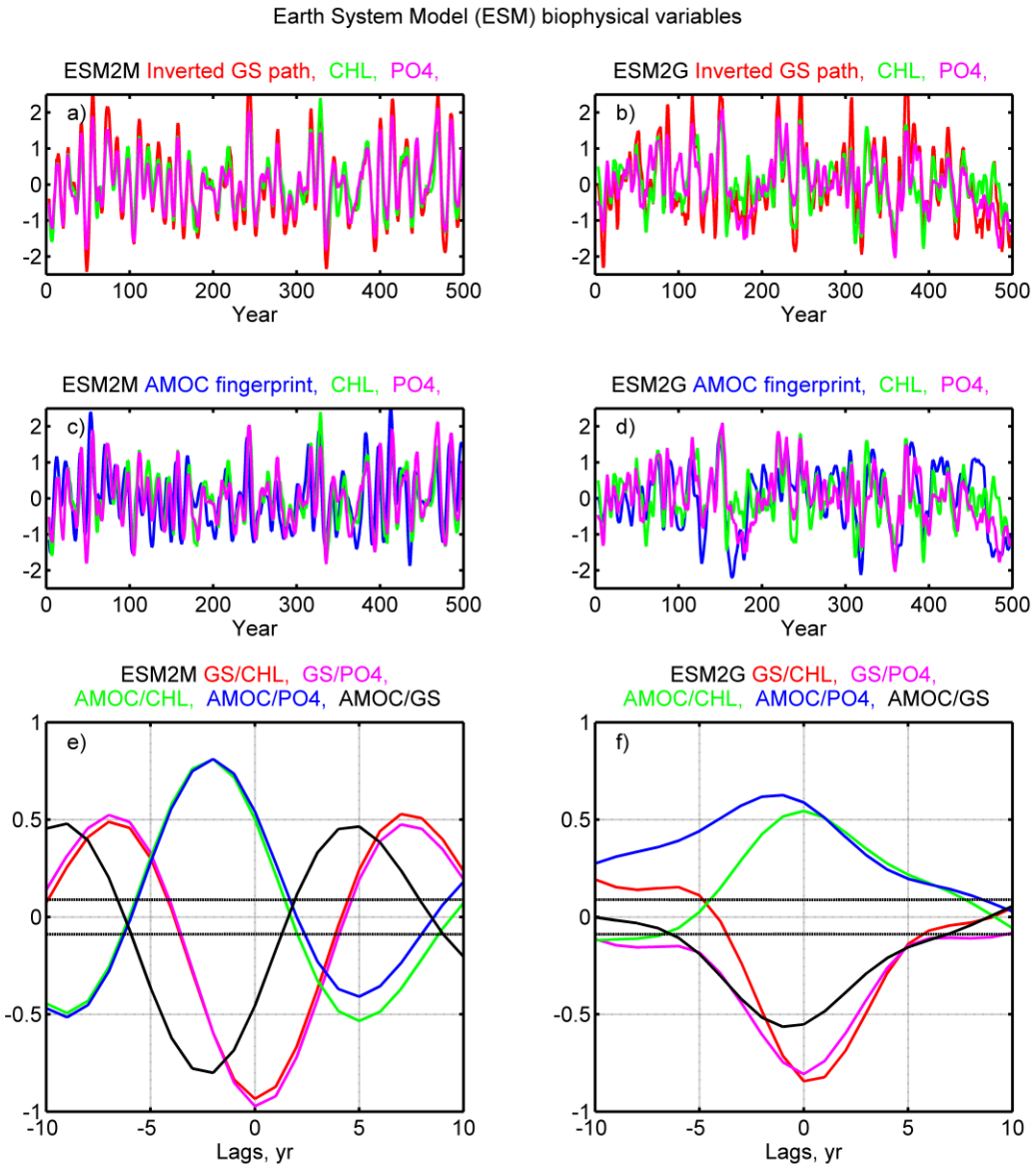

Figure 5.2: Simulated physical and biogeochemical variables from two ESMs (Left column - ESM2M, and right column - ESM2G). (a,b,c,d) Inverted GS path (red line), AMOC fingerprint

(blue line), chlorophyll index (green line), and PO_4 index (purple line). A 5 year running mean is applied and all variables are normalized by their standard deviations.

There are two regions of positive anomalies in the leading mode of chlorophyll concentrations in the subdomain (Fig. 5.3a). The first (and largest) is just south of the Scotian shelf, extending zonally from Georges Bank to the New England Seamounts. The second region stretches just south of the GS path, between 65°W and 55°W (Fig. 5.3a). The leading mode of nutrient (PO_4) concentrations in the subdomain exhibits highest anomalies along the GS path, especially in the region between 70°W and 55°W (Fig. 5.4a). Fig. 5.2a, c suggests that these increases in chlorophyll and nutrient (PO_4) concentrations in the GS region occur when the GS path is shifted southward, and lag the positive AMOC fingerprint by ~ 2 years, and vice versa. In

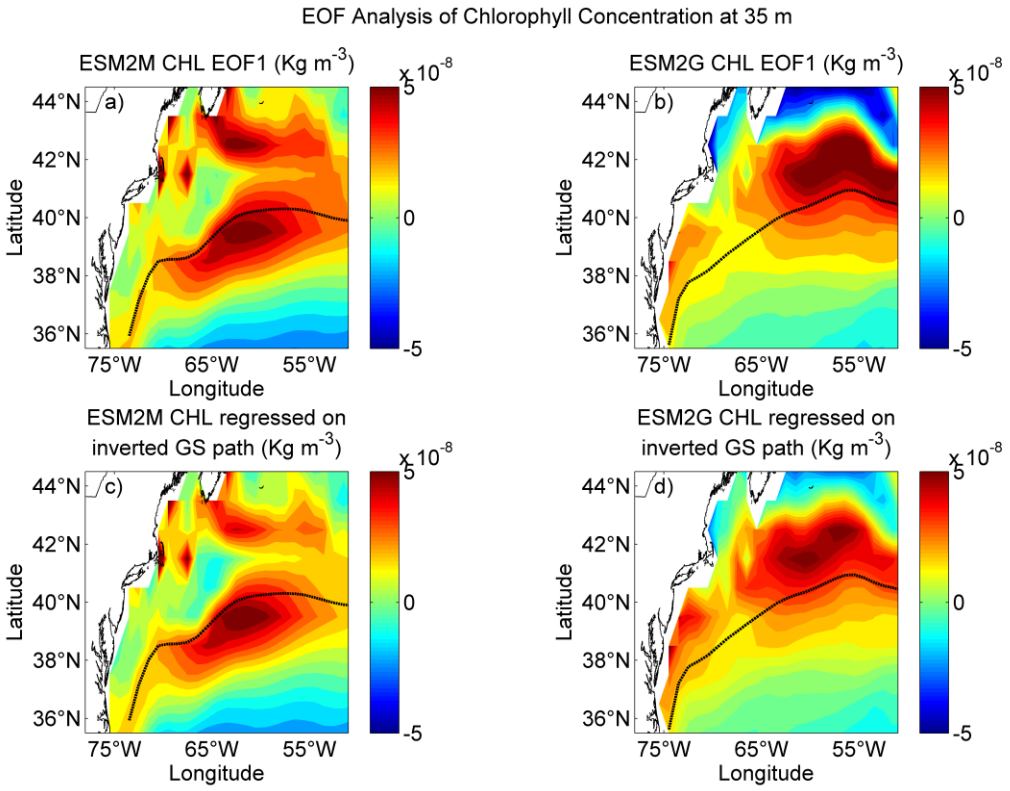

Figure 5.3: Spatial pattern of variability in chlorophyll concentrations. (a) ESM2M and (b) ESM2G leading mode, EOF1, of the annually mean chlorophyll concentrations (Kg m^{-3}) at 35 m. (c) ESM2M and (d) ESM2G annually mean chlorophyll concentrations at 35 m regressed onto the corresponding unfiltered, inverted GS path. The black lines indicate the location of the climatological mean GS path in ESM2M and ESM2G respectively.

ESM2M, the GS path is anti-correlated with the AMOC fingerprint with 2-year lag (r = -0.8, smoothed with a 5-year running mean, significant at 99% level) at decadal time scale, similar to that found in GFDL CM2.1 and in observations.

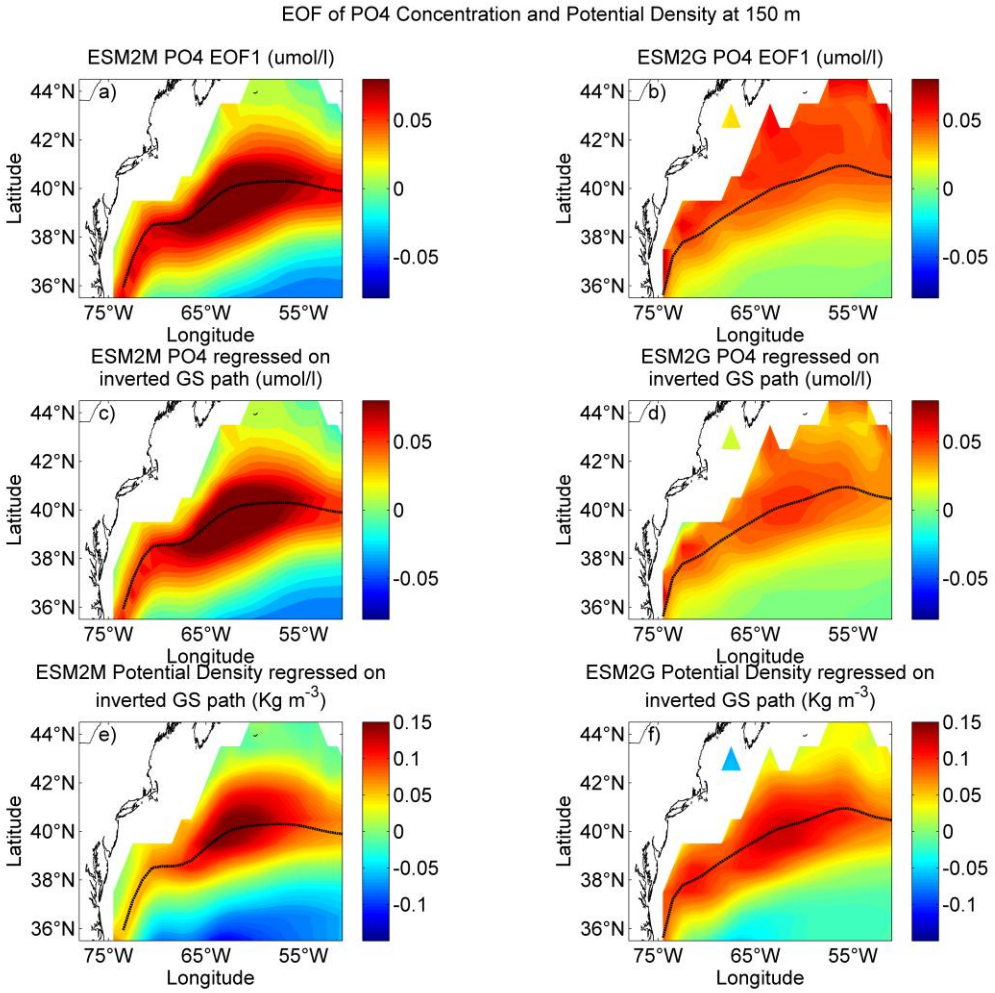

Figure 5.4: Spatial pattern of variability in PO_4 concentrations and potential density. (a) ESM2M and (b) ESM2G leading mode, EOF1, of the annually mean PO_4 concentrations (µmol/l) at 150 m. (c) ESM2M and (d) ESM2G annually mean PO_4 concentrations at 150 m regressed onto the corresponding unfiltered, inverted GS path. (e) ESM2M and (f) ESM2G annually mean potential

density (Kg m^{-3}) at 150 m regressed onto the corresponding unfiltered, inverted GS path. The black lines indicate the location of the climatological mean GS path in ESM2M and ESM2G respectively.

In ESM2G, the GS path, AMOC fingerprint, chlorophyll and nutrient (PO4) indexes show comparable decadal to multi-decadal variations (Fig. 5.2b, d), similar to ESM2M results. In particular, the GS path is anti-correlated with the chlorophyll index and the nutrient (PO_4) index at zero lag, (r = -0.84, -0.80 respectively, smoothed with a 5-year running mean, both significant at 95% levels). Meanwhile, the AMOC fingerprint is positively correlated with the chlorophyll index at zero lag (r = 0.54, smoothed with a 5-year running mean, significant at 95% level) and positively correlated with the nutrient (PO_4) index with 1-year lead (r = 0.62, smoothed with a 5-year running mean, significant at 95% level). In ESM2G the strongest positive anomalies in the leading mode of chlorophyll concentrations in the subdomain are mainly located north of the GS path, east of the Georges Bank region, south of the Scotian shelf (Fig. 5.3b). The leading mode of nutrient (PO_4) concentrations in the subdomain in ESM2G also shows positive anomalies along and north of the GS path (Fig. 5.4b), but have smaller amplitudes and extend further north than those in ESM2M (Fig. 5.4a). Fig. 5.2b, d suggests that these increases in chlorophyll and nutrient (PO_4) concentrations in the GS region occur when the GS path is shifted southward and the AMOC fingerprint is positive, and vice versa. In ESM2G, the GS path is anti-correlated with the AMOC fingerprint with 1-year lag (r = -0.56, smoothed with a 5-year running mean, significant at 95% level) at decadal time scale, similar to that found in GFDL CM2.1 and in observations.

5.3.3 Mechanisms for decadal variability of chlorophyll and nutrient concentrations

The region north of the GS path typically features high climatological chlorophyll concentrations associated with the spring bloom (Fig. 5.5). For both ESM2M and ESM2G, the anomalous chlorophyll concentrations regressed on the inverted GS path (Fig. 5.3c, d) exhibit very similar spatial patterns to the corresponding leading modes in chlorophyll concentrations (Fig. 5.3a, b), indicating that the variability of chlorophyll concentration in this region (near Georges Bank and along the GS path) is strongly linked to the anti-correlated variability in the GS path. The climatological mean nutrient (PO_4) concentrations increase with the latitude and depth in the GS region (Fig. 5.6, 5.7). The anomalous nutrient (PO_4) concentrations regressed on the inverted GS path (Fig. 5.4c, d) also show very similar spatial patterns as the corresponding leading modes in PO_4 concentrations (Fig. 5.4a, b), indicating the variability of the GS path dominates the variability of nutrient concentrations in the GS region.

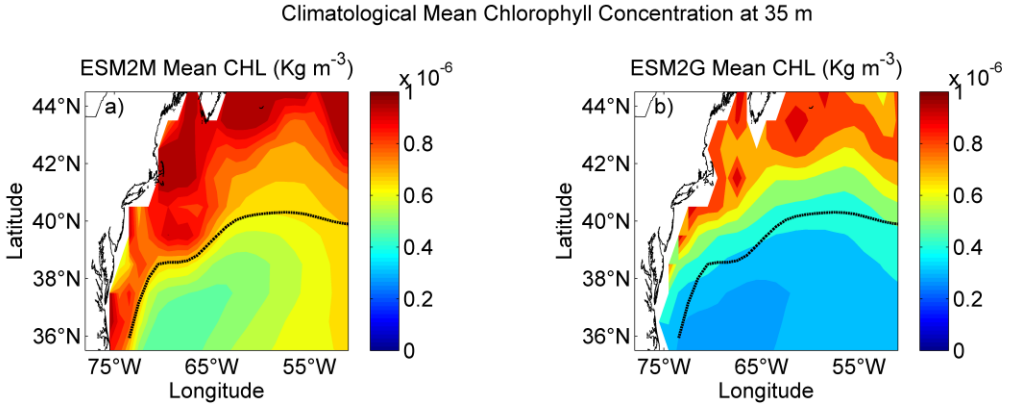

Figure 5.5: Climatological mean chlorophyll concentrations (Kg m^{-3}) at 35 m in both ESM2G and ESM2M.

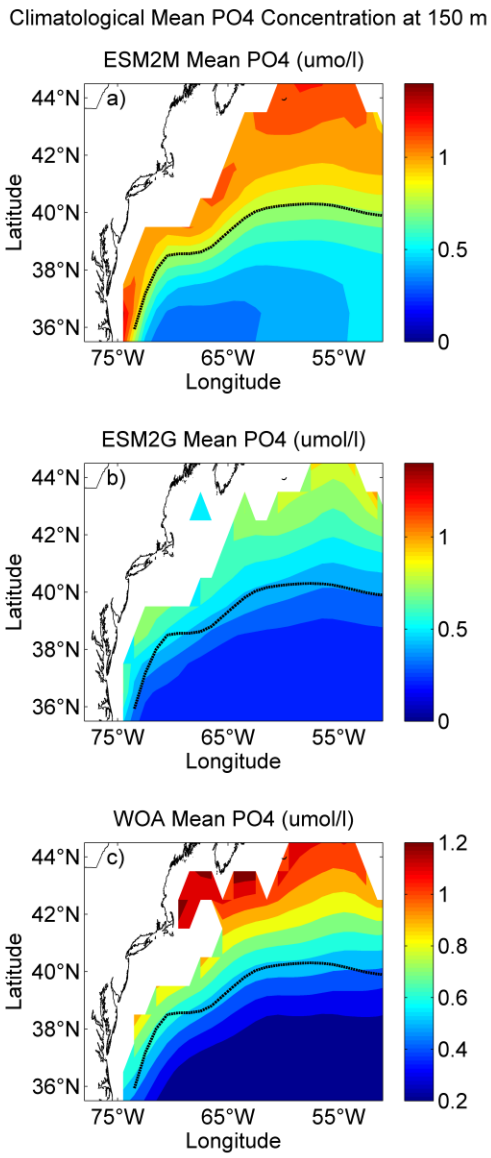

Figure 5.6: Climatological mean PO_4 concentrations (µmol/l) at 150m in ESM2M, ESM2G, and World Ocean Atlas.

Fig. 5.4 (e, f) shows the anomalous annual mean potential density at 150 m regressed on the inverted GS path in ESM2M and ESM2G respectively. The GS path-centric pattern is strikingly similar to the spatial distribution in the corresponding leading modes in nutrient

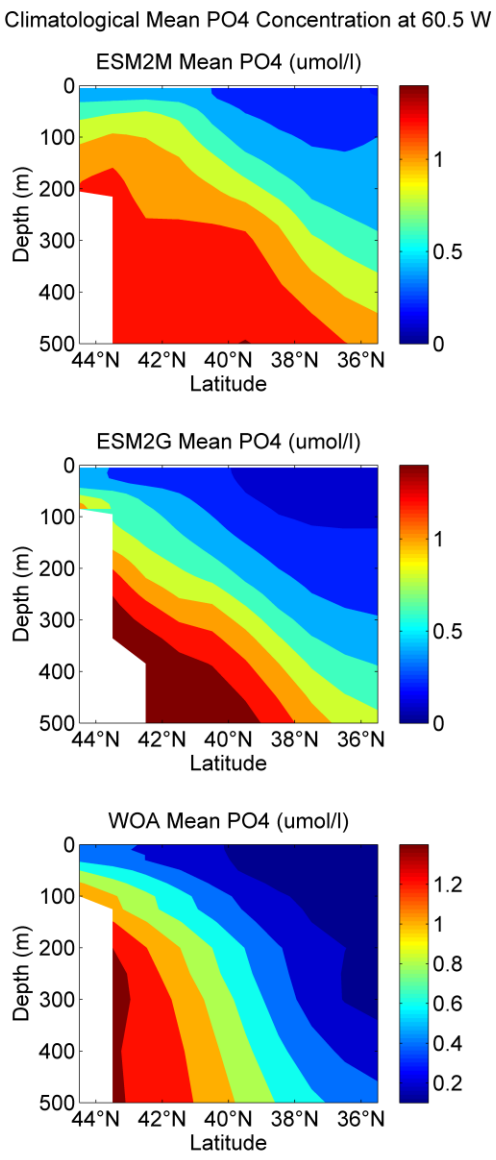

Figure 5.7: Climatological mean PO_4 concentrations (µmol/l) along the vertical section at 60.5°W in ESM2M, ESM2G, and World Ocean Atlas.

concentrations in both ESM2M and ESM2G, though it is more apparent for ESM2M than it is for ESM2G. This implies the GS path-centric pattern in the variability of nutrient concentrations is closely tied to the physical transport associated with isopycnal processes. The positive potential density anomalies at this depth (i.e. shallowing of isopycnals) are associated with

southward shifts in the GS path, and vice versa. A stronger AMOC leads to steepened isopycnal slopes in the GS front (mainly due to the strengthening of the cyclonic NRG thus cooling in the region north of the GS path), as well as a southward shift of the GS front. Hence the isopycnals are shallower and nutrient concentrations are higher along the climatological mean GS path as well as north of it, and the isopycnals are deeper and nutrient concentrations are lower in the south. Note that the amplitude of the anomalous nutrient concentrations near the GS path is smaller in ESM2G than that in ESM2M (Fig. 5.4a,b,c,d), although the two ESMs have very similar amplitudes of potential density anomalies there (Fig. 5.4e,f). This is because the climatological mean nutrient concentrations around the GS path are lower in ESM2G than that in ESM2M and in the observations (Fig. 5.6).

Both the remineralization process of organic matter and the physical transport of nutrients can influence the subsurface nutrient distribution [*Kremeur et al.*, 2009]. Here the variability of subsurface nutrient distribution is due to the physical transport in the water column, not due to the remineralization biogeochemical processes. *Levy et al.* [2009] also found that the subsurface nutrient concentrations in western North Atlantic change with the isopycnals, i.e. higher nutrient concentrations (shallowing of nutriclines) are associated with shallowing of isopycnals in the region north of the subtropical gyre and lower nutrient concentrations (deepening of nutriclines) are associated with deepening of isopycnals in the subtropical gyre as a result of the southward shift of the gyre boundary.

The enhanced nutrient in the GS region has contributed to the enhanced chlorophyll concentrations around the GS path as well as north of the GS path. The spatial patterns of anomalous chlorophyll concentrations do not match the spatial patterns for anomalous nutrient concentration exactly (Fig. 5.3, 5.4), i.e. the maximum anomalies in chlorophyll concentrations

are located both slightly further north (ESM2M and ESM2G) and slightly south (ESM2M) than the locations for maximum anomalies in nutrient concentration in both ESM2M and ESM2G. This is because stronger chlorophyll concentration variability near Georges Bank is mainly induced by stronger upwelling north of the GS path. An enhanced AMOC and associated North Atlantic deep flow leads to an enhanced NRG [*Zhang and Vallis*, 2007], thus enhanced upwelling and surface cooling in the cyclonic NRG. An increase in upwelling would lead to increased nutrient supply, consequently increasing the chlorophyll concentration for this region.

Schollaert et al. [2004] found that at inter-annual time scale, a northward shift in the GS position at the Oleander track coincides with an increase in the Slope Sea's spring bloom over the four-year period from 1997 to 2001 using satellite data. However, we found no obvious trend in the averaged GS path from 75^{o}W to 55^{o}W over this four-year period (Fig. 5.1a). Here our modeling results are focused on decadal time scale, and the currently available observed data for chlorophyll/nutrient concentrations in the GS region are too short to verify their decadal variability and the mechanisms discussed here.

5.5 Conclusions and Discussions

To summarize, results here suggest that the underlying physical driver for the decadal variability in the GS path and the regional biogeochemical cycling is linked to the low frequency variability in the AMOC. These results indicate that the coherence between AMOC variations and the anti-correlated shifts of the GS path are much higher at decadal time scale than that at inter-annual time scale in both observations and modeling results. An enhanced AMOC leads to a stronger NRG; thus cooling in the Slope Sea as well as a southward shift of the GS path, results in steepened isopycnal slopes in the GS front and stronger upwelling north of the GS path. This is concurrent with the increase in chlorophyll and nutrients in the GS region. Nutrient reservoirs in

the GS region move along with the steepened isopycnals in the GS front induced by the enhanced AMOC, hence nutrient concentrations are higher along the climatological mean GS path as well as north of it in response to the shallower isopycnals there. The enhanced nutrient in the GS region has contributed to the enhanced chlorophyll concentrations around the GS path, meanwhile the enhanced chlorophyll north of the GS path is mainly due to AMOC-induced upwelling there. These results suggest that physical processes rather than biogeochemical processes (remineralization) are the primary driving mechanism for the simulated decadal biogeochemical variability in the GS region. The impact of the AMOC and the GS path on the decadal variability of another nutrient, nitrate (NO_3), is very similar to that found for phosphate (PO_4). The analysis of the full biogeochemical cycle in the GS region is beyond the scope of this paper.

Our results have shown how changes in the basin wide ocean circulation, such as AMOC, are teleconnected with regional scale physical and biogeochemical variations near the North American eastern seaboard at decadal time scales; such connections are useful for understanding and predicting future physical and biogeochemical variations in this region. Further, AMOC induced decadal variability in chlorophyll and nutrient concentrations in the GS region could be important for changes in the localized carbon cycle and fisheries at decadal time scale.

Last, we note differences of simulated chlorophyll and nutrient concentrations in the GS region between ESM2M and ESM2G might be attributed to differences between each model's oceanic physical components. Vertical pressure coordinates are used for ESM2M, where isopycnal coordinates are used for ESM2G [*Dunne et al.*, 2012]. Nevertheless, the simulated impact of the AMOC and the anti-correlated GS path on the decadal variability in chlorophyll and nutrient concentrations in the GS region are generally consistent between the two ESMs,

suggesting the robustness of the results. Meanwhile, one should pay caution in linking GS variability and biogeochemical cycling when using models with relatively coarse resolution [*Henson et al.*, 2009]. In particular, the amplitudes of the decadal variability in chlorophyll and nutrient concentrations in the GS region might be underestimated due to the coarse resolution used in ESM2M and ESM2G ocean components. The ESMs results here need to be improved with high resolution ESMs in the future.

Chapter 6

Summary and Conclusion

When investigating large-scale ocean processes there are various merits to analyzing current flow from parameters constructed using different datasets. In this dissertation a combination of observational data and model output has been used to explore Gulf Stream dynamics and the role it plays in North Atlantic circulation.

In the first section, various measures of position and transport variability between the Gulf Stream and the Florida Current are investigated using time series analysis. Direct observations and satellite-derived data were used to track various different proxies of Gulf Stream position and found significantly correlated. The local measures of Gulf Stream path were compared with a zonally averaged Gulf Stream position index verifying the estimates are internally consistent. Finally cross-correlation analysis between the Gulf Stream position/transport measures and the Florida Current indicated the Florida Current does not have a detectable signal in the Gulf Stream east of Cape Hatteras.

Chapter 3 found the Gulf Stream's interannual migration correlated specifically to the Icelandic Low (IL; pressure and longitude) component of the North Atlantic Oscillation (NAO). Sea surface temperature (SST) composites of the North Atlantic showed that during anomalously low IL, cold anomalies were observed all over the north Atlantic, spreading from the eastern

Labrador Sea south to the Scotian shelf and northeast into the Irminger and Norwegian Seas. The SST composite for anomalously low IL pressure with a two-year lag showed warm SST anomalies primarily south of the Scotian shelf and the Grand Banks, extending zonally in the northern subtropical gyre. Similar results were observed with IL longitude, providing further support for the buoyancy-driven forcing mechanisms. Finally, the link between Gulf Stream and IL (and Southern Oscillation Index) was used to develop a prediction scheme for predicting the Gulf Stream Northwall one year later.

The oceanic link between the Gulf Stream and the IL was further explored in Chapter 4's investigation of the Labrador Current, the Slope Sea, and Gulf Stream path's interconnection. Results suggested both Slope Sea and Labrador Current play a statistically significant role in the Gulf Stream's interannual migration. Slope Sea structure and properties were defined and compared with the Gulf Stream's interannual migration. The nature of the relationship between the Slope Sea and Gulf Stream suggested a feedback loop, where increases (decreases) in Slope Sea southwest transport follow southward (northward) shifts in Gulf Stream position; and changes in Slope Sea temperature precede shifts in Gulf Stream position, yet follow changes in Slope Sea transport. Last, the Labrador Current was shown to lead Gulf Stream low frequency variability by 2 years, where increases (decreases) in Labrador Current equatorward transport precede southward (northward) shifts in Gulf Stream position.

The last chapter looked at the relationship between the Gulf Stream path, the Atlantic meridional overturning circulation (AMOC) fingerprint, and biogeochemical cycling. Increases (decreases) in nutrients/chlorophyll concentrations and southward (northward) shifts in GS path were shown to follow periods of enhanced (weakened) AMOC fingerprint. The chlorophyll/nutrients were found related to the physical variables via upwelling and isopycnal

processes. The Gulf Stream's shift south indicated a shallowing of isopycnals in the Slope Sea, thus allowing nutrients to get re-introduced into the surface layer for primary production.

Overall this dissertation has aimed to give a comprehensive report on the structure and dynamics Gulf Stream's interannual migration. Establishing the underlying driving mechanism for the Stream's low frequency latitudinal shift was of particular interest. Analyses presented here supported evidence for the Gulf Stream's shift being forced by ocean-atmosphere processes in the subpolar gyre, rather than processes in the subtropical gyre (e.g. Rossby waves and/or the Florida Current). Though results shown here are predominantly indicative of buoyancy-driven mechanisms as the Gulf Stream's primary driving force, the related dynamical processes are still unclear. The need for further investigation and longer observational datasets stresses the importance of continuing to monitor the Gulf Stream.

Bibliography

Bane Jr., J. M., O. B. Brown, R. H. Evans, and P. Hamilton (1988), Gulf Stream Remote Forcing of Shelfbreak Currents in the Mid-Atlantic Bight, *Geophysical Research Letters*, *15*(5), 405--407.

Baringer, M. O. N., and J. C. Larsen (2001), Sixteen years of Florida Current Transport at 27 N, *Geophysical Research Letters*, *28*(16), 3179-3182.

Behrenfeld, M., R. O'Malley, D. Siegel, C. McClain, J. Sarmiento, G. Feldman, A. Milligan, P. Falkowski, R. Letelier, and E. Boss (2006), Climate-driven trends in contemporary ocean productivity, *Nature*, *444*, 752-755.

Behringer, D., L. Regier, and H. Stommel (1979), Thermal feedback on wind-stress as a contributing cause of the Gulf Stream, *Journal of Marine Research*, *37*, 699-709.

Bersch, M., I. Yashayaev, and K. P. Koltermann (2007), Recent changes in the thermohaline circulation in the subpolar North Atlantic, *Ocean Dynamics*, *57*, 223-235.

Borkman, D. G., and T. J. Smayda (2009), Gulf Stream position and winter NAO as drivers of long-term variations in the bloom phenology of the diatom Skeletonema costatum "species-complex" in Narragansett Bay, RI, USA, *Journal of Plankton Research*, *31*(11), 1407-1425, doi:10.1093/plankt/fbp072.

Bower, A. S., and H. D. Hunt (2000), Lagrangian Observations of the Deep Western Boundary Current in the North Atlantic Ocean. Part I: Large-Scale Pathways and Spreading Rates, *Journal of Physical Oceanography*, *30*, 764-783.

Brown, O. B., R. H. Evans, J. W. Brown, H. R. Gordon, R. C. Smith, and K. S. Baker (1985), Phytoplankton Blooming Off the U.S. East Coast: A Satellite Description, *Science*, *229*, 163-167, doi:10.1126/science.229.4709.163.

Cornillon, P., and R. D. Watts (1987), Satellite Thermal Infrared and Inverted Echo Sounder Determinations of the Gulf Stream Northern Edge, *Journal of Atmospheric and Oceanic Technology*, *4*, 712-723.

Csanady, G. T. (1990), Physical basis of coastal productivity, *EOS, 71*, 1060-1065.

Csanady, G. T., and P. Hamilton (1988), Circulation of slopewater, *Continental Shelf Research, 8*, 565-624.

Cunningham, S. A., et al. (2007), Temporal Variability of the Atlantic Meridional Overturning Circulation at 26.5°N, *Science, 317*, 935-938.

De Coetlogon, G., C. Frankignoul, M. Bentsen, C. Delon, H. Haak, S. Masina, and A. Pardaens (2006), Gulf Stream Variability in Five Oceanic General Circulation Models, *Journal of Physical Oceanography, 36*, 2119-2135.

Delworth, T. L., and e. al (2006), GFDL's CM2 Global Coupled Climate Models. Part I: Formulation and Simulation Characteristics, *Journal of Climate, 19*, 643-674.

DiNezio, P. N., L. J. Gramer, W. E. Johns, C. S. Meinen, and M. O. Baringer (2009), Observed Interannual Variability of the Florida Current: Wind Forcing and the North Atlantic Oscillation, *Journal of Physical Oceanography, 39*, 721-736.

Doney, S. C. (2006), Plankton in a warmer world, *Nature, 444*, 695-696.

Dunne, J. P., et al. (2012), GFDL's ESM2 Global Coupled Climate-Carbon Earth System Models. Part I: Physical Formulation and Baseline Simulation Characteristics, *Journal of Climate, 25*, 6646-6665.

Dunne, J. P., et al. (2013), GFDL's ESM2 Global Coupled Climate-Carbon Earth System Models. Part II: Carbon System Formulation and Baseline Simulation Characteristics, *Journal of Climate, 26*, 2247-2267.

Fedorov, A. V., and S. G. Philander (2000), Is El Nino changing?, *Science, 288*, 1997-2002.

Firing, E., J. Ramada, and P. Caldwell (1995), Processing ADCP data with the CODAS software system version 3.1, edited, Joint Institute for Marine and Atmospheric Research University of Hawaii & National Oceanographic Data Center., Bremerhaven, PANGAEA.

Flagg, C. N., M. Dunn, D.-P. Wang, H. T. Rossby, and R. L. Benway (2006), A study of the currents of the outer shelf and upper slope from a decade of shipboard ADCP observations in the Middle Atlantic Bight, *Journal of Geophysical Research, 111*(C6), doi:10.1029/2005jc003116.

Flagg, C. N., G. Schwartze, E. Gottlieb, and H. T. Rossby (1998), Operating an Acoustic Doppler Current Profiler aboard a Container Vessel, *Journal of Atmospheric and Oceanic Technology, 15*, 257-271.

Follows, M., and S. Dutkiewicz (2002), Meteorological modulation of the North Atlantic spring bloom, *Deep Sea Research II: Topical Studies in Oceanography*, *49*, 321-344.

Frankignoul, C., G. De Coetlogon, T. Joyce, and S. Dong (2001), Gulf Stream Variability an Ocean-Atmosphere Interactions, *Journal of Physical Oceanography*, *31*, 3516-3528.

Fuglister, F. C., and A. D. Voorhis (1965), A New Method of Tracking the Gulf Stream, *Limnology and Oceanography*, *10*, 115.

Greene, C. H., and A. J. Pershing (2003), The flip-side of the North Atlantic Oscillation and modal shifts in slope-water circulation patternss, *Limnology and Oceanography*, *48*, 319-322.

Hameed, S., and S. Piontkovski (2004), The dominant influence of the Icelandic Low on the position of the Gulf Stream northwall, *Geophysical Research Letters*, *31*(9), doi:10.1029/2004gl019561.

Han, G. (2006), Low-frequency variability of sea level and currents off Newfoundland, *Advances in Space Research*, *38*, 2141-2161.

Han, G., N. Chen, and Z. Ma (2014), Is there a north-south phase shift in the surface Labrador Current transport on the interannual-to-decadal scale?, *Journal of Geophysical Research*, *119*, 276-287, doi:10.1002/2013JC009102.

Han, G., K. Ohashi, N. Chen, P. G. Myers, N. Nunes, and J. Fischer (2010), Decline and partial reboun of the Labrador Current 1993-2004: Monitoring ocean currents from altimetric and conductivity-temperature-depth data, *Journal of Geophysical Research*, *115*, doi:10.1029/2009JC006091.

Han, G., and C. L. Tang (2000), Interannual Variations of Volume Transport in the Western Labrador Sea Based on TOPEX/Poseidon and WOCE Data, *Journal of Physical Oceanography*, *31*, 199-211.

Henson, S. A., D. Raitsos, J. P. Dunne, and A. McQuatters-Gollop (2009), Decadal variability in biogeochemical models: Comparison with a 50-year ocean colour dataset, *Geophysical Research Letters*, *36*, doi:10.1029/2009GL040874.

Iselin, C. O. D. (1936), A study of circulation of the western North Atlantic, *MIT-Woods Hole Oceanographic Institution*, *4*(4), 101 pp.

Jenkins, W. J., and S. C. Doney (2003), The subtropical nutrient spiral, *Global Biogeochemical Cycles*, *17*(4), doi:10.1029/2003GB002085.

Jennings, E., and N. Allott (2006), Position of the Gulf Stream influences lake nitrate concentrations in SW Ireland, *Aquatic Sciences*(68), 482-489.

Joyce, T., C. Deser, and M. A. Spall (2000), The Relation between Decadal Variability of Subtropical Mode Water and the North Atlantic Oscillation, *Journal of Climate*, *13*, 2550-2569.

Joyce, T., Y.-O. Kwon, and L. Yu (2009), On the relationship between synoptic wintertime atmospheric variability and path shifts in the Gulf Stream and Kuroshio Extension, *Journal of Climate*, *22*, 3177-3192.

Joyce, T., and R. Zhang (2010), On the Path of the Gulf Stream and the Atlantic Meridional Overturning Circulation, *Journal of Climate*, *23*(11), 3146-3154, doi:10.1175/2010jcli3310.1.

Kalnay, E., et al. (1996), The NCEP/NCAR 40-year Reanalysis Project, *Bulletin of the American Meteorological Society*, *77*, 437-471.

Kelly, K. A. (1991), The meandering Gulf Stream as seen by the Geosat Altimeter: Surface Transport, Position and Velocity Variance from 73 to 46W, *Journal of Geophysical Research*, *96*, 16,721-716,738.

Kelly, K. A., M. J. Caruso, S. Singh, and B. Qiu (1996), Observations of atmosphere-ocean coupling in midlatitude western boundary currents, *Journal of Geophysical Research*, *101*, 6295-6312.

Kelly, K. A., and S. T. Gille (1990), Gulf Stream surface transport and statistics at 69 W from the Geosat altimeter, *Journal of Geophysical Research*, *95*, 3149-3161.

Krauss, W., E. Fahrbach, A. Aitsam, J. Elken, and P. Koske (1987), The North Atlantic Current and its associated eddy field southeast of Flemish Cap, *Deep-Sea Research*, *34*(1163-1185).

Kremeur, A.-S., M. Levy, O. Aumont, and G. Reverdin (2009), Impact of the subtropical mode water biogeochemical properties on primary production in the North Atlantic: New insights from an idealized model study, *Journal of Geophysical Research*, *114*, doi:10.1029/2008JC005161.

Lee, T., and P. Cornillon (1995), Temporal variation of meandering intensity and domain-wide lateral oscillations of the Gulf Stream, *Journal of Geophysical Research*, *100*, 13,603-613,613.

Lee, T., and P. Cornillon (1996), Propagation and Growth of Gulf Stream Meanders between 75° and 45°W, *Journal of Physical Oceanography*, *26*, 225-241.

Levitus, S., J. Antonov, and T. Boyer (2005), Warming of the world ocean, 1955-2003, *Geophysical Research Letters*, *32*, doi:10.1029/2004GL021592.

Levy, M., D. Iovino, S. Masson, G. Madec, P. Klein, A.-M. Treguier, and K. Takahashi (2009), Remote impacts of Sub-Mesoscale Dynamics on new production, *Mercator Ocean Quarterly Newsletter*, *35*, 13-19.

Linder, C. A., and G. Gawarkiewicz (1998), A climatology of the shelfbreak front in the Middle Atlantic Bight, *Journal of Geophysical Research, 103*, 18,405-418,423.

Lozier, M. S., A. C. Dave, J. B. Palter, L. M. Gerber, and R. T. Barber (2011), On the relationship between stratification and primary productivity in the North Atlantic, *Geophysical Research Letters, 38*, L18609, doi:doi:10.1029/2011GL049414.

Mahajan, S., R. Zhang, T. Delworth, S. Zhang, A. Rosati, and Y.-S. Chang (2011), Predicting Atlantic meridional overturning circulation (AMOC) variations using subsurface and surface fingerprints, *Deep-Sea Research II, 58*, 1895-1903.

Martinez, E., D. Antoine, F. D'Ortenzio, and B. Gentili (2009), Climate-driven basin-scale decadal oscillations of oceanic phytoplankton, *Science, 326*, 1253-1256.

McGrath, G. G., H. T. Rossby, and J. T. Merril (2010), Drifters in the Gulf Stream, *Journal of Marine Research, 68*, 699-721.

McLellan, H. J. (1957), On the Distinctness and Origin of the Slope Water off the Scotian Shelf and its Easterly Flow South of the Grand Banks, *Journal of the Fisheries Research Board of Canada, 14*, 213-239.

Meinen, C. S., M. O. Baringer, and R. F. Garcia (2010), Florida Current transport variability: An analysis of annual and longer-period signals, *Deep-Sea Research I, 57*, 835-846.

Minobe, S., A. Kuwano-Yoshida, N. Komori, S.-P. Xie, and R. J. Small (2008), Influence of the Gulf Stream on the trophosphere, *Nature, 452*, 206-209.

Mountain, D. G. (2012), Labrador slope water entering the Gulf of Maine-response to the North Atlantic Oscillation, *Continental Shelf Research, 47*, 150-155.

Nye, J., T. Joyce, Y.-O. Kwon, and J. S. Link (2011), Silver hake tracks changes in Northwest Atlantic circulation, *Nature Communications, 2*, doi:10.1038/ncomms1420.

Parsons, A. T. (1969), A two-layer model of Gulf Stream separation, *Journal of Fluid Mechanics, 39*, 511-528.

Pavlis, N. K., S. A. Holmes, S. C. Kenyon, and J. K. Factor (2012), The development and evaluation of the Earth Gravitational Model 2008 (EGM2008), *Journal of Geophysical Research, 117*, doi:10.1029/2011JB008916.

Pelegri, J. L., and G. T. Csanady (1991), Nutrient transport and mixing in the Gulf Stream, *Journal of Geophysical Research, 96*, 2577-2583.

Peña-Molino, B., and T. Joyce (2008), Variability in the Slope Water and its relation to the Gulf Stream path, *Geophysical Research Letters, 35*(3), doi:10.1029/2007gl032183.

Peng, G., Z. Garraffo, G. R. Halliwell, O.-M. Smedstad, C. S. Meinen, V. Kourafalou, and P. Hogan (2009), Temporal variability of the Florida Current transport at 27 N, in *Ocean Circulation and El Nino: New Research*, edited by F. Columbus, NOVA Science Publishers, Hauppauge, NY.

Pershing, A. J., C. H. Greene, C. Hannah, D. Sameoto, E. Head, D. G. Mountain, J. W. Jossie, M. C. Benfield, P. C. Reid, and T. G. Durbin (2001), Oceanographic responses to climate in the Northwest Atlantic, *Oceanography*, *14*(3), 76-82.

Pickart, R. S., T. K. McKee, D. J. Torres, and S. A. Harrignton (1999), Mean Structure and Interannual Variability of the Slopewater System South of Newfoundland, *Journal of Physical Oceanography*, *29*, 2541-2558.

Pickart, R. S., and W. M. Smethie Jr. (1993), How Does the Deep Western Boundary Current Cross the Gulf Stream?, *Journal of Physical Oceanography*, *23*, 2602-2616.

Pickart, R. S., D. J. Torres, and R. A. Clarke (2002), Hydrography of Labrador Sea during Active Convection, *Journal of Physical Oceanography*, *32*, 428-457.

Planque, B., and A. H. Taylor (1998), Long-term changes in zooplankton and the climate of the North Atlantic, *Journal of Marine Science*, *55*, 644-654.

Quenouille, M. H. (1952), *Associated Measurements*.

Robson, J., R. Sutton, and D. Smith (2014), Decadal predictions of the cooling and freshening of the North Atlantic in the 1960s and the role of ocean circulation, *Climate Dynamics*, *42*, 2353-2365.

Rossby, H. T. (1999), On gyre interactions, *Deep Sea Research Part II*, *46*, 139-164.

Rossby, H. T., and R. L. Benway (2000), Slow variations in mean path of the Gulf Stream east of Cape Hatteras, *Geophysical Research Letters*, *27*(1), 117-120.

Rossby, H. T., C. N. Flagg, and K. Donohue (2005), Interannual variations in upper-ocean transport by the Gulf Stream and adjacent waters between New Jersey and Bermuda, *Journal of Marine Research*, *63*, 203-226.

Rossby, H. T., C. N. Flagg, and K. Donohue (2010), On the variability of Gulf Stream transport from seasonal to decadal timescales, *Journal of Marine Research*, *68*, 503-522.

Rossby, H. T., C. N. Flagg, K. Donohue, A. Sanchez-Franks, and J. Lillibridge (2014), On the long-term stability of the Gulf Stream transport based on 20 years of direct measurements, *Geophysical Research Letters*, *41*(doi:10.1002/2013GL058636).

Rossby, H. T., and E. Gottlieb (1998), The Oleander Project: Monitoring the Variability of the Gulf Stream and Adjacent Waters between New Jersey and Bermuda, *Bulletin of the American Meteorological Society, 79*(1), 5-18.

Rossby, H. T., and T. Rago (1985), Hydrographic evidence for seasonal and secular change in the Gulf Stream, *IOC Technical Report, 30*, 25-28.

Rossby, H. T., and H.-M. Zhang (2001), The near-surface velocity and potential vorticity structure of the Gulf Stream, *Journal of Marine Research, 59*, 949-975.

Schollaert, S. E., H. T. Rossby, and J. A. Yoder (2003), Gulf Stream cross-frontal exchange: possible mechanisms to explain interannual variations in phytoplankton chlorophyll in the Slope Sea during SeaWiFS years, *Deep-Sea Research II, 51*, 173-188.

Smeed, D. A., et al. (2014), Observed decline of the Atlantic meridional overturning circulation 2004-2012, *Ocean Science, 10*, 29-38.

Smith, P. C., R. W. Houghton, R. G. Fairbanks, and D. G. Mountain (2001), Interannual variability of boundary fluxes and water mass properties in the Gulf of Maine and on Georges Bank: 1993-1997, *Deep Sea Research II: Topical Studies in Oceanography, 48*, 37-70.

Spall, M. A. (1996), Dynamics of the Gulf Stream/Deep Western Boundary Current Crossover. Part I: Entrainment and Recirculation, *Journal of Physical Oceanography, 26*, 2152-2168.

Talley, L. D., and M. S. McCartney (1982), Distribution and Circulation of Labrador Sea Water, *Journal of Physical Oceanography, 12*, 1189-1205.

Taylor, A. H. (1995), North-South shifts of the Gulf Stream and their climatic connection with the abundance of zooplankton in the UK and its surrounding areas, *ICES Journal of Marine Science, 52*, 711-721.

Taylor, A. H., and A. Gangopadhyay (2001), A simple model of interannual displacements of the Gulf Stream, *Journal of Geophysical Research*, *106*(C7), 13849-13860, doi:10.1029/1999jc000147.

Taylor, A. H., M. B. Jordan, and J. A. Stephens (1998), Gulf Stream shifts following ENSO events, *Nature, 393*, 638.

Taylor, A. H., and J. A. Stephens (1980), Latitudinal displacements of the Gulf Stream (1966 to 1977) and their relation to changes in temperature and zooplankton abundance in the NE Atlantic, *Oceanologica Acta*, 145-149.

Taylor, A. H., and J. A. Stephens (1998), The North Atlantic Oscillation and the latitude of the Gulf Stream, *Tellus, 50A*, 134-142.

Thompson, D. J., and W. J. Schmitz (1989), A Limited-Area Model of the Gulf Stream: Design, Initial Experiments, and Model-Data Intercomparison, *Journal of Physical Oceanography, 19*, 791-814.

Worthington, L. V. (1976), *On the North Atlantic Circulation*, John Hopkins University Press, Baltimore.

Yeager, S., and M. Jochum (2009), The connection between Labrador Sea buoyancy loss, deep western boundary current strength, and Gulf Stream path in an ocean circulation model, *Ocean Modelling, 30*, 207-224.

Yoder, J. A., S. E. Schollaert, and J. E. O'Reailly (2002), Climatological phytoplankton chlorophyll and sea-surface temperature patterns in continental shelf and slope waters off the Northeast U.S. coast., *Limnology and Oceanography, 47*, 672-682.

Zhang, R. (2008), Coherent surface-subsurface fingerprint of the Atlantic meridional overturning circulation, *Geophysical Research Letters, 35*, doi:10.1029/2008GL035463.

Zhang, R., T. Delworth, A. Rosati, W. Anderson, K. Dixon, H.-C. Lee, and F. Zeng (2011), Sensitivity of the North Atlantic Ocean circulation to an abrupt change in the Nordic Sea overflow in a high resolution global coupled climate model, *Journal of Geophysical Research, 116*, C12024, doi:doi:10.1029/2011JC007240.

Zhang, R., and G. Vallis (2007), The Role of Bottom Vortex Stretching on the Path of the North Atlantic Western Boundary Current and on the Northern Recirculation Gyre, *Journal of Physical Oceanography, 37*(8), 2053-2080, doi:10.1175/jpo3102.1.